

UNCLASSIFIED

AD NUMBER
ADB009765
NEW LIMITATION CHANGE
TO Approved for public release, distribution unlimited
FROM Distribution authorized to U.S. Gov't. agencies only; Test and Evaluation; AUG 1975. Other requests shall be referred to Air Force Armament Laboratory, Attn: DLMQ, Eglin AFB, FL 32542.
AUTHORITY
USADTC ltr, 30 May 1979

THIS PAGE IS UNCLASSIFIED

✓

28



AFATL-TR-75-103 ✓

**THE INFRARED SIGNATURE OF  
THE HIGH ALTITUDE SUPERSONIC TARGET (HAST)  
AT SEA LEVEL**

TARGETS BRANCH  
GUIDED WEAPONS DIVISION

ADB009765

AUGUST 1975

DDC  
RECEIVED  
MAR 22 1976  
C

FINAL REPORT: FEBRUARY 1975 - JUNE 1975

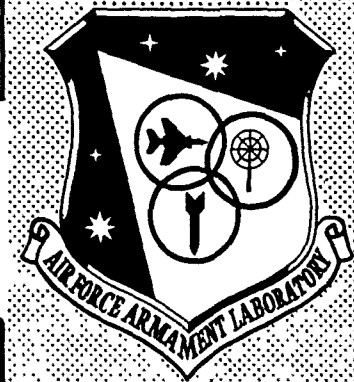
AD NO. \_\_\_\_\_  
DDC FILE COPY

Distribution limited to U. S. Government agencies only; this report documents test and evaluation; distribution limitation applied August 1975. Other requests for this document must be referred to the Air Force Armament Laboratory (DLMO), Eglin Air Force Base, Florida 32542.

**AIR FORCE ARMAMENT LABORATORY**

AIR FORCE SYSTEMS COMMAND • UNITED STATES AIR FORCE

**EGLIN AIR FORCE BASE, FLORIDA**



UNCLASSIFIED

SECURITY CLASSIFICATION OF THIS PAGE (When Data Entered)

REPORT DOCUMENTATION PAGE		READ INSTRUCTIONS BEFORE COMPLETING FORM
1. REPORT NUMBER <b>14</b> AFATL-TR-75-103	2. GOVT ACCESSION NO.	3. RECIPIENT'S CATALOG NUMBER
4. TITLE (and Subtitle) <b>6</b> THE INFRARED SIGNATURE OF THE HIGH ALTITUDE SUPERSONIC TARGET (HAST) AT SEA LEVEL.	5. TYPE OF REPORT & PERIOD COVERED <b>9</b> Final Report, January 1975 - June 1975	
7. AUTHOR(s) <b>10</b> D. B. Ebeoglu C. W. Martin	8. CONTRACT OR GRANT NUMBER(s) <b>112</b> 152 p.	
9. PERFORMING ORGANIZATION NAME AND ADDRESS Guided Weapons Division (DLMQ) Air Force Armament Laboratory Eglin Air Force Base, Florida 32542	10. PROGRAM ELEMENT, PROJECT, TASK AREA & WORK UNIT NUMBERS Proj. Element No. 62602F, Proj. No. 192103; Proj. Element No. 63232F, Proj. No. 469A0501	
11. CONTROLLING OFFICE NAME AND ADDRESS Air Force Armament Laboratory, Armament Development and Test Center, Air Force Systems Command Eglin Air Force Base, Florida 32542	12. REPORT DATE <b>11</b> August 1975	13. NUMBER OF PAGES 116
14. MONITORING AGENCY NAME & ADDRESS (if different from Controlling Office) <b>16</b> AF-1921, AF-469A <b>17</b> 192103, 5	15. SECURITY CLASS. (of this report) UNCLASSIFIED	
15a. DECLASSIFICATION/DOWNGRADING SCHEDULE		
16. DISTRIBUTION STATEMENT (of this Report) Distribution limited to U. S. Government agencies only; this report documents test and evaluation; distribution limitation applied August 1975. Other requests for this document must be referred to the Air Force Armament Laboratory (DLMQ), Eglin Air Force Base, Florida 32542.		
17. DISTRIBUTION STATEMENT (of the abstract entered in Block 20, if different from Report)		
18. SUPPLEMENTARY NOTES Available in DDC.		
19. KEY WORDS (Continue on reverse side if necessary and identify by block number)		
20. ABSTRACT (Continue on reverse side if necessary and identify by block number) Detailed measurements of the infrared signature of the High Altitude Supersonic Target (HAST) hybrid rocket engine have been obtained for the first time at sea level and at several measured O/F ratios representing its entire operating range. Secondary injection, as an infrared signature augmentation technique, has been evaluated on both the full-scale HAST engine and a special subscale model. The latter has also been operated with subsonic envelopes of inert gas (nitrogen) and air to eliminate or reduce the effect of afterburning as a radiation mechanism. The infrared measurements show excellent correlation between full-scale and subscale total radiation and also indicate that maximum radiation per unit area remains constant		

DDC  
 RECEIVED  
 AUG 23 1975  
 C

UNCLASSIFIED

SECURITY CLASSIFICATION OF THIS PAGE(When Data Entered)

Item 20 (Continued):

at beam aspect. It has been determined that the HAST hybrid engine infrared radiation is surface area dependent, varies linearly with flow rate, and is affected primarily by O/F ratio. These measurements have permitted closer evaluation of in-flight performance and have resulted in realistic recommendations for a HAST augmentation technique.



ACCESSION for	
NTIS	Write Section <input type="checkbox"/>
DOC	Ref Section <input checked="" type="checkbox"/>
UNCLASSIFIED	<input type="checkbox"/>
JUSTIFICATION .....	
BY .....	
DISTRIBUTION/AVAILABILITY STATEMENTS	
Dist.	AVAIL. AND/OR SPECIAL
<b>B</b>	

UNCLASSIFIED

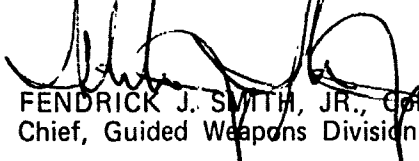
SECURITY CLASSIFICATION OF THIS PAGE(When Data Entered)

## PREFACE

This technical report describes the results of measurements and analyses performed by the Targets Branch (DLMQ) of the Air Force Armament Laboratory, Eglin Air Force Base, Florida, in simultaneous support of Program Element No. 62602F, Project No. 192103, "Infrared Plume Simulation Technology," and Program Element No. 63232F, Project No. 469A0501, "Plume Injection Infrared Augmentation." The effort was conducted during the period 20 January 1975 through 1 June 1975 by Dr. D. B. Ebeoglu, Lieutenant C. W. Martin, Mr. D. E. Fink, and Mr. I. W. Semmes (AFATL/DLMQ). The interferometer data were obtained and reduced by Captain W. B. Jollie (ADTC/TSGPA). The outstanding technical cooperation and support of Mr. A. L. Holzmar, Mr. R. A. Jones, and Dr. B. L. Iwanciw of Chemical Systems Division (CSD), United Technologies, Sunnyvale, California, is gratefully acknowledged. The results of the experimental and analytical effort conducted by CSD are contained in technical report AFATL-TR-75-90, "High Altitude Supersonic Target (HAST) Infrared Augmentation," Eglin Air Force Base, Florida, July 1975.

This technical report has been reviewed and is approved for publication.

FOR THE COMMANDER



FENDRICK J. SMITH, JR., Colonel, USAF  
Chief, Guided Weapons Division

## TABLE OF CONTENTS

Section	Title	Page
I	INTRODUCTION . . . . .	1
II	MEASUREMENT CONDITIONS . . . . .	3
	1. Experimental Geometry . . . . .	3
	2. Instrumentation . . . . .	3
	3. Calibration and Data Verification . . . . .	5
III	EXPERIMENTAL RESULTS . . . . .	7
	1. Subscale HAST Measurements . . . . .	7
	2. Full-Scale HAST Measurements . . . . .	12
IV	COMPARISON AGAINST ANALYTIC PREDICTIONS . . . . .	17
V	CONCLUSIONS AND RECOMMENDATIONS . . . . .	21
	LIST OF REFERENCES . . . . .	24
Appendix A	ADDITIONAL FULL-SCALE HAST ENGINE PLUME THERMAL SCANNER DATA DISPLAYS . . . . .	93

## LIST OF FIGURES

Figure	Title	Page
1	Subscale HAST Infrared Measurements Geometry . . . . .	25
2	Full-Scale HAST Infrared Measurements Geometry . . . . .	26
3	Subscale HAST Engine/Infrared Instrumentation Arrangement . . . . .	27
4	Full-Scale HAST Engine/Infrared Instrumentation Arrangement . . . . .	28
5	Time Sequences for Subscale HAST Engine Secondary Injection . . . . .	29
6	Subscale Engine Spectrum - No Injection, No Flow . . . . .	30
7	Subscale Engine Spectrum - O <sub>2</sub> Injection, No Flow . . . . .	31
8	Subscale Engine Spectrum - CH <sub>4</sub> Injection, No Flow . . . . .	32
9	Subscale Engine Spectrum - O <sub>2</sub> Injection, Mach 0.3 N <sub>2</sub> Flow . . . . .	33
10	Subscale Engine Spectrum - CH <sub>4</sub> Injection, Mach 0.3 N <sub>2</sub> Flow . . . . .	34
11	Subscale Engine Spectrum - No Injection, Mach 0.3 N <sub>2</sub> Flow . . . . .	35
12	Subscale Engine Spectrum - No Injection, No Flow . . . . .	36

## LIST OF FIGURES (CONCLUDED)

Figure	Title	Page
13	Subscale Engine Spectrum - No Injection, Mach 0.7 Airflow . . .	37
14	Subscale Engine Spectrum - POPS Injection, Mach 0.7 Airflow . .	38
15	Subscale Engine Spectrum - POPS Injection, No Flow . . . . .	39
16	Full-Scale HAST Engine - Boost Phase Duty Cycle . . . . .	40
17	Full-Scale HAST Engine - Sustain Phase Duty Cycle . . . . .	41
18	Full-Scale HAST Engine Boost Phase - J (4 to 5 Micrometers) Versus Time . . . . .	42
19	Full-Scale HAST Engine Sustain Phase - J (4 to 5 Micrometers) Versus Time . . . . .	43
20	Full-Scale HAST Engine Boost Phase - Typical Spectrum . . . . .	44
21	Full-Scale HAST Engine Sustain Phase - Typical Spectrum . . . .	45
22	Predicted HAST Plume Isothermal Contours (Sea Level Static) - Non-Equilibrium Chemistry . . . . .	46
23	Predicted HAST Plume Spectral Radiant Intensity at 30 Degrees from Tail - 1 to 8 Micrometers . . . . .	47
24	Measured Fuel/Particulate Rich Spectral Distribution from 3 to 14 Micrometers . . . . .	48
25	Predicted HAST Plume at Sea Level Static Conditions . . . . .	49
26	Predicted HAST Plume Spectral Radiant Intensity - 1.8 to 2.5 Micrometers (Sea Level Static) . . . . .	50
27	Predicted HAST Plume Spectral Radiant Intensity - 4.0 to 5.5 Micrometers (Sea Level Static) . . . . .	51

## LIST OF TABLES

Table	Title	Page
1	Time Sequences for Full-Scale HAST Engine Secondary Injection for Boost and Sustain Phases . . . . .	53
2	Infrared Measurement Comparisons Against an Extended Source . .	55
3	Radiometric Data for Subscale HAST Engine . . . . .	56

LIST OF TABLES (CONTINUED)

Table	Title	Page
4	Relative Radiation Emitted by Subscale HAST Engine in Three Spectral Bands . . . . .	61
5	Subscale Engine Plume Spatial Distribution - No Injection, No Flow . . . . .	66
6	Subscale Engine Plume Spatial Distribution - O <sub>2</sub> Injection, No Flow . . . . .	67
7	Subscale Engine Plume Spatial Distribution - CH <sub>4</sub> Injection, No Flow . . . . .	68
8	Subscale Engine Plume Spatial Distribution - O <sub>2</sub> Injection, Mach 0.3 N <sub>2</sub> Flow . . . . .	69
9	Subscale Engine Plume Spatial Distribution - CH <sub>4</sub> Injection, Mach 0.3 N <sub>2</sub> Flow . . . . .	70
10	Subscale Engine Plume Spatial Distribution - No Injection, Mach 0.3 N <sub>2</sub> Flow . . . . .	71
11	Subscale Engine Plume Spatial Distribution - No Injection, No Flow . . . . .	72
12	Subscale Engine Plume Spatial Distribution - No Injection, Mach 0.7 Airflow . . . . .	73
13	Subscale Engine Plume Spatial Distribution - POPS Injection, Mach 0.7 Airflow . . . . .	74
14	Subscale Engine Plume Spatial Distribution - POPS Injection, No Flow . . . . .	75
15	Subscale HAST Engine Scanner, Radiometric Data with and without Reflected Radiation . . . . .	77
16	Full-Scale HAST Engine Boost Phase - Infrared Radiant Intensity Between 4 and 5 $\mu$ . . . . .	82
17	Full-Scale HAST Engine Sustain Phase - Infrared Radiant Intensity Between 4 and 5 $\mu$ . . . . .	83
18	Full-Scale HAST Engine Boost Phase Spatial Distribution, T = 5 to 6 Seconds . . . . .	84
19	Full-Scale HAST Engine Boost Phase Spatial Distribution, T = 7 to 8 Seconds . . . . .	85
20	Full-Scale HAST Engine Boost Phase Spatial Distribution, T = 14 to 15 Seconds . . . . .	86

## LIST OF TABLES (CONCLUDED)

Table	Title	Page
21	Full-Scale HAST Engine Boost Phase Spatial Distribution, T = 21 to 22 Seconds . . . . .	87
22	Full-Scale HAST Engine Boost Phase Spatial Distribution, T = 26 to 27 Seconds . . . . .	88
23	Full-Scale HAST Engine Boost Phase Spatial Distribution, T = 41 to 42 Seconds . . . . .	89
24	Full-Scale HAST Engine Boost Phase Spatial Distribution, T = 29 to 30 Seconds . . . . .	90
25	Comparison Between Calculated and Measured Data (Sea Level Static Conditions - Sustain Phase) . . . . .	91
26	Comparison Between Calculated and Measured Data (Sea Level Static - Boost Phase) . . . . .	91

## SECTION I

### INTRODUCTION

The infrared data described in this report were obtained on two hybrid rocket engines developed by Chemical Systems Division (CSD), United Technologies (formerly United Technology Center, Division of United Aircraft), Sunnyvale, California. These engines utilize a case bonded solid fuel grain (80 percent polybutadiene and 20 percent polymethylmetacrylate) having a hollow core through which is injected an atomized liquid oxidizer [inhibited red fuming nitric acid (IRFNA)].

The full-scale engine operates at total flow rates of between 1000 and 2000 grams per second and is the propulsion system for the HAST. A subscale engine having the same general geometry and propellants, and operating at a flow rate of about 100 grams per second, was developed to permit the study of secondary injection as an infrared augmentation technique over a wide range of primary and secondary conditions.

The purpose of this effort was to obtain a set of detailed and unambiguous measurements of the infrared signature of the HAST engine at sea level, analyze infrared performance, evaluate and recommend viable augmentation techniques and extrapolate the data to determine inflight infrared performance. Previous analyses (Reference 1) had concluded that, to the maximum extent possible, the target propulsion system should be used as the infrared source. Experimental investigations (Reference 2) had established the major parameters affecting infrared radiation from rocket engine plumes. An experimental investigation was thus recommended and was undertaken by CSD to apply the fundamental knowledge gained in maximizing radiation from plumes to the specific details of the HAST hybrid engine configuration, temperature, and fuel chemistry.

The detailed IR signature measurements, which were conducted by AFATL, determined total radiant intensity between 4 and 5 micrometers, spectral radiant intensity between 2 and 5 micrometers and spatial radiant intensity distributions over its entire plume between 4 and 5.5 micrometers. These data were obtained for each operating condition. Both engines were operated by CSD using a complement of instrumentation to control, monitor, and record engine operating conditions.

This report describes the geometry for the measurements, the final reduced data from each instrument and the agreement between instruments. It discusses the infrared performance of the hybrid engine with and without augmentation, with and without subsonic co-flowing air envelope, and with and without a subsonic nitrogen envelope. This

#### References

1. Report of the Plume Emissions Panel, Advisory Committee to the Air Force Systems Command, National Academy of Sciences, June 1973.
2. D. B. Ebeorju, Fundamental Parameters Affecting Plume Infrared Radiation, AFATL-TR-74-84, Eglin Air Force Base, Florida, April 1974.

report also reviews previous infrared plume prediction calculations performed for the HAST, compares them against the measured data and evaluates their effectiveness. Based on the conclusions reached from all the data analysis, recommendations are made for implementing improved techniques to provide significant inflight infrared enhancement of the HAST engine exhaust plume.

## SECTION II

### MEASUREMENT CONDITIONS

#### 1. EXPERIMENTAL GEOMETRY

Figures 1 and 2 show the geometry chosen for the subscale and full-scale engine measurements, respectively. Corresponding photographs of the engine/instrumentation arrangements are shown in Figures 3 and 4. Both engines were operated at a height of 39.4 centimeters from ground to centerline.

There was a vertical wall approximately 69.9 centimeters from the subscale engine parallel to the centerline (off the right-hand side of Figure 3). The scanner measurements detected an infrared reflection of the plume from this wall during the subscale engine tests and from the ground plane<sup>1</sup> during the full-scale engine tests. However, the reflected radiation in each case contributed an apparent increase in total radiation of less than 20 percent. In view of the low levels encountered, no serious attempts were undertaken to eliminate reflections. [These conclusions become apparent from the infrared scanner data on the subscale engine (Tables 5 through 14) and on the full-scale engine (Tables 16 and 18 through 24)].

For the subscale measurements, the AFATL and CSD radiometers were placed next to each other at a point approximately 30 degrees from the plume axis (tail-on angle being 0 degree). Agreement between the radiometers was repeatedly found to be within 6 percent. Thus, for the full-scale measurements, the radiometers were placed at separate locations in order to gain another data point. In the latter case, the AFATL unit was placed at 60 degrees and the CSD unit at 30 degrees. (However, due to the lay of the land, the CSD unit had to be at a height of approximately 10 meters above the engine axis.) The interferometer and the scanner were always operated at 90 degrees aspect angle, care being taken to ensure that they did not fall within each other's field of view.

#### 2. INSTRUMENTATION

Most of the infrared instrumentation has been described in detail previously and thus only salient points are reviewed here. The AFATL radiometer is a Hewlett Packard 8330A/8334A thermopile with a 3.92- to 5.1-micrometer bandpass filter, a 7-1/2-degree non-attenuated field of view and a CaF<sub>2</sub> window. The CSD radiometer, designed and fabricated by CSD, uses a pyroelectric detector with a 3.86- to 5.31-micrometer bandpass filter, a non-attenuated field of view of approximately 7.2 degrees, and a germanium window. Both radiometers have a flat spectral response and were operated over a flat field of view.

---

#### Footnote

<sup>1</sup>The full-scale measurements were conducted on a rainy day, and the wet pavement might have enhanced the amount of radiation reflected in that instance.

A BOFORS scanner with a Barnes digital data acquisition system (Reference 3) was used to obtain infrared spatial distributions. The instrument has a 25-degree (horizontal) by 12.5-degree (vertical) field of view, giving a two-dimensional matrix of 56 (horizontal) by 94 (vertical) total digital picture elements over this field of view, with a digital dynamic range of each picture element from 0 to 127. The bandpass selected was 4 to 5.5 micrometers.

A Block Model 600 interferometer spectrometer was used to measure spectral distributions between 2 and 5 micrometers. Data were collected at a resolution of  $4 \text{ cm}^{-1}$  at a rate of 16 scans per second, generally, over a 1-second duration. The instrument was operated with about a 25-degree field of view (of which approximately 16 degrees were taken up by the full-scale plume).

An automatic sequencing system developed by CSD was used with both the engines to control the duration of each sequence of operation during a given firing. Figure 5 shows the time sequences used for the subscale HAST firing. The standard time sequence shown in Figure 5(a) allowed the examination of (a) the static plume, (b) the static plume with fuel augmentation, (c) the static plume with oxygen augmentation, (d) the dynamic plume (with subsonic air or nitrogen envelope), (e) the dynamic plume with fuel augmentation, and (f) the dynamic plume with oxygen augmentation. The sequence was changed only once, as shown in Figure 5(b), to allow the evaluation of the Atlantic Research Corporation Pyrotechnic Optical Plume Simulator (POPS) as a HAST plume augmentation device.

Table 1 shows the sequences for both the boost and sustain phases of the full-scale HAST firing. The infrared instruments were operated continuously from a point in time preceding engine firing to after the end of a complete set of sequences. The sequencer was used to produce time marks in conjunction with an IRIG time-code generator. The full-scale engine could only be evaluated at static conditions; thus, time sequences were selected to allow infrared measurements of the plume with and without fuel augmentation and with and without oxygen augmentation at set intervals. These intervals encompassed a range of engine O/F ratios and total mass flow rates for all the missions contemplated for the HAST.

The interferometer data were collected in two ways. First, interferograms were recorded on analog tape (using a Bell & Howell CPR-4040 Instrumentation Recorder) along with IRIG time code, the automatic sequencer sync pulse, and voice annotation. In this way, the entire spectral history of each rocket motor firing was preserved. Second, interferograms were randomly digitized and recorded in real time using the data system of the spectrometer to provide spectral information free from any possible recorder noise. This real time data provided a check on the quality of the recorded data and provided a means of on-the-spot data evaluation.

---

#### Reference

3. C. W. Martin, R. F. Askew, and D. B. Ebeoglu, Operation of an Infrared Thermal Scanner for Plume Measurements, AFATL-TR-74-204, Eglin Air Force Base, Florida, December 1974.

For each run, data were reduced over the intervals of time shown in Figure 5 and Table 1. The data system digitized and co-added 16 interferograms to create the final data interferogram for each specified time. It then performed a Fourier transform on the final interferogram to produce a raw target spectrum. This spectrum was corrected with the instrument response curve and plotted as a fully calibrated spectrum. Each spectrum was then recorded on digital magnetic tape to make a permanent record of the final data. The same procedures were used to reduce the data collected in real time, except that a separate real time instrument response curve was used to correct the raw data.

The thermal scanner data were continuously recorded on digital tape and the time sequences shown in Figure 5 and Table 1 used for final data reduction. Frames were selected using timing pulses from the firing sequencer on a strip chart recorder and the octal frame counter on the scanner. (The scanner operates at a scan rate of 2.87 frames per second.) The radiant intensity figures presented for each sequence are averages of the total radiant intensity measured in three frames. The data recorded from the scanner were visually reviewed on an oscilloscope and gross effects, such as saturation or reflections, noted for correction. Final numerical data reduction was performed on a CDC 6600 computer.

### 3. CALIBRATION AND DATA VERIFICATION

A 1.25-square-centimeter blackbody source at 900 degrees Centigrade was used at the test locations to obtain the response of each instrument configuration. Interferograms from the blackbody were collected on both analog tape and in real time. These data were reduced to provide an instrument response curve in order to calibrate the spectral information from the target. Analog voltages from the scanner due to the blackbody radiation were checked on-site and the radiation recorded on digital tape.

Full calibration procedures were performed at the Air Force Armament Laboratory using the same blackbody source at different locations, an extended blackbody source, a propane/oxygen torch, and all three infrared instruments. Data were taken for a number of extended sources having about a 10:1 range of radiance and radiant intensity levels. Total radiant intensity between 4 and 5 micrometers, as measured by the thermopile radiometer, and total radiant intensity between 4 and 5.5 micrometers, as summed by the scanner (operated at the same sensitivity and attenuator levels used for the HAST plume measurements) were found to agree within 18 percent.

The comparison of these data against integrated radiant intensity between 4 and 5 micrometers, as measured by the interferometer, showed the latter, in certain configurations, to yield approximately one-half the radiant intensity measured by the other two instruments. This occurred consistently for all cases in which the interferometer viewed an extended source filling the field of view. It was determined that better than 20 percent agreement could be obtained for a small extended source placed in the center of the field of view.

The interferometer has a sharp drop-off in sensitivity beyond a central solid angle of 5 degrees with the optical configuration used in the HAST measurements. This drop-off causes integrated values of radiant intensity between 4 and 5 micrometers to be, very roughly, halved. This factor applied for all the spectral radiant intensity data collected on the full-scale HAST. The interferometer was only used to measure the relative radiant intensity of the subscale HAST. This correction factor, therefore, is not relevant to the latter data.

The radiometric data comparison described above is summarized in Table 2. Runs 1 through 5 were performed with the interferometer viewing sources filling its field of view. In runs 6 through 9 the extended sources did not fill the field of view of the interferometer. The result was better than 20 percent agreement between the interferometer and the thermopile radiometer.

## SECTION III

### EXPERIMENTAL RESULTS

#### 1. SUBSCALE HAST MEASUREMENTS

Infrared measurements were performed at sea level on the subscale HAST engine during 18 firings, two of which included augmentation by the Atlantic Research Corporation POPS device. The engine was operated at O/F ratios between 1.95 and 4.01 and at total mass flow rates between 86 and 172 grams per second. Chamber pressures varied between 4.86 and 10.2 kg/cm<sup>2</sup>. Six data points were taken at each firing (except for the POPS run, which only required four). Oxygen (O<sub>2</sub>) and methane (CH<sub>4</sub>) augmentation were evaluated at static conditions and also with a co-flowing airstream at Mach 0.7 or with a co-flowing nitrogen stream at Mach 0.3.

This procedure resulted in approximately 100 data points being taken by each instrument and allowed the infrared signature of the engine to be verified several ways. Since the data are similar in many respects, data taken by these instruments are presented in their entirety for only a few representative firings.

##### a. Radiometric Data

The complete set of data collected with the radiometers and the radiometric data from the scanner are presented in Table 3 which relates them to key engine parameters. Additional diagnostic engine data taken for each firing included fuel grain size, nozzle diameter and expansion ratio, chamber pressure, characteristic velocity, IRFNA mass flow rate, total mass flow rate and thrust. These may be found in the CSD final report (Reference 4) and can be cross-referenced by using the run number. They are not repeated here since analyses of the data have shown them to have a relatively minor effect on the infrared performance of the engine.

For each firing of the subscale HAST, Table 3 shows:

- (1) O/F ratio
- (2) Secondary material injected

##### Reference

4. A. L. Holzman and R. A. Jones, High Altitude Supersonic Target (HAST) Infrared Augmentation, AFATL-TR-75-90, Eglin Air Force Base, Florida, July 1975.

- (3) Ratio of secondary to primary mass flow rate ( $\dot{m}_s/\dot{m}_p$ )
- (4) Co-flowing air or nitrogen Mach number ( $M_\infty$ ); with the latter flow condition being designated by the symbol  $N_2$  following the Mach number
- (5) The radiant intensity,  $J$ , in watts/steradian, between 4 and 5 micrometers measured by the radiometers
- (6) The radiant intensity,  $J$ , in watts/steradian, between 4 and 5.5 micrometers measured by the scanner
- (7) The figure of merit,  $\bar{J}$ , in watts/steradian/gram/second, computed from the radiometer data
- (8) The infrared augmentation ratio  $(J_{aug}/J)_{flow}$  is the ratio of the radiant intensity of the plume with and without secondary injection, based on the radiometer data obtained with air or nitrogen flow
- (9) Injection mode, whether via a discrete number of holes or an annular slot

The radiometric data shown in Table 3 are those measured by the CSD radiometer. The latter numerical values were used directly since agreement with the AFATL radiometer was within 10 percent for every single data point. These radiometric data therefore provide a consistent standard of comparison for previous and subsequent measurements performed by CSD.

The static data consistently show  $O_2$  injection to produce a fraction of the augmentation produced by  $CH_4$  injection, the latter in some cases exceeding 100 percent. It is quite certain, however, that these data merely show the enhancement of afterburning by hot  $CH_4$  rather than augmentation of the exhaust plume itself. The static augmentation data is only recommended for use in determining the extent to which the subscale infrared plume is an extrapolation of the full-scale infrared plume.

Afterburning is the primary radiation mechanism in a rocket engine exhaust plume at static altitude conditions (Reference 5). Afterburning increases when the O/F ratio is decreased as more hot unburned fuel is released into the ambient air, causing the large increase in radiant intensity noted at low O/F ratios. The HAST engine operates below

#### Reference

5. D. B. Ebeoglu and C. W. Martin, Effect of Mixture Ratio on UV, Visible and Infrared Radiation for Exhaust Plumes, AFATL-TR-75-79, Eglin Air Force Base, Florida, May 1975.

stoichiometry for all presently postulated mission profiles, resulting in significant afterburning at static altitude conditions. Oxygen injection at static conditions produces minimal infrared augmentation probably by permitting slightly more efficient combustion of the fuel rich exhaust than with stagnant air. Methane injection, at static conditions, on the other hand, directly increases afterburning. The effect of fuel injection is the same as lowering the O/F ratio and thus large increases of infrared radiant intensity are produced.

Afterburning is reduced significantly in an airstream. In the case of an unchoked exhaust the attenuation is quite severe; reductions of two orders of magnitude are possible at low subsonic air velocities (Reference 6). In the case of a choked rocket engine exhaust in a supersonic airstream, radiant intensity may be reduced by a factor as high as 20.

The air or nitrogen ambient flow data were thus used as the basis for evaluating the secondary injection plume augmentation technique. The ratio of  $J_{\text{flow}}/J_{\text{static}}$  gives a direct indication of the operational HAST plume signature attenuation by air velocity in flight. Normalizing the radiant intensity data of the subscale HAST engine with ambient flow, so that  $J$  for the plume without augmentation becomes 1.0, permits a direct indication of the effectiveness of  $O_2$  and  $CH_4$  augmentation

The ratio of the plume radiant intensity at static sea level conditions to that in a subsonic airstream gives an optimistic indication of the attenuation that can be expected in flight since (a) the air is only at subsonic velocity and (b) the airflow does not fully encompass the plume. The data collected with the plume in a subsonic co-flowing nitrogen stream give a more pessimistic approximation of the ultimate airborne radiant intensity. Although signature attenuation due to the kinetic effects of a supersonic airstream are not simulated, the nitrogen stream overcompensates by eliminating all the afterburning that the HAST engine exhaust could be expected to produce in actual flight at altitude. On the other hand, it has been shown that radiant intensity increases with altitude (Reference 2) in inverse proportion to the square root of ambient pressure due to the expansion and increase in length of the exhaust plume.

Using these criteria for evaluation, the data show that:

- (1) Augmentation by fuel or oxygen injection depends on the engine O/F ratio at any ambient condition. With either a co-flowing air or nitrogen stream the data show that fuel injection produces more augmentation at rocket engine O/F ratios larger than about 3.0,

#### Reference

6. D. B. Ebeoglu, The Infrared Signature of Pyrophorics, AFATL-TR-74-92, Eglin Air Force Base, Florida, May 1974.

whereas oxygen injection is more effective for O/F ratios less than 3.0. The POPS device, which produces an exhaust rich in carbon particulates, gives about the same augmentation as CH<sub>4</sub>.

- (2) Maximum augmentation of about 50 to 60 percent is possible, albeit at different O/F ratios, for either O<sub>2</sub>, CH<sub>4</sub>, or POPS injection. These measurements are all in co-flowing subsonic streams, and require secondary total mass flow rates of about 5 to 10 percent of that of the HAST engine total propellant flow rate. Further increases of the secondary mass flow rate, of either oxidizer or fuel, do not measurably increase the enhancement.
- (3) Annular or multipoint secondary injection produces higher augmentation than single hole injection at any condition.

#### b. Spectral Data

Spectral radiant intensity distributions for either of the HAST engines, for any operating condition, and for any augmentation condition, bear striking resemblances to each other. Spectra are presented in Figures 6 through 11 for the subscale engine for all six conditions of one run (number 5579) illustrating O<sub>2</sub>/CH<sub>4</sub> injection, with and without Mach 0.3 nitrogen flow. Figures 12 through 15 show all four conditions of one run (number 5587) with POPS injection, with and without Mach 0.7 airflow.

The spectra show CO<sub>2</sub> radiation between 4 and 5 micrometers, CO<sub>2</sub> and H<sub>2</sub>O radiation between 2.5 and 3 micrometers, superimposed on a strong graybody continuum peaking below 2 micrometers. POPS injection does not alter the spectral distribution in any appreciable fashion. The exhaust plume spectra are quite similar to those produced by a highly fuel rich combustion at which the point of carbon luminosity has been reached. [For example, the spectrum of freeburning kerosene (Reference 5)].

In general, the graybody contribution is more pronounced with air or nitrogen flow than at static conditions. Run 5579 was chosen as an example because it exhibits the largest difference in graybody level from static to dynamic condition than any other run and thus best illustrates this point. The change in spectral distribution indicates that afterburning (which predominates in a static environment) produces more CO<sub>2</sub> and H<sub>2</sub>O emission than hot carbon emission. As with the radiometric data, the ambient flow measurements give a fairly realistic representation of spectral distributions that can be expected from this engine in flight.

Relative radiation emitted in three spectral bands, 2.2 to 3, 2.2 to 4, and 4 to 5 micrometers are presented in Table 4 for each sequence of each firing of the subscale HAST engine. These data can be used to assess the distribution of radiation within the 2- to 5-micrometer band. The data with nitrogen or airflow show that secondary injection of CH<sub>4</sub>

and O<sub>2</sub> affect infrared radiation in any of these three bandpasses in nearly the same amounts. The 4- to 5-micrometer band data are generally proportional to the radiometric data presented in Table 3, although no attempt was made to ensure that the interferometer viewed the entire plume.

In the case of the POPS tests the interferometer data for the 4- to 5-micrometer band are directly proportional to the radiometer readings. The spectral data with airflow show the POPS to augment primarily by increasing graybody radiation when injected into a high O/F ratio exhaust. Table 4 shows that at an O/F ratio of 2.46 (Run 5587) POPS is not effective in any band; on the other hand, at an O/F ratio of 3.99 (Run 5588), augmentation in the 2.2- to 3- and 2.2- to 4-micrometer bands is significantly higher than in the 4- to 5-micrometer band. This suggests that at the lower O/F ratio, the graybody radiation from the engine plume is too high for augmentation by particulates from the POPS device. At the higher O/F ratio, POPS injection doubles the graybody radiation from the plume and consequently increases radiant intensity in the 4- to 5-micrometer band.

### c. Spatial Data

Typical infrared plume spatial distributions for the subscale HAST exhaust are shown in Tables 5 through 14. These cover the same two runs which were used to describe the interferometer data. These data represent one file out of the data recorded on a continuous time base during each firing sequence. The horizontal increment is 2.54 cm, the vertical increment is 0.72 cm, and the unit of radiation in each spatial element is 0.01 watt/steradian.

The radiation reflected from the wall behind the engine is evident at the top of the static plume scans. In order to determine the radiation from the plume alone and assess quantitatively the contribution of the reflected radiation, a special data reduction computer program for line subtraction was written and applied to the data. Table 15 compares radiant intensity with and without reflection for all the subscale engine runs and lists the percent contribution due to the reflection.

The spatial measurements were all made at the same attenuator and sensitivity settings in order to obtain a direct comparison of data. The difference between the spatial distributions of plumes in a static and in a subsonic flow environment are significant. As Tables 5 through 14 typically show, the subsonic ambient flow causes plumes to be reduced by at least a third in each dimension, and plume maximum intensity per unit area to drop at least one-half. Secondary injection without airflow produces augmentation by increasing plume dimensions as well as increasing radiance, indicating augmentation to be due to a large extent to afterburning. Secondary injection with ambient flow, on the other hand, does not appreciably increase plume dimensions - primarily, the magnitude of the scanned matrix elements increase.

POPS produces a spatially skewed augmented plume due to its being injected at a relatively high velocity through a single point in the subscale HAST engine exit nozzle. The POPS injection data also show the low radiant intensity of its own exhaust as it is injected into the subscale HAST engine plume. The POPS exhaust can be seen in a single vertical column in the top left-hand side of Tables 13 and 14 (the scanner data being inverted).

For all the ambient flow conditions, Table 15 shows that the subscale HAST scanner radiometric data agree closely with the thermopile and pyroelectric radiometer data; whereas, in the static case, the scanner and radiometer data differ by a constant amount. This is due entirely to aspect angle. The HAST propellant exhaust is highly rich in fuel and particulates and thus is quite likely to be optically opaque. Therefore, it is postulated that the radiation emitted by the plume is proportional to the plume surface area rather than the plume volume. The radiometers placed at 30 degrees and the scanner placed at 90 degrees view different aspects, and thus different size surface areas, of the plume. At static conditions the surface area of the plume at beam aspect is much larger than that at 30-degree aspect. With a co-flowing stream the plume length is decreased and the surface area projected at 90 degrees becomes closer to that at 30 degrees.

## 2. FULL-SCALE HAST MEASUREMENTS

The full-scale engine infrared measurements were performed over a set of mixture ratios covering the full HAST inflight operating range. Data were obtained continuously during operating conditions representing both boost and sustain phase. The secondary injection cycle is shown in Figures 16 and 17 together with the actual O/F ratios at those points. O/F ratios were obtained by an indirect measurement of the solid fuel flow rate during firings via a continuous engine-weighing process developed by CSD.

O/F ratios varied between 1.5 and 3.2 during boost and between 3.1 and 2.0 during sustain phase. Total propellant flow rates were between 1500 and 2200 grams per second during boost and from approximately 1200 down to 500 grams per second during sustain phase. Either methane ( $\text{CH}_4$ ) or oxygen ( $\text{O}_2$ ) were injected, both symmetrically and asymmetrically, at two flow rates of approximately 23 and 53 grams per second. Chamber pressures increased from about 15 to 27  $\text{kg/cm}^2$  during boost and decreased from about 13 to 3.5  $\text{kg/cm}^2$  during sustain phase.

The only infrared anomaly noted occurred in the first 10 seconds of boost phase. The initial 10 seconds of boost phase is not representative of conditions that can be reproduced during significant time periods in which the HAST would be presented as an inflight infrared target. During the first 10 seconds, extra fuel is used for reliable ignition producing an O/F of 1.5. The high infrared radiant intensity produced during this period is due to this extremely low O/F ratio and also to the exhaust of burned igniter material.

#### a. Radiometric Data

Figure 28 shows infrared radiant intensity versus time for the boost phase. The data shown were taken with the AFATL thermopile detector at the 60-degree aspect angle position. The time profile agrees extremely well with that observed at the 30-degree aspect angle by the CSD pyroelectric detector. Variations in infrared radiant intensity with O/F ratio and with secondary injection are clearly evident.

Figure 18 shows secondary injection to produce the same effect on the full-scale HAST engine plume radiation as on the subscale engine at static conditions. Significant augmentation occurs during CH<sub>4</sub> injection, with negligible or negative effects being produced with O<sub>2</sub> injection. As has been indicated, however, these effects are solely manifestations of afterburning which predominates at static conditions. They are not representative of in-flight performance.

Table 16 presents the radiometric data obtained between 4 and 5 micrometers by all of the infrared instruments during boost phase. The injection mode is designated at Hi O (high oxygen), Lo F (low methane), etc. Thermal scanner data were lost due to saturation during 10 seconds of the run (Figure 18) when its sensitivity setting was erroneously changed from 50 to 20. Interferometer data were not taken during the initial 10 seconds. The integrated interferometer readings have been corrected grossly for spatial non-linearity. The integrated thermal scanner data is presented with and without the reflection from the ground, as is the percent reflection. The contribution of reflection differs with aspect angle and, therefore, these corrections only apply to the scanner and interferometer data which were taken at 90 degrees. Table 16 shows reflection corrected data only in the scanner column so marked.

Table 16 generally illustrates the variation of radiant intensity with aspect angle in boost phase. This distribution is quite similar to the cardioid pattern observed in a turbojet engine exhaust. Maximum radiant intensity is observed at 60 degrees. Beam aspect is somewhat lower, with 30-degree aspect radiation being lower still. As has been discussed, however, it is believed that the HAST rocket engine produces a plume that is optically thick, and that it thus emits infrared radiation which is surface, rather than volume, dependent. Turbojets, on the other hand, generally emit optically thin, and thus volume dependent, radiation, with the possible exception being those engines operating at high afterburner power. The variation of radiant intensity with aspect angle of the full-scale HAST plume, therefore, may not always exhibit the familiar cardioid pattern in flight.

Figure 19 shows the radiometric performance versus time during the sustain phase, as observed with the AFATL radiometer at 60 degrees aspect angle. As in boost phase, the initial 10 seconds are not representative of long-term performance. The infrared time profile shown, tracks all the variations in engine and injection operation cycles at this aspect

angle. On the other hand, the output of the CSD radiometer at 30 degrees did not follow these variations and did not maintain relative agreement with the 60-degree readings. After other possibilities were eliminated, it was concluded that these anomalies were due to plume separation in the nozzle. Separation will occur when the full-scale engine is operated at sea level and at low chamber pressures during the sustain phase.

Table 17 summarizes all the useful radiometric data obtained during the sustain phase. Injection modes are designated as in Table 16, with the exception of Asy to mean asymmetric secondary injection. The interferometer data shown has been corrected roughly for its non-flat field of view. The 30-degree aspect angle data were discarded since they were dominated by the separated plume; scanner data were not collected in usable form due to operator error. The data are consistent with the boost data and subscale engine infrared performance.  $T$  appears to be reasonably constant at a given O/F ratio for this range of operating conditions indicating that plume radiant intensity varies fairly linearly with total flow rate over a fairly wide range of flow rates between about 90 and 2200 grams per second.

#### b. Spectral Data

The spectral variant intensity distribution of the full-scale HAST engine was determined to be very similar to that observed with the subscale engine. A representative spectrum for boost and sustain phase, respectively, are presented in Figures 20 and 21. Relative radiation emitted in the three subdivisions of the 2- and 5-micrometer band are equally similar to that observed with the subscale engine.

These data support the thesis presented earlier (Reference 5) that all hydrocarbon exhausts emit infrared energy within a very limited number of spectral distributions, which change noticeably only at the extremes of O/F ratio. The HAST engine spectra show that changing engine size has no effect on infrared spectral distribution. In this case, it can also be postulated that even changing the oxidizer (from IRFNA to  $O_2$ , for example) might not have had an appreciable effect on the spectrum.

#### c. Spatial Data

The BOFORS infrared scanner has two controls which permit gain to be changed in steps varying between 2 and 3, provided both controls are set properly. One of these is electronic and can be controlled from the control panel. The other is in the form of neutral density attenuators which have to be physically replaced on the camera head itself. These gain settings determine the size signal that will be registered by each cell in the matrix of 56 by 94. If the controls are set too low, some cells become saturated, i.e., their output becomes pegged at a maximum level that might be any fraction of the actual radiant intensity falling on the detector. The data in those cells, and probably for the total plume, become numerically unusable. If, on the other hand, the controls are set too high, dynamic range is lost since the output signal from each cell remains well below the maximum possible.

Usually, these instrument idiosyncrasies do not pose difficulties in that test runs can be performed in the beginning of a set of measurements to select the controls for optimum signal output. In the case of the full-scale HAST measurements test runs could obviously not be made and, since the first phase, boost, was only 45 seconds long, controls had to be preset based on extrapolations from the subscale data.

The assumptions that had to be made were (1) full-scale engine plume length (to determine the distance at which to place the detector), and (2) the maximum radiation expected within a rectangle  $\Delta x$  by  $\Delta y$  on the plume (represented by each cell of the matrix). These required further assumptions of (1) J, (2) the area or volume dependence of the radiation from the plume, and (3) the relative shape of the visible versus the infrared plume at sea level. Calculations were then performed using equations developed earlier (Reference 3) to estimate control settings.

Maximum infrared plume length during boost phase was estimated to be not more than 3.66 meters (12 feet), based on linear extrapolations of the subscale engine infrared and visible plumes, and previous photographs of a full-scale engine plume. A plume-to-detector distance of 9.14 meters (30 feet) was selected that would provide for a small margin of error by allowing plumes up to 4.27 meters (14 feet) to be imaged. The scanner was positioned at a point about 2 meters downstream perpendicular to the plume axis.

At this distance,  $\Delta x = 7.5$  cm by  $\Delta y = 2.13$  cm on the plume, producing a cell having an area of  $16.26 \text{ cm}^2$ . The subscale engine data, for an O/F similar to boost phase, showed plume radiation per unit area to be  $1.06 \text{ w/st/cm}^2$ . The estimated maximum radiation for the full-scale HAST in the above geometry is then  $17.23 \text{ w/st}$  per cell. Next, at 9.14 meters the solid angle subtended by the camera can be shown to be  $1.33 \text{ by } 10^{-4}$  steradians, and the latter two parameters combined to give:

$$CF_{\max} = 4.36 \times 10^4$$

which corresponds to an amplifier setting of 50 in conjunction with neutral density attenuator  $1/K_0$  factor of 2465.

It was thus decided to use an attenuator setting of 75 during the first 10 seconds of the boost, when unusually high exhaust radiation would prevail which did not correspond to a normal engine cycle, and set the control at 50 after the first 10 seconds.

A second estimate was also performed assuming volume dependent radiation and radiation per unit volume. Naturally, this assumption defined a different set of scanner gain control settings. This estimate was performed as backup to be used in the sustain phase in case the assumption of surface area dependent radiation proved to be inaccurate.

The boost phase data for the HAST were successfully obtained at these specific control settings, indicating the accuracy of the estimates. Conversely, they also proved that (1) the subscale engine plume data could be accurately extrapolated to predict full-scale engine total radiant intensity, (2) the radiation from HAST engine plumes was surface area dependent, and (3) the maximum radiation per unit area for the subscale plume was the same as that emitted by the full-scale plume.

The basic scanner data obtained during the boost phase of the HAST are presented in Tables 18 through 23. These correspond to the time frames shown in Table 16. The accuracy of the extrapolation was explicitly proven further when the operator attempted to obtain data at an attenuator setting of 20 (instead of 50) during the 10 seconds of the run shown in Figure 18. The four scanner matrices obtained during this brief period had a sizeable number of saturated cells. One of these matrices (taken at  $t = 29$  to 30 seconds) is shown as an example in Table 24 with saturated cells indicated by asterisks. These four scanner plots could not be numerically reduced with any accuracy and were discarded from the final data.

The scanner data just presented were treated additionally to obtain further displays that can be used for the verification of analytical predictions and for direct comparisons against the airborne turbojet plume data format. These corresponding displays are presented in the Appendix. The first displays show radiant intensity versus axial distance along the plume (also known as station radiation). The second displays present a compact two-dimensional display of plume geometry, with radiant intensity shown as a quasi-gray level. The third displays give a three-dimensional format with length, width, and radiant intensity projected on the three axes. The latter display format is presently used to present all BASES (Beam Approach Seeker Evaluation System) airborne data.

## SECTION IV

### COMPARISON AGAINST ANALYTIC PREDICTIONS

A variety of models were previously used to calculate plume infrared properties from propellant and engine design parameters (References 7 and 8). Emissions from hot CO<sub>2</sub>, H<sub>2</sub>O, CO and, in one case, particulates, were calculated over a band of infrared wavelengths between 1 and 8 micrometers, ignoring atmospheric absorption.

Briefly, the first prediction calculations (Reference 9) used a chemical equilibrium program called Isp, followed by the Dynamic Sciences Generalized Kinetics Program (GKP) (Reference 10). The output was fed into a Low Altitude Plume Program (LAPP) (Reference 11) as well as a Naval Weapons Center/Brigham Young University plume model (Reference 12). The plumes predicted by these codes were then used as the basis for plume IR predictions for the HAST engine using two different gaseous radiation band models. These were a code developed to predict radiant base heating from the plume of NASA's Saturn IV rocket (Reference 13) and one developed by the Army Missile Command to predict plume IR signatures of jet aircraft engines (Reference 14).

The first set of predictions were all made for an O/F ratio of 3.2 and cruise mode for a number of altitude/flight velocity conditions. A valid comparison can be made between the predictions for sea level static ambient conditions and the radiometric, spatial, and spectral measurement data for the unaugmented engine operating at an O/F of 3.1 in the sustain phase.

#### References

7. W. J. Rothschild, Analysis of the HAST Rocket Exhaust Plume Infrared and Radar Characteristics, AFRPL-TR-73-16, Edwards Air Force Base, California, May 1973.
8. J. W. Fisher, High Altitude Supersonic Target (HAST) Exhaust Plume Analysis, AFATL-TR-71-154, Eglin Air Force Base, Florida, December 1971.
9. R. Hall and C. Selph, United States Air Force Rocket Propulsion Laboratory's Theoretical Isp Program, Revised February 1971.
10. D. E. Coates, H. M. Frey, and G. R. Nickerson, Generalized Kinetic Analysis Program, Dynamic Science, Irvine, California, June 1971.
11. R. R. Mikatarian and H. S. Pergament, Aerochem Axisymmetric Mixing with Non-equilibrium Chemistry Computer Program, AFRPL-TR-69-167, June 1969.
12. P. O. Hedman, J. M. Simonsen, and L. D. Smooth, Development and Evaluation of a Flight Attenuation Model, NWC-TP-5048, November 1971.
13. M. Dash and R. M. Huffaker, A General Program for the Calculation of Radiation from an Inhomogeneous, Nonisobaric, Nonisothermal Rocket Exhaust Plume, NASA TM-X53-622, June 1967.
14. H. T. Jackson, An Analytical Model for Predicting the Radiation from Jet Plumes, Army Missile Command, RE-TR-70-7, April 1970.

Table 25 compares two of the predicted variations of total radiant intensity (in the nominal 4- to 5-micrometer band) with aspect angle with the measured data. The radiometric predictions compare within a factor of 2 with the worst error occurring in the extrapolated calculation. There is no discernible trend to the calculations; they are neither consistently high nor consistently low.

The predicted plume spatial radiation distributions are in the form of isothermal contours as shown in Figure 22. It is thus possible only to compare approximate plume lengths and widths; it is not possible to make station radiation comparisons. The predicted plume boundary (600 degrees Kelvin contour) is 47 feet long by 2.4 feet in diameter. Even if the plume boundary is assumed to be at a higher temperature (1000 degrees Kelvin), the calculations predict a plume of 22 feet long by 0.75 foot in diameter. The actual plume is considerably shorter (about 8 feet at an O/F = 3.1 in sustain phase with an absolute measured maximum of 12 feet even in boost phase) and somewhat wider (about 2.6 feet) in both sustain and boost. Some of the discrepancy may be due to flow separation within the nozzle that is believed to occur during sustain mode at sea level. However, the predictions differ from the boost data at an O/F of 3.2 where separation is not a problem, and where the flow rates are higher. There is thus some question as to the validity of more detailed spatial distribution calculations that could be made based on these predictions.

The spectrum between 1 and 8 micrometers predicted for the HAST engine at sea level static conditions for a 30-degree aspect angle is shown in Figure 23. These calculations ignored the contribution of emission by particulates and thus this spectrum differs significantly from any of the measured spectra. Abundant graybody radiation is emitted by the HAST propellant at any flow rate over a fairly wide range of O/F ratios including the one at which the predictions were performed. This is evident from all the spectra presented in this report and also from Figure 24 which shows a measured spectrum for this type of fuel and particulate-rich exhaust carried forward to 14 micrometers.

Another prediction of the HAST infrared signature was also previously made (Reference 8), this time with graybody radiation included in the calculations. In this instance the signature was calculated at sea level in boost phase at an O/F believed to be 3.5.

This prediction is based on an equilibrium thermochemical program developed at Naval Weapons Center (Reference 15) which was input to an equilibrium method of

---

#### Reference

15. H. N. Browne, D. R. Cruise, and M. M. Williams, The Theoretical Computation of Equilibrium Compositions, Thermodynamic Properties and Performance Characteristics of Propellant Systems, NAVWEPS Report No. 7043, June 1960.

characteristics (Reference 16) and an equilibrium mixing (Reference 17) program. The results of the plume flow-field analyses were finally used to predict spectral radiant intensity distributions using the computer solution described in Reference 13.

The radiometric comparison of the data is shown in Table 26. The predicted radiation at 30 degrees aspect angle is off by a factor of 2; otherwise, there is reasonable agreement. It is again, however, misleading to compare single radiometric values to see if valid plume predictions have been made.

Spatial estimates in this instance are limited to a prediction of a maximum plume diameter of about 11 inches, and the determination that the first Mach disc would occur at about 9.9 inches with a shock at about 17.5 inches. This prediction is shown in Figure 25. The prediction of plume boundary does not agree with the measured diameter of about 29 inches. The Mach discs and shocks at sea level do not show up in infrared or visible imagery at discrete locations but tend to run into each other creating a luminous core, as shown in the thermalscanner displays in Section III and in the Appendix. The prediction of a precise location for only the first Mach disc and the first shock, therefore, is of little practical value and almost impossible to verify.

The last prediction at sea level is of spectral distribution. Spectral radiant intensity distributions were predicted for two bands, 1.8 to 2.5 and 4.0 to 5.6 micrometers (as shown in Figures 26 and 27) for the 90-degree aspect angle. These data show more graybody radiation than do the first set of predictions. However, the beginning of the H<sub>2</sub>O and CO<sub>2</sub> band emissions in the 2.2 to 2.5-micrometer region is much too high and the prediction of graybody radiation increasing at wavelengths beyond 5 micrometers is wrong; graybody radiation monotonically decreases beyond 5 micrometers.

Taking also into account the gap in the predictions between 2.5 and 4.0 micrometers can only lead to the inevitable conclusion that these predictions are unsatisfactory. The method of characteristics prediction technique is really only useful for very high altitude (well above 100,000 feet) rocket engines exhausts where there is a large distance between shocks, and the length of the plume to the first Mach disc and shock is of interest. Its use for sea level or even low altitude plume prediction is questionable.

#### References

16. M. W. Garbrick, Analysis of an Inviscid Exhaust Plume, Martin Marietta Corporation Report No. OR 9171, December 1967.
17. M. W. Dowdy, et. al., Missile Exhaust Plume and Shock Layer Studies, Martin Marietta Corporation Report No. OR 10,338, December 1969.

The lack of agreement between predictions and measurements at static altitude has also been previously reported for a kerosene/oxygen rocket engine (Reference 18). Causes for some of the discrepancies have been suggested in this reference. The HAST engine case points up another major deficiency in the codes used: incorrect predictions of graybody radiation emission. This point was not evident in the case of the simple kerosene/oxygen engine exhaust which primarily emitted molecular radiation.

---

Reference

18. D. B. Ebeoglu and C. W. Martin, Experimental Verification of Infrared Plume Predictions for a Rocket Engine, AFATL-TR-74-191, Eglin Air Force Base, Florida, November 1974.

## SECTION V

### CONCLUSIONS AND RECOMMENDATIONS

#### 1. CONCLUSIONS

A detailed discussion of the conclusions reached from the infrared measurements and analysis performed on the subscale and full-scale HAST engines accompany the data presented in Sections III and IV. Following is a summary of these conclusions:

- (1) The subscale engine provides a valid spatial and spectral infrared simulation of the exhaust plume of the full-scale HAST.
- (2) The full-scale infrared plume performance can be linearly extrapolated from the subscale data.
- (3) Co-flowing streams of air or nitrogen provide more valid ambient conditions for testing the effectiveness of augmentation techniques than do static sea level conditions.
- (4) Oxygen injection produces about a 50 percent increase in radiant intensity with a Mach 0.5 nitrogen ambient at an O/F less than 3.0 at less than 6 percent primary flow rate.
- (5) Methane injection produces about a 50 percent increase in radiant intensity with a Mach 0.5 air ambient at an O/F greater than 3.0 at less than 6 percent primary flow rate.
- (6) Atlantic Research Corporation POPS device produces approximately the same performance as methane.
- (7) Multi-point (or preferably annular) secondary injection is required to achieve the augmentation cited. One-point and even two-point injections do not give consistent or satisfactory results.
- (8) The analytic predictions of the HAST infrared performance made to date are not valid.
- (9) A problem of flow separation exists when the full-scale engine is operated in sustain mode at static sea level conditions.

## 2. RECOMMENDATIONS

On the basis of the data presented in previous sections and the conclusions reached from them, the following recommendations were made immediately after the measurements:

- (1) Perform remaining infrared augmentation experimentation on the subscale engine with co-flowing air or nitrogen streams; do not perform any further static tests.
- (2) Determine the capability of bi-propellant injection (simultaneous injection of gaseous fuel and oxidizer) to increase secondary combustion.
- (3) Determine the capability of high temperature fuel injection to increase secondary combustion.
- (4) Determine the capability of hydrogen injection to increase the energy level of emission from the exhaust plume.
- (5) Determine the capability of CO<sub>2</sub> injection (as CO plus O<sub>2</sub> bi-propellant) on augmenting CO<sub>2</sub> radiation.
- (6) Increase the ratio of secondary to primary propellant flow rate for all techniques to determine optimum augmentation, i.e., beyond the 3 to 6 percent originally proposed for fuel or oxidizer injection.
- (7) Determine the capabilities of IRFNA as well as O<sub>2</sub> injection (in order to make use of on-board oxidizer and thus reduce HAST payload).
- (8) Establish a verified analytic prediction capability in line with previous recommendations (References 1, 18).

Most of the steps recommended above were performed between February and May 1975. The results of these experiments are reported in the CSD report (Reference 4). In summary the data show that:

- (1) Bi-propellant injection [high temperature methyl acetylene-propadiene (MAPP) gas and oxygen as well as methane and oxygen] produces 300 to 600 percent augmentation with Mach 0.5 airflow.
- (2) Hydrogen injection gives quite similar performance.
- (3) These performances are achieved for approximately 20 percent secondary to primary ratio of flow rates. Augmentation does not increase appreciably

at higher secondary flow rates; augmentation is reduced at lower secondary flow rates to about the monopropellant performance at 3 to 6 percent secondary to primary ratios.

- (4) Increasing monopropellant injection flow rates does not increase augmentation measurably.
- (5) High temperature fuel (MAPP) injection by itself gives about the same augmentation performance as methane.
- (6) MAPP/oxygen injection produces approximately twice as much augmentation as methane/oxygen.
- (7) CO<sub>2</sub> injection does not give appreciable augmentation.
- (8) IRFNA injection decreases the infrared radiant intensity as does any liquid fuel or oxidizer injection tested to date.

The bi-propellant and hydrogen injection results show the feasibility of producing significant augmentation by maximizing secondary combustion in the plume. Augmentation improves by an order of magnitude in a non-afterburning environment indicating that the same performance can be sustained during flight. Bi-propellant injection can therefore be considered a possible major breakthrough in infrared augmentation technology.

It is thus finally recommended that the technique be evaluated on a subscale HAST engine in an environment simulating flight altitude as well as air velocity. It is also recommended that the applicability of the technique to augment other primary propellants and engines be investigated. The feasibility of the concept of augmenting through secondary combustion has been shown. The technique of bi-propellant injection should be exploited for as many other target systems as possible.

## LIST OF REFERENCES

1. Report of the Plume Emissions Panel, Advisory Committee to the Air Force Systems Command, National Academy of Sciences, June 1973.
2. D. B. Ebeoglu, Fundamental Parameters Affecting Plume Infrared Radiation, AFATL-TR-74-84, Eglin Air Force Base, Florida, April 1974.
3. C. W. Martin, R. F. Askew, and D. B. Ebeoglu, Operation of an Infrared Thermal Scanner for Plume Measurements, AFATL-TR-74-204, Eglin Air Force Base, Florida, December 1974.
4. A. L. Holzman and R. A. Jones, High Altitude Supersonic Target (HAST) Infrared Augmentation, AFATL-TR-75-90, Eglin Air Force Base, Florida, July 1975.
5. D. B. Ebeoglu and C. W. Martin, Effect of Mixture Ratio on UV, Visible and Infrared Radiation for Exhaust Plumes, AFATL-TR-75-79, Eglin Air Force Base, Florida, May 1975.
6. D. B. Ebeoglu, The Infrared Signature of Pyrophorics, AFATL-TR-74-92, Eglin Air Force Base, Florida, May 1974.
7. W. L. Rothschild, Analysis of the HAST Rocket Exhaust Plume Infrared and Radar Characteristics, AFRPL-TR-73-16, Edwards Air Force Base, California, May 1973.
8. J. W. Fisher, High Altitude Supersonic Target (HAST) Exhaust Plume Analysis, AFATL-TR-71-154, Eglin Air Force Base, Florida, December 1971.
9. R. Hall and C. Selph, United States Air Force Rocket Propulsion Laboratory's Theoretical Isp Program, Revised February 1971.
10. D. E. Coates, H. M. Frey, and G. R. Nickerson, Generalized Kinetic Analysis Program, Dynamic Science, Irvine, California, June 1971.
11. R. R. Mikatarian and H. S. Pergament, Aerochem Axisymmetric Mixing and Non-equilibrium Chemistry Computer Program, AFRPL-TR-69-167, June 1969.
12. P. O. Hedman, J. M. Simonsen, and L. D. Smooth, Development and Evaluation of a Flight Attenuation Model, NWC-TP-5048, November 1971.
13. M. Dash and R. M. Huffaker, A General Program for the Calculation of Radiation from an Inhomogeneous, Nonisobaric, Nonisothermal Rocket Exhaust Plume, NASA-TM-X53-622, June 1967.
14. H. T. Jackson, An Analytical Model for Predicting the Radiation from Jet Plumes, Army Missile Command, RE-TR-70-7, April 1970.
15. H. N. Browne, D. R. Cruise, and M. M. Williams, The Theoretical Computation of Equilibrium Compositions, Thermodynamic Properties and Performance Characteristics of Propellant Systems, NAVWEPS Report No. 7043, June 1960.
16. M. W. Garbrick, Analysis of an Inviscid Exhaust Plume, Martin Marietta Corporation Report No. OR 9171, December 1967.
17. M. W. Dowdy, et. al., Missile Exhaust Plume and Shock Layer Studies, Martin Marietta Corporation Report No. OR 10,338, December 1969.
18. D. B. Ebeoglu and C. W. Martin, Experimental Verification of Infrared Plume Predictions for a Rocket Engine, AFATL-TR-74-191, Eglin Air Force Base, Florida, November 1974.

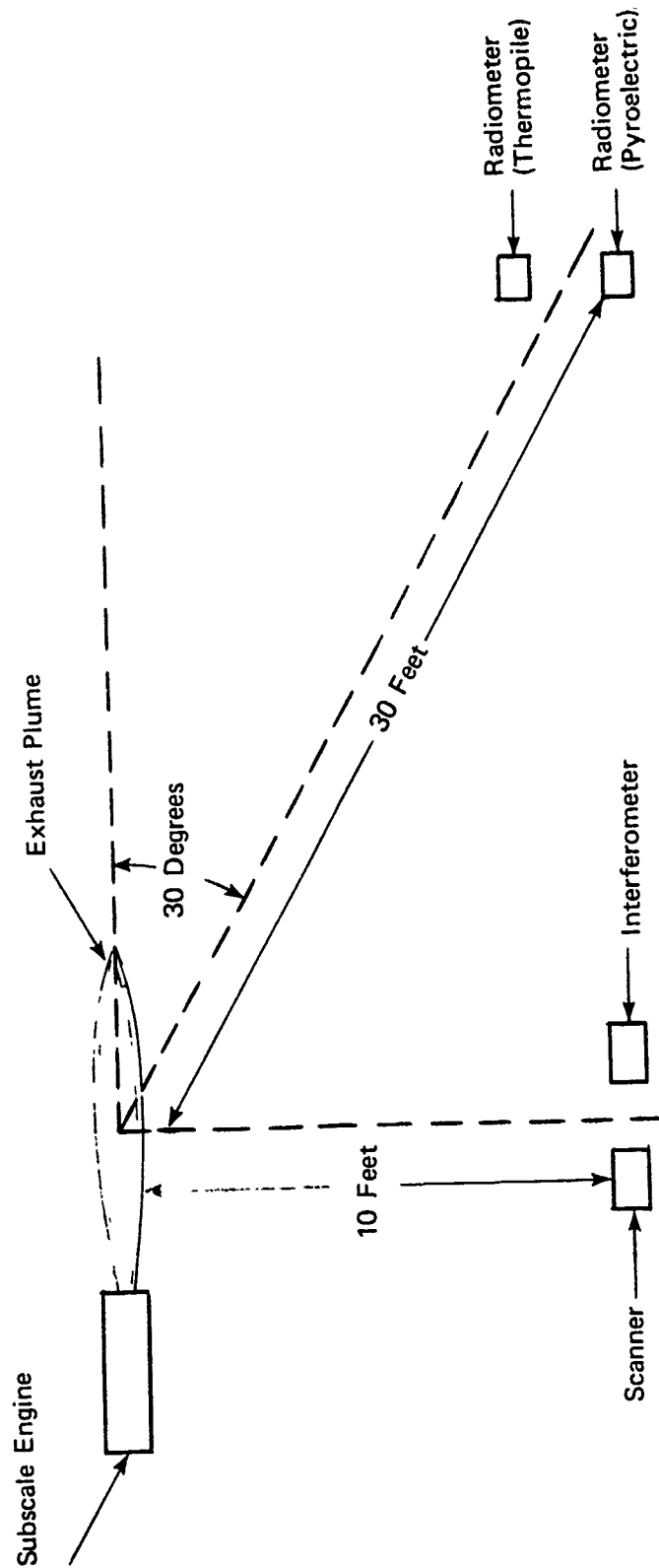


Figure 1. Subscale HAST Infrared Measurements Geometry

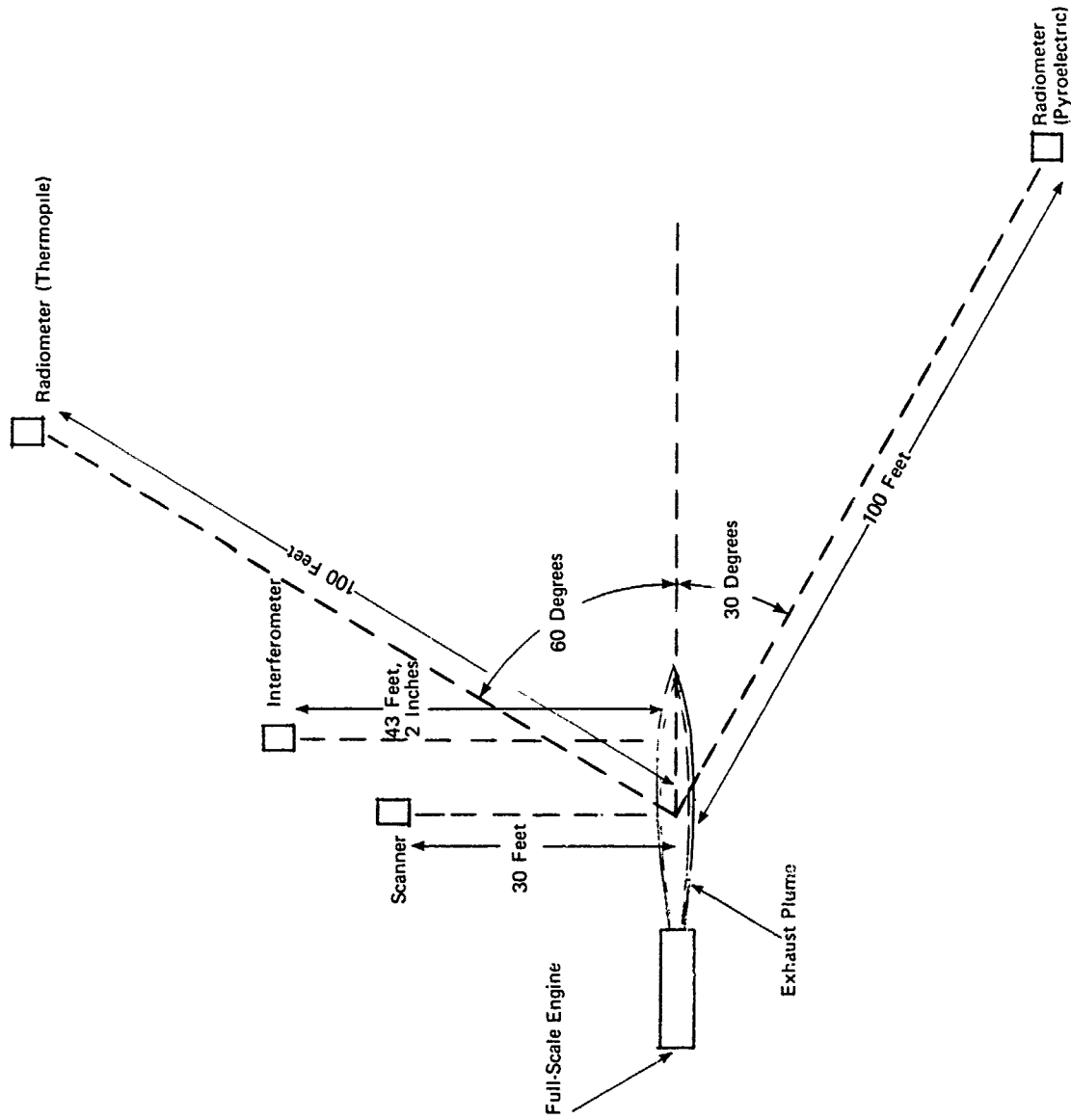


Figure 2. Full-Scale HAST Infrared Measurements Geometry

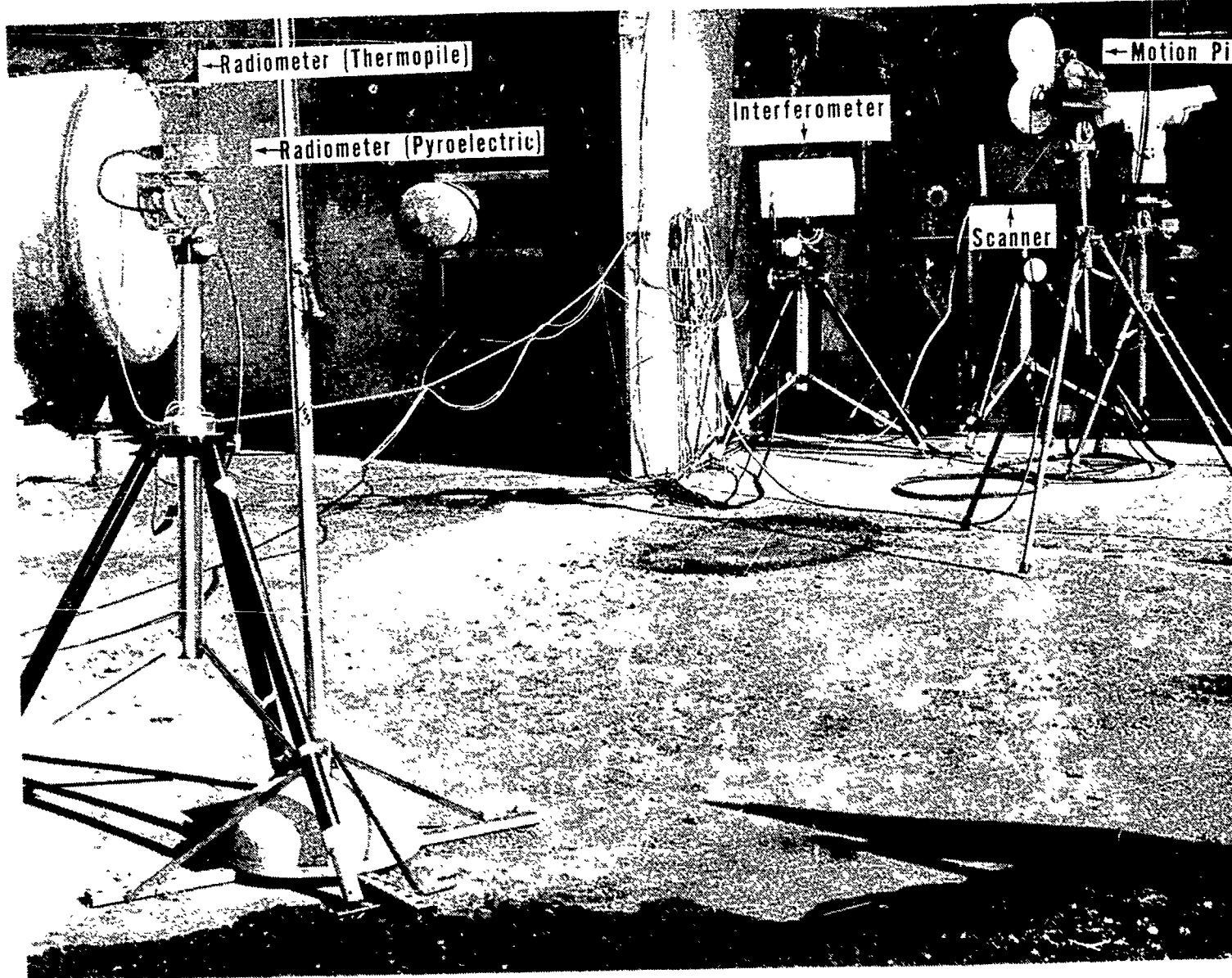


Figure 3.

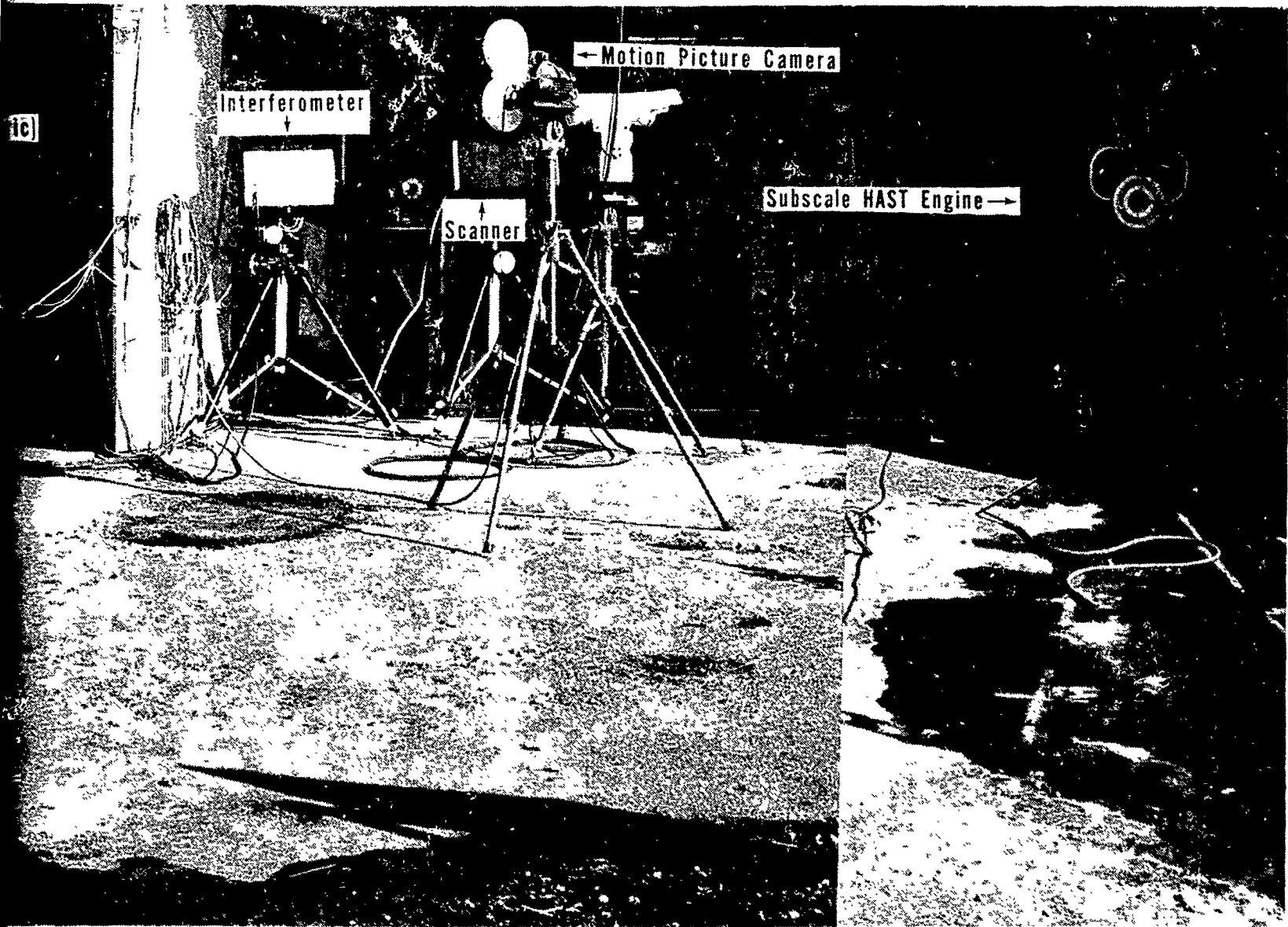


Figure 3. Subscale HAST Engine/Infrared Instrumentation Arrangement

2

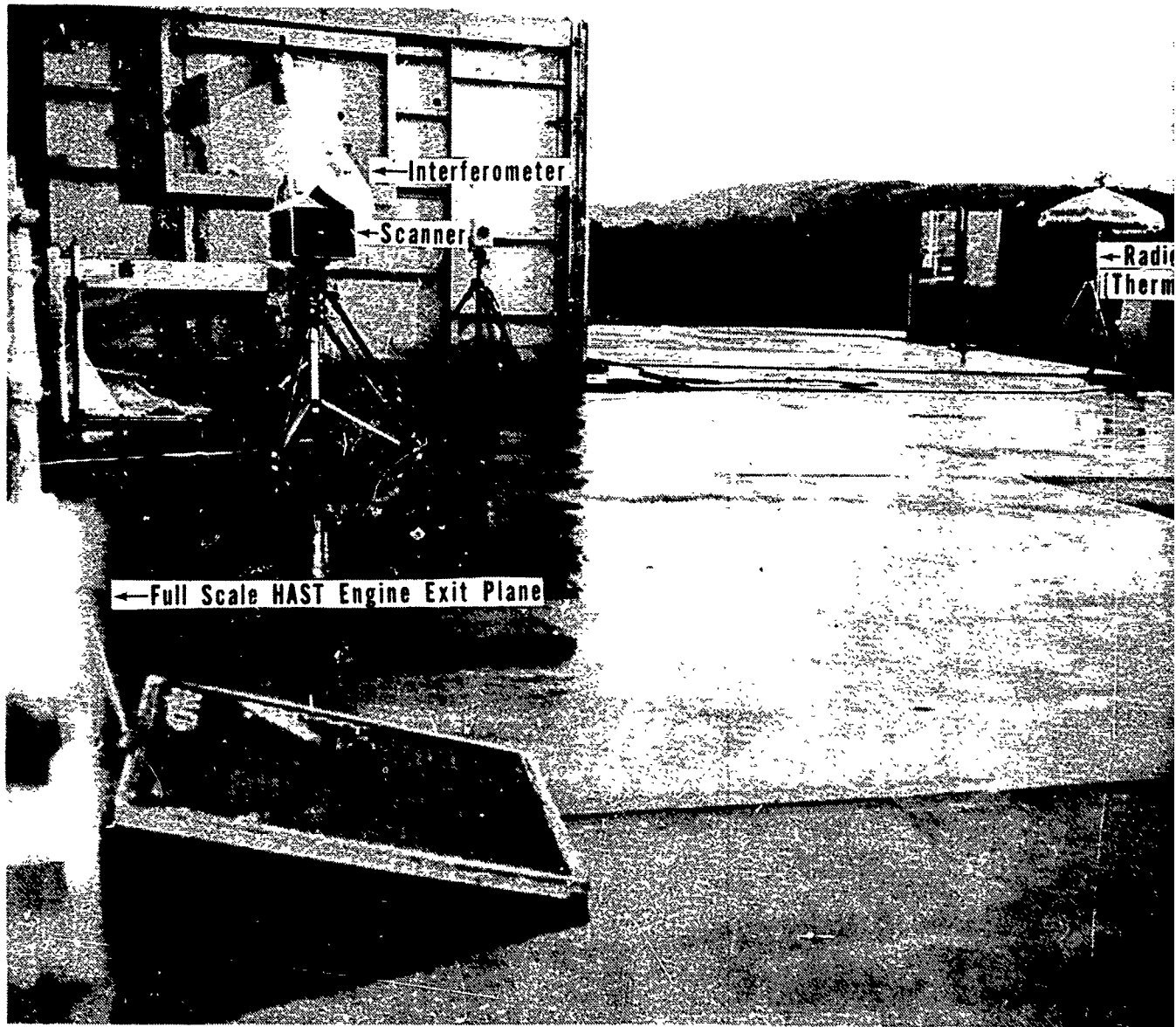


Figure 4. Full-Scale HAST Engine/Infrared

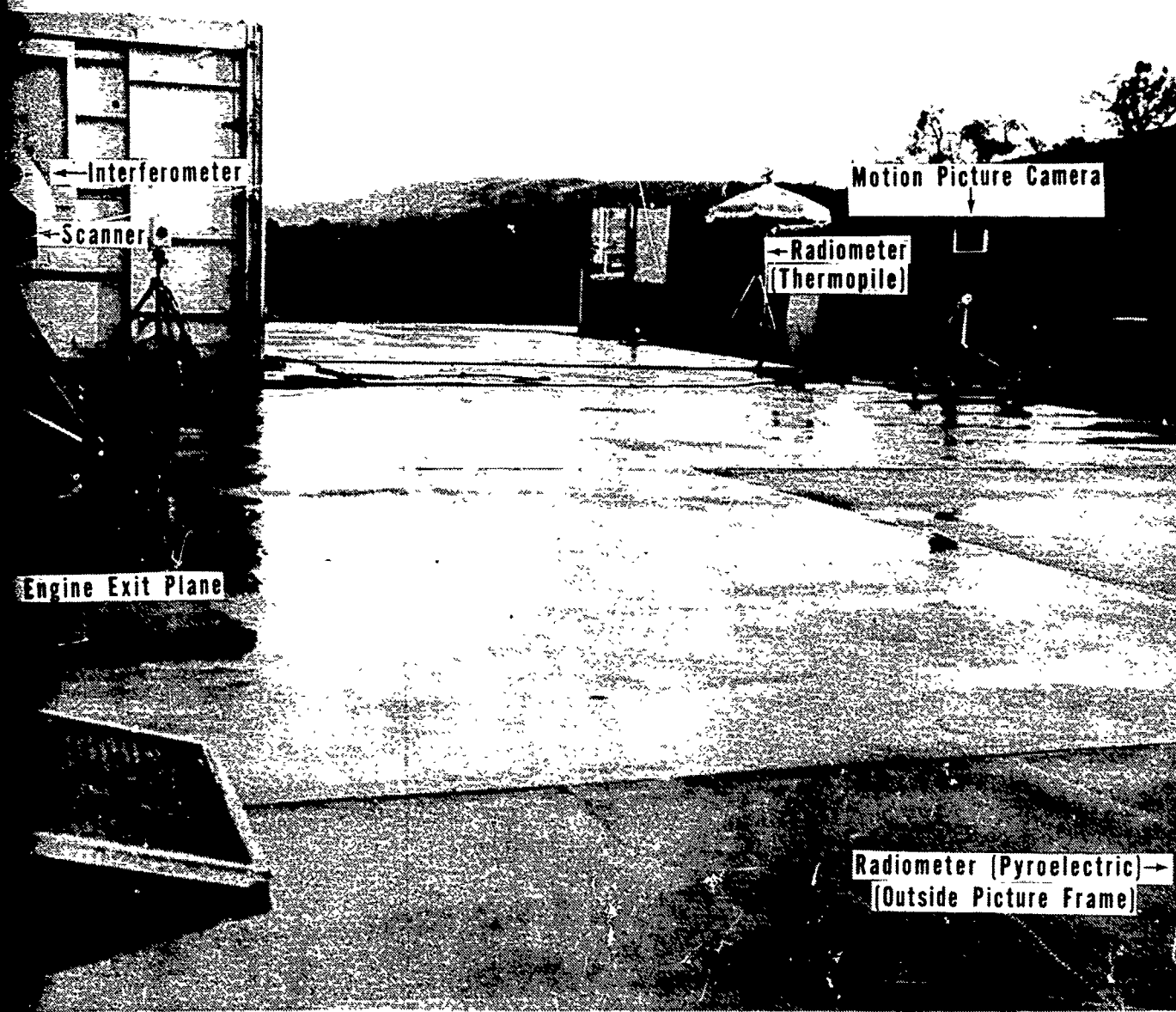
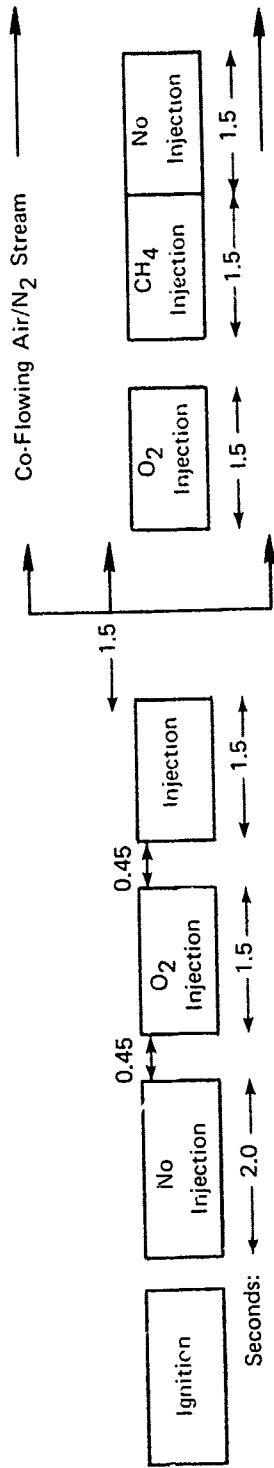
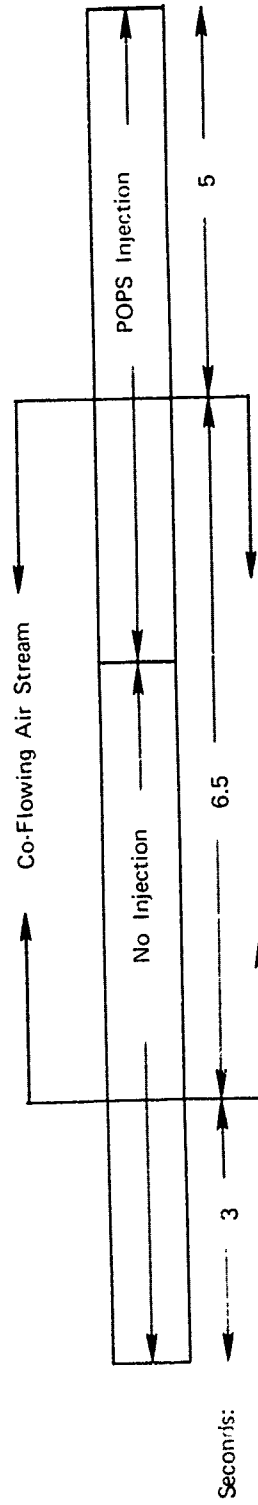


Figure 4. Full-Scale HAST Engine/Infrared Instrumentation Arrangement

7



(a) O<sub>2</sub>/CH<sub>4</sub> Injection



(b) POPS Injection

Figure 5. Time Sequences for Subscale HAST Engine Secondary Injection

5-102

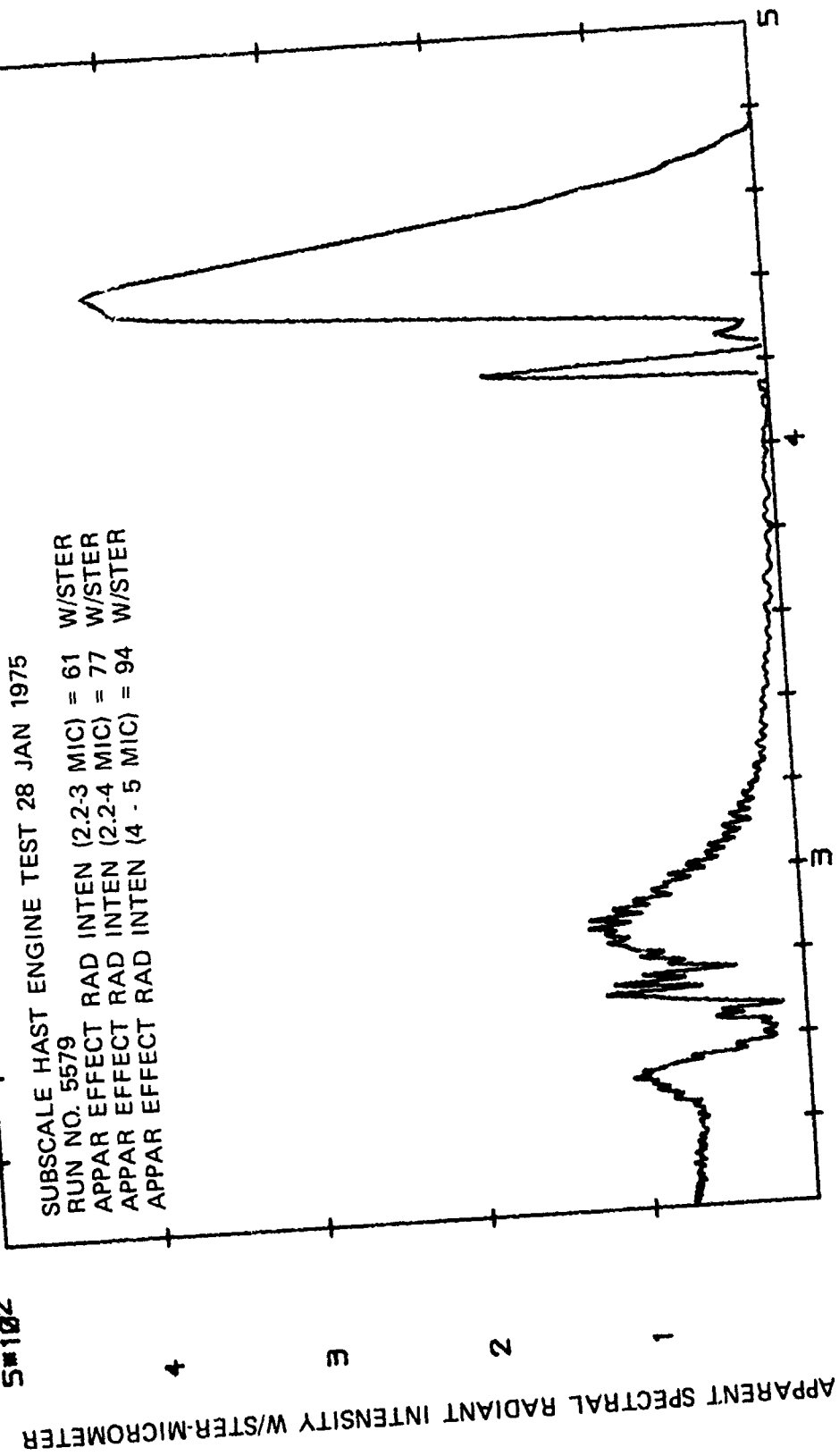


Figure 6. Subscale Engine Spectrum - No Injection, No Flow

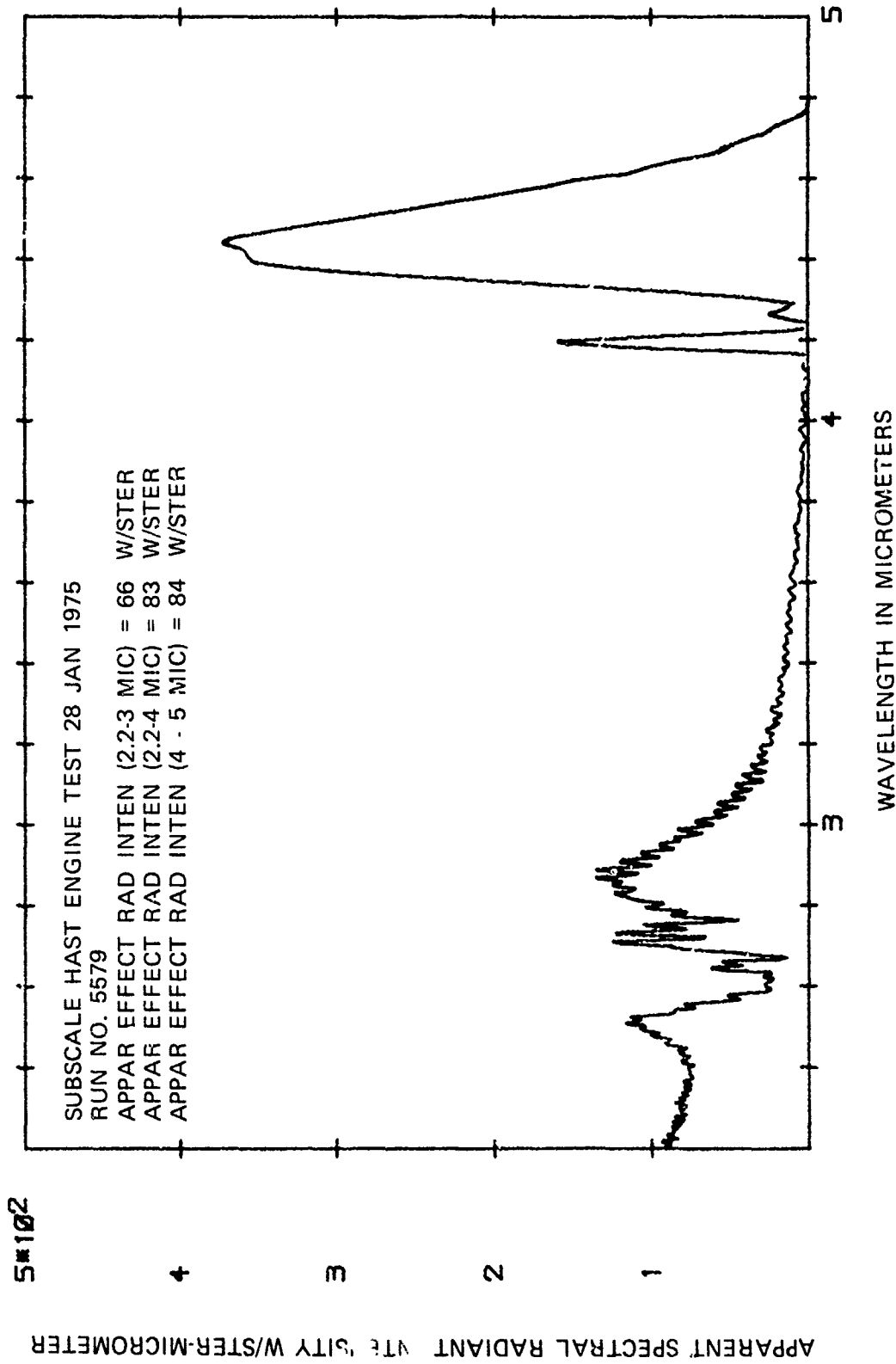


Figure 7. Subscale Engine Spectrum - O<sub>2</sub> Injection, No Flow

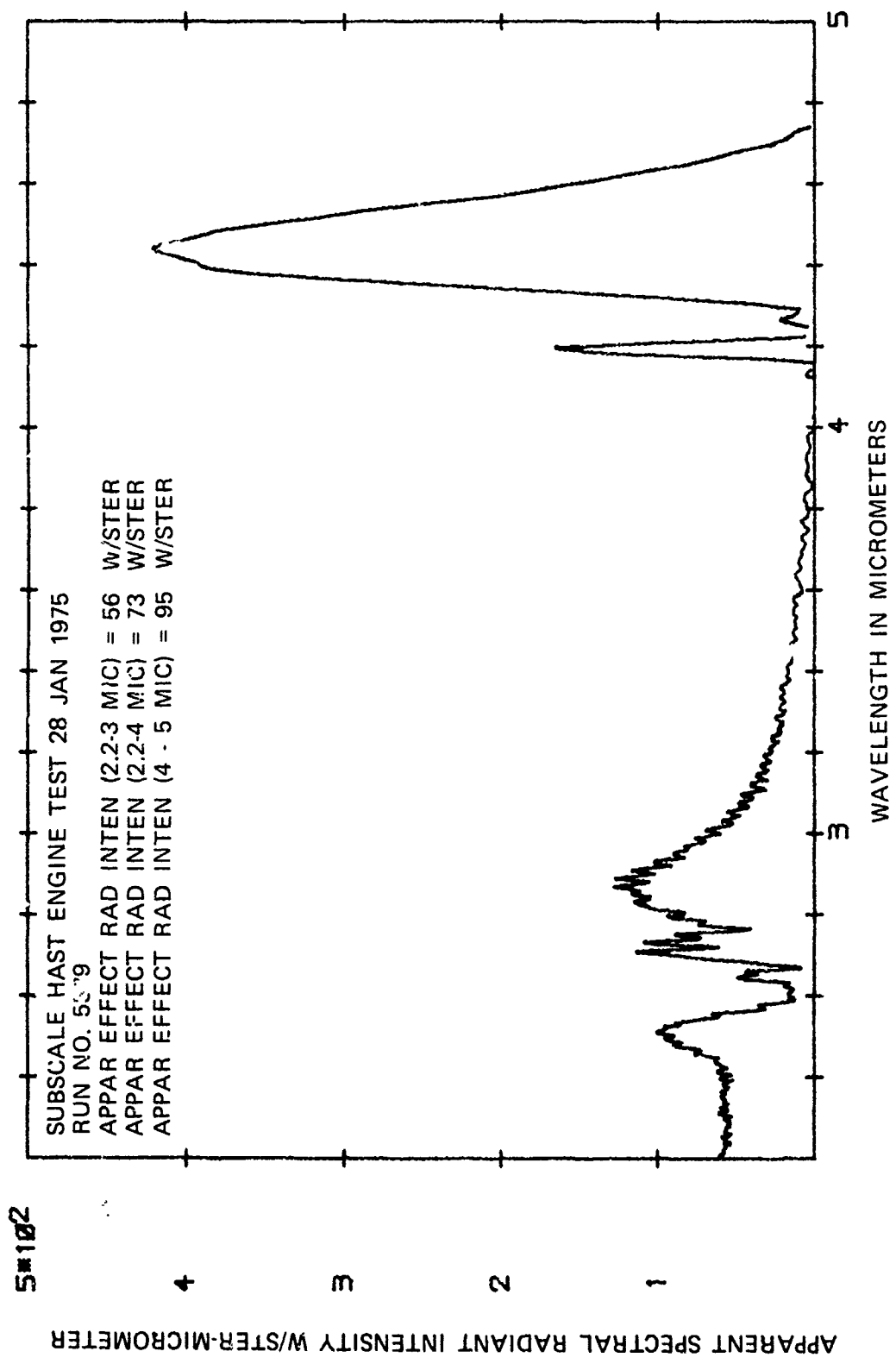


Figure 8. Subscale Engine Spectrum - CH<sub>4</sub> Injection, No Flow

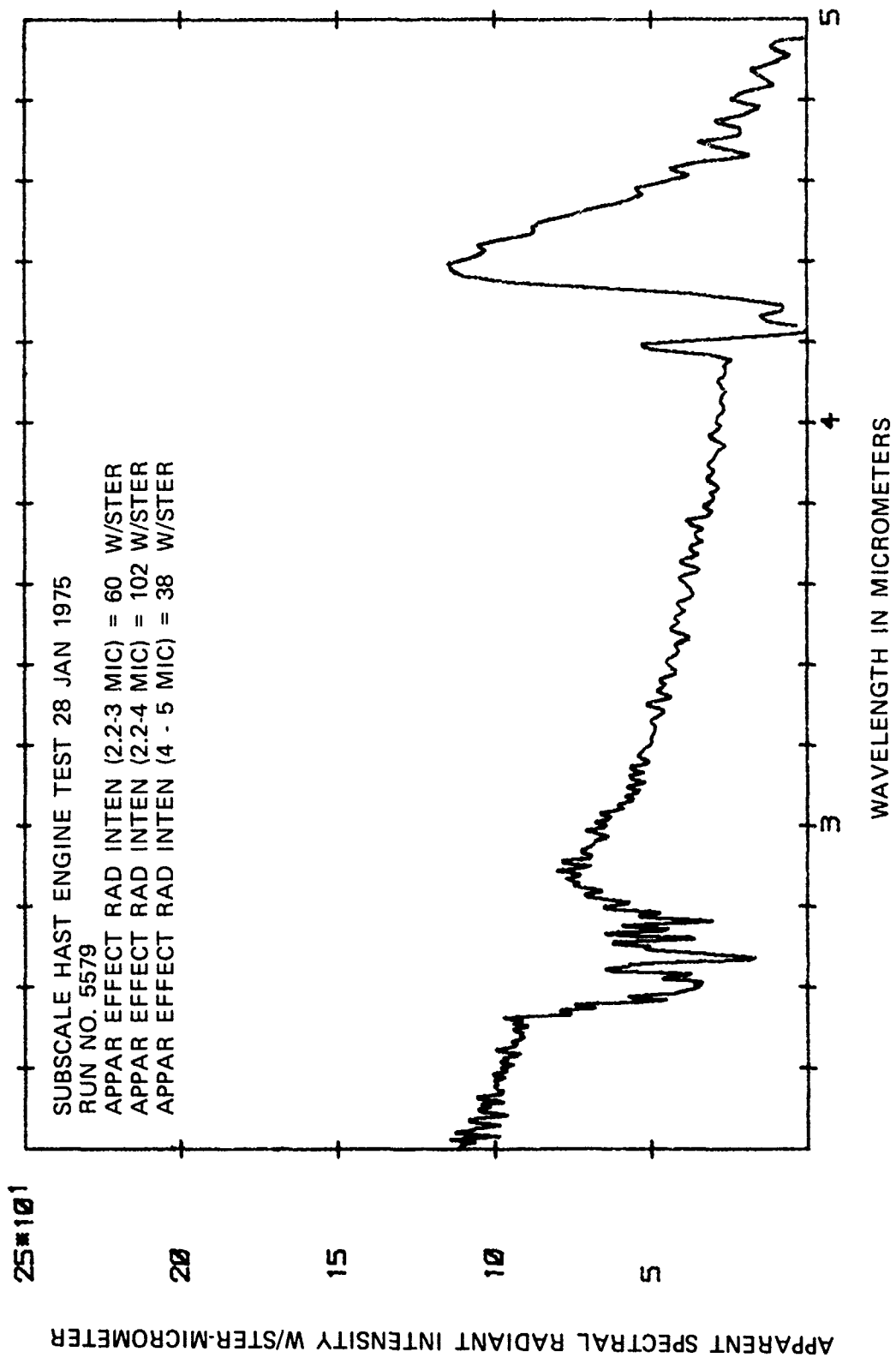


Figure 9. Subscale Engine Spectrum - O<sub>2</sub> Injection, Mach 0.3 N<sub>2</sub> Flow

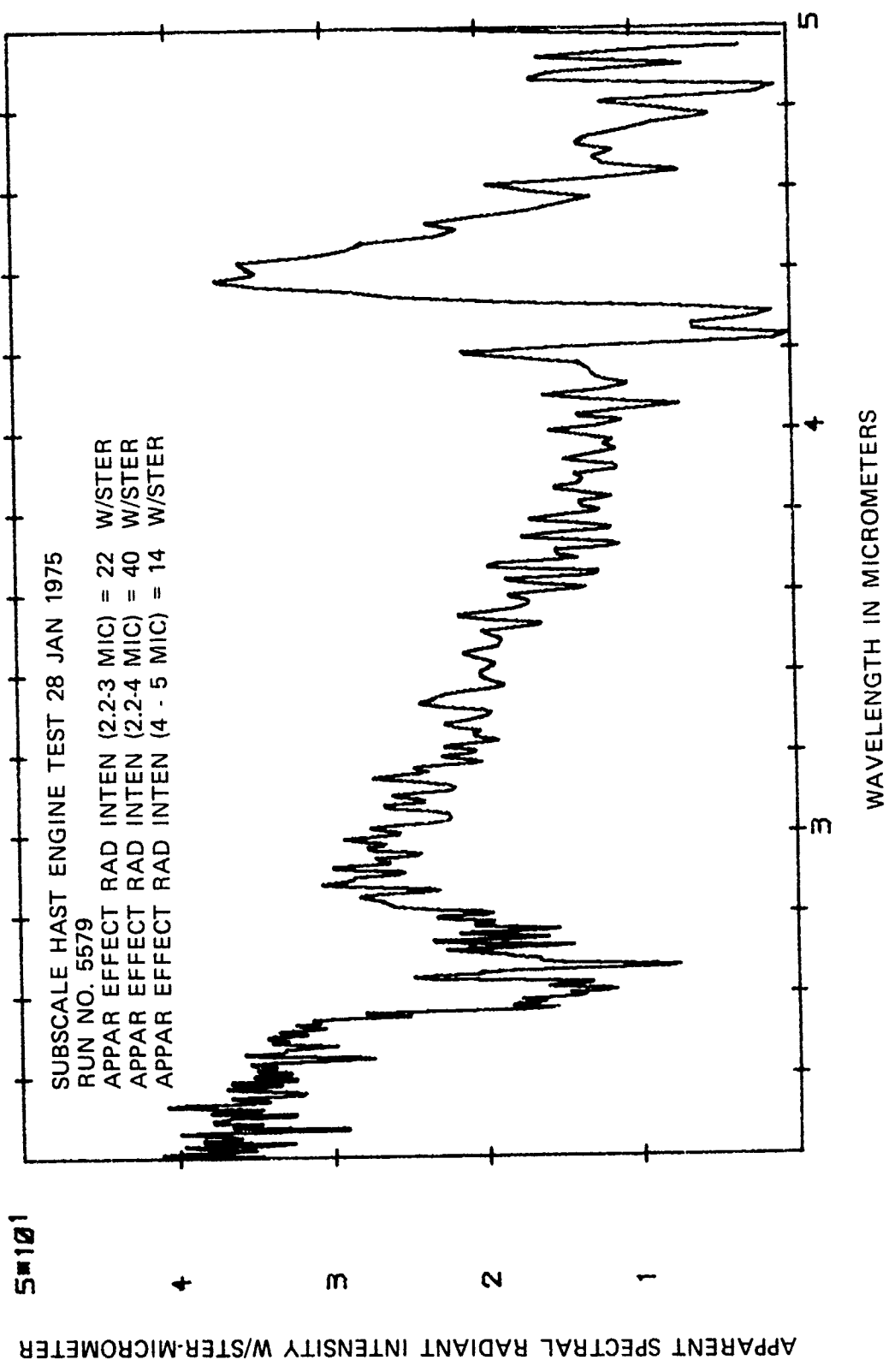


Figure 10. Subscale Engine Spectrum - CH<sub>4</sub> Injection, Mach 0.3 N<sub>2</sub> Flow

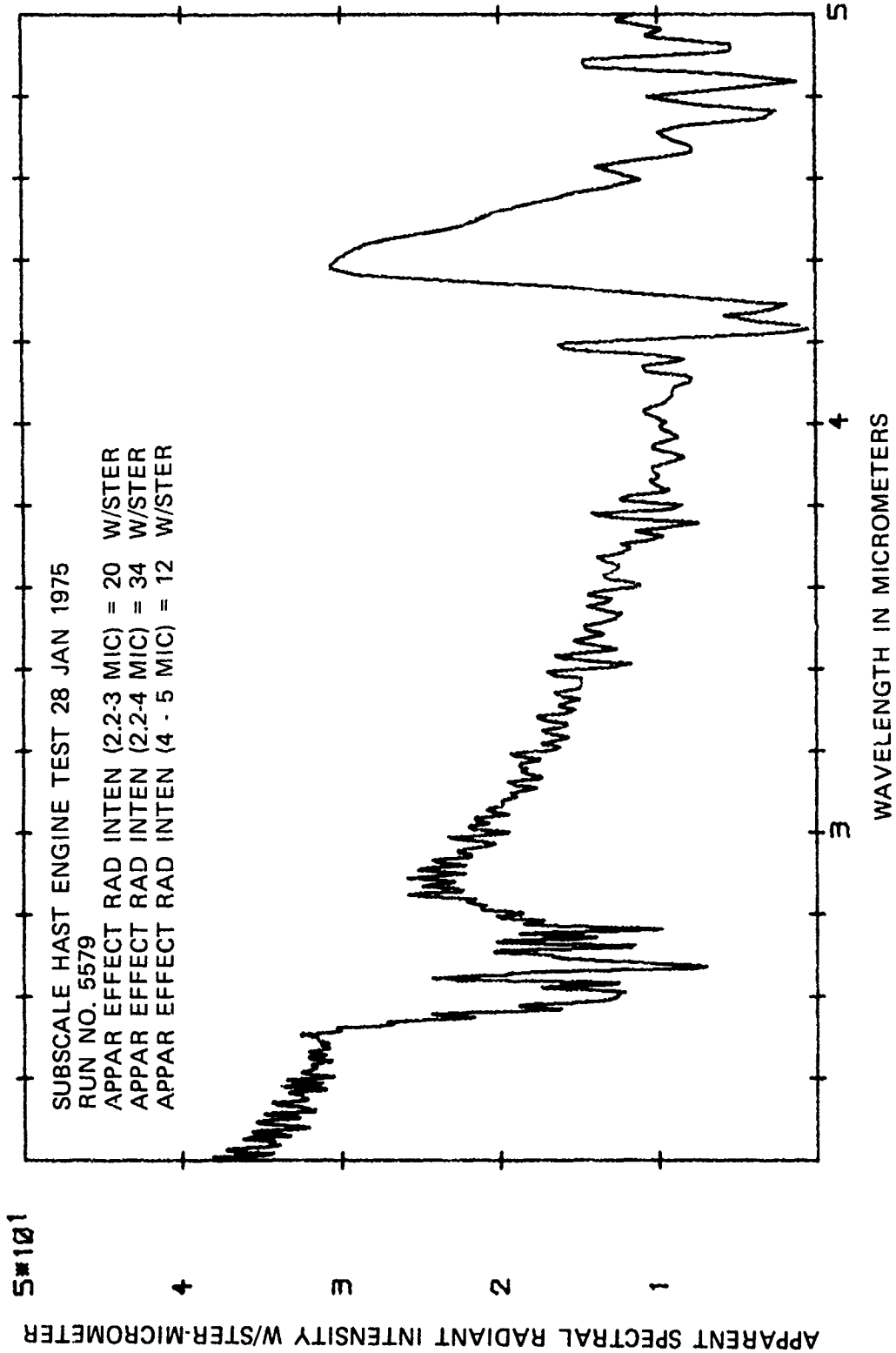


Figure 11. Subscale Engine Spectrum, No Injection, Mach 0.3 N<sub>2</sub> Flow

This document is the property of the Defense Research Agency, Ottawa, Ontario, Canada. It is loaned to you for your personal use only. It is not to be distributed outside your organization.

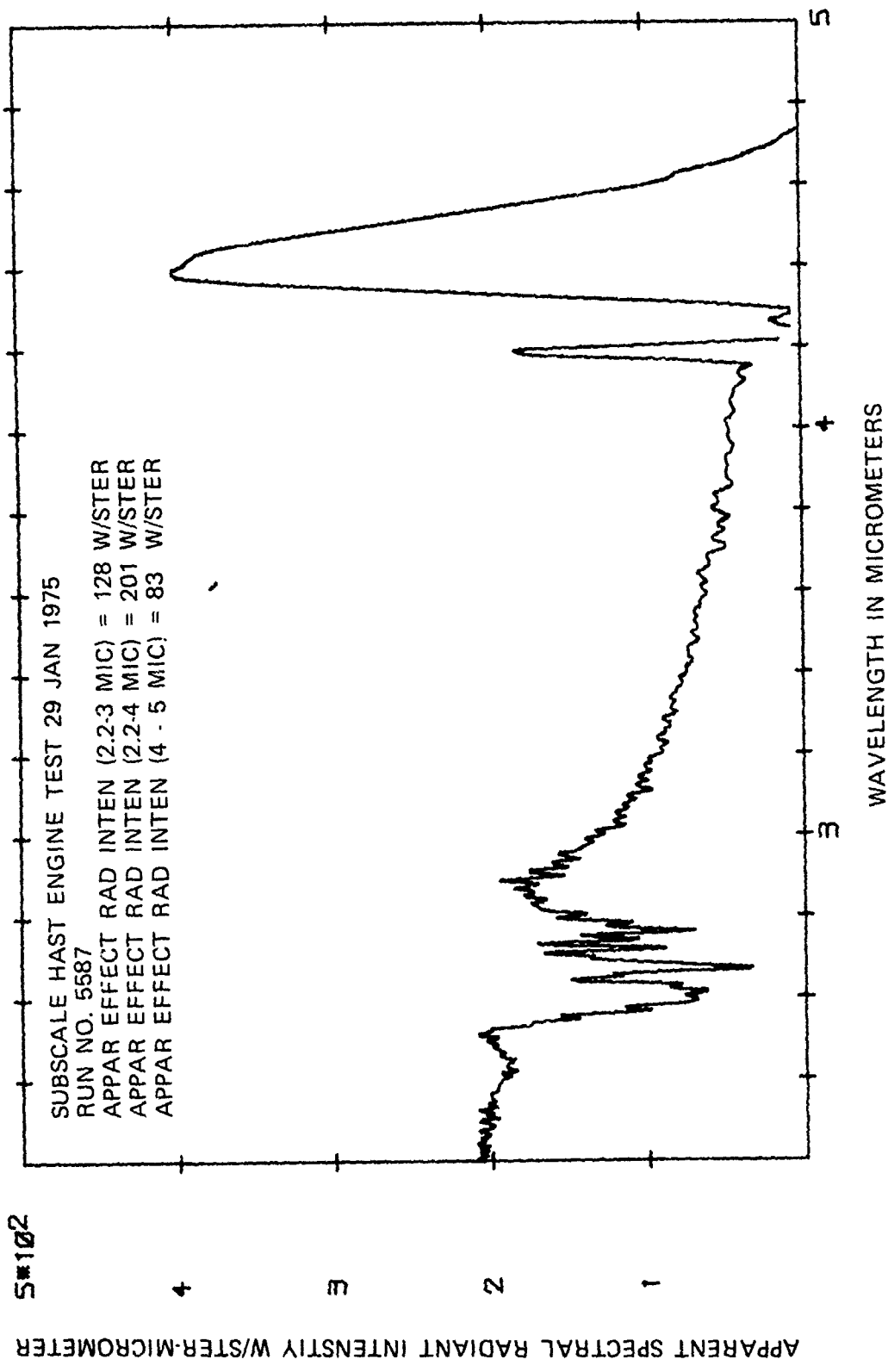


Figure 12. Subscale Engine Spectrum, No Injection, No Flow

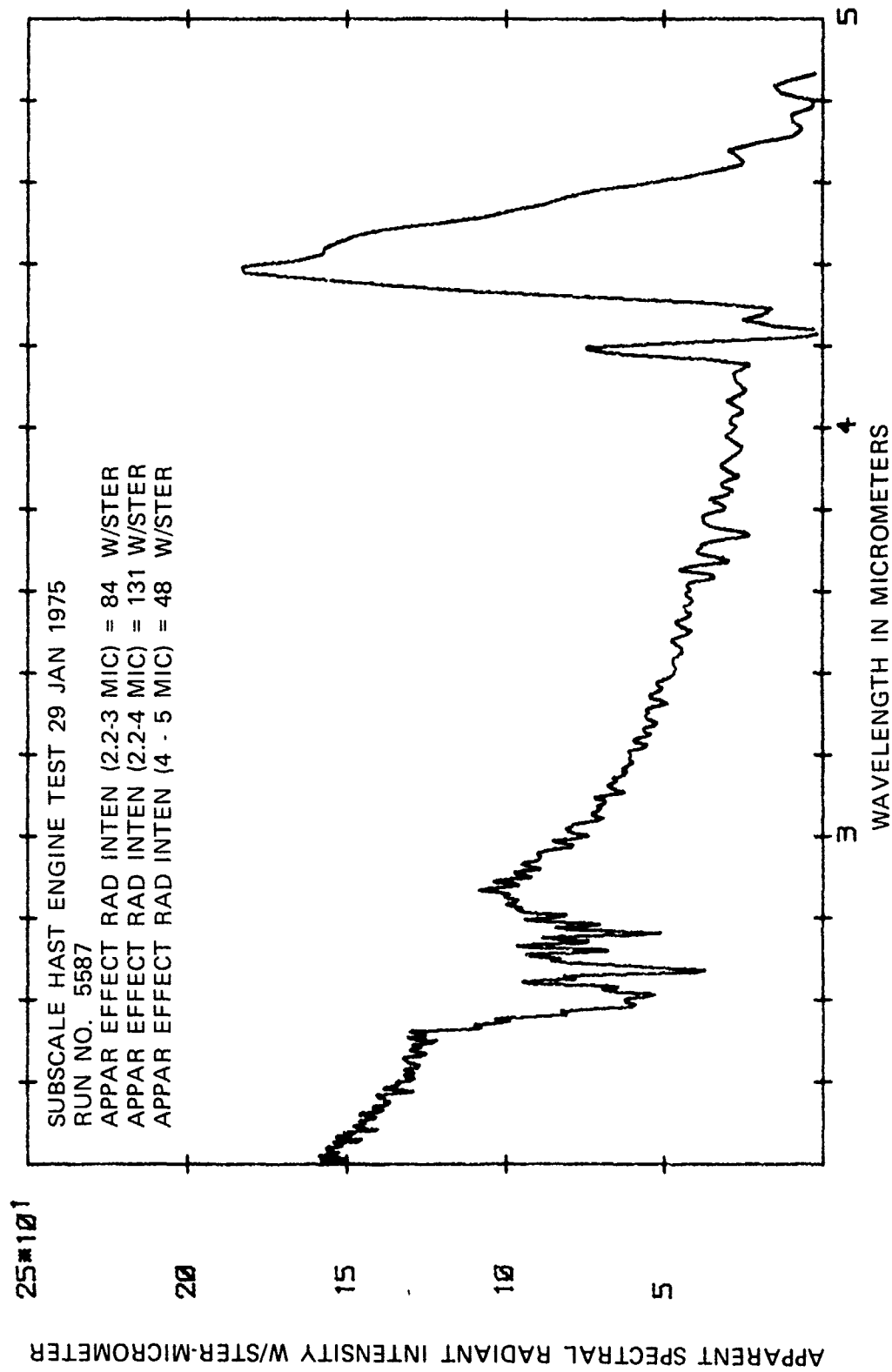


Figure 13. Subscale Engine Spectrum, No Injection, Mach 0.7 Airflow

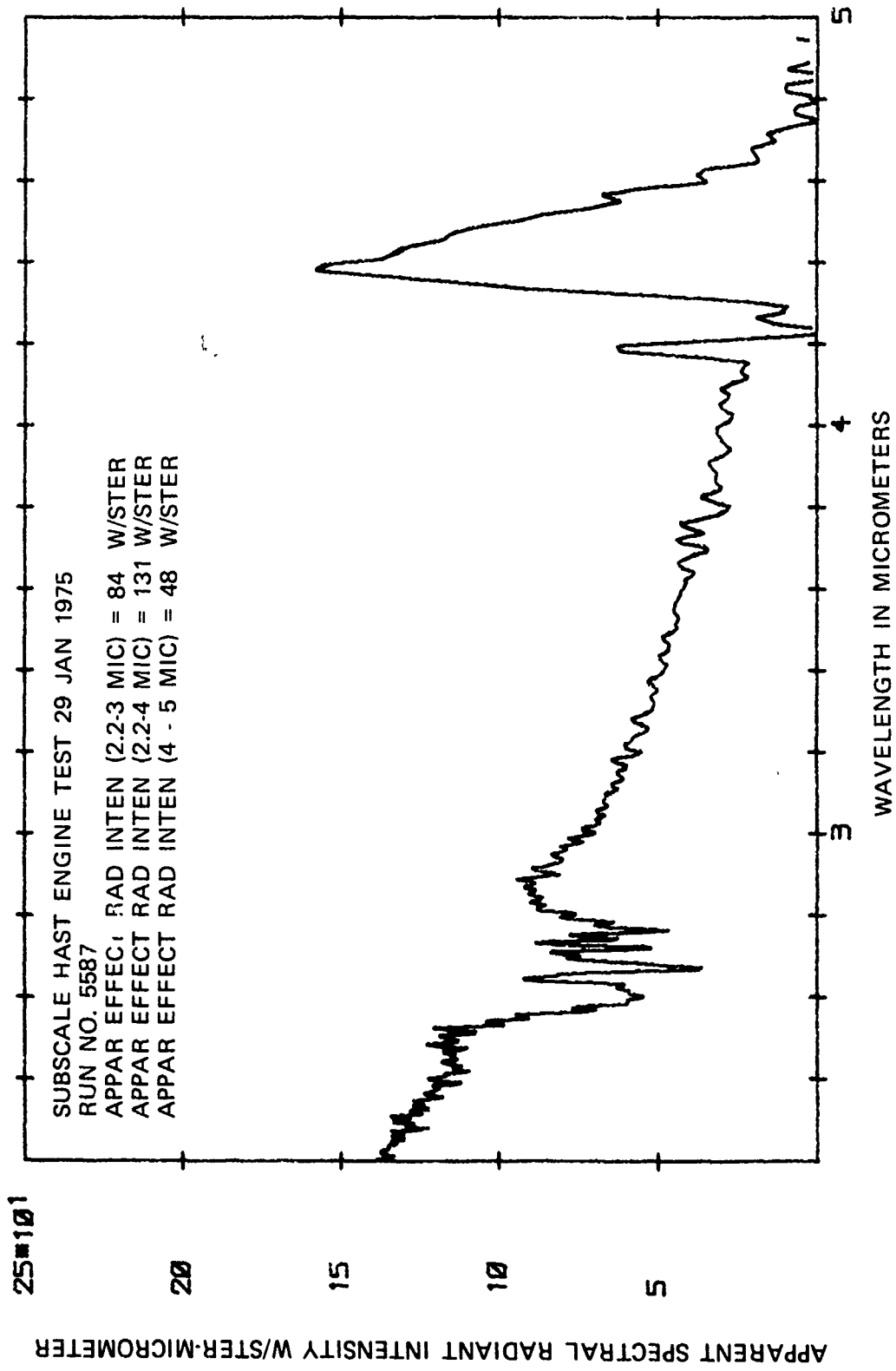


Figure 14. Subscale Engine Spectrum, POPS Injection, Mach 0.7 Airflow

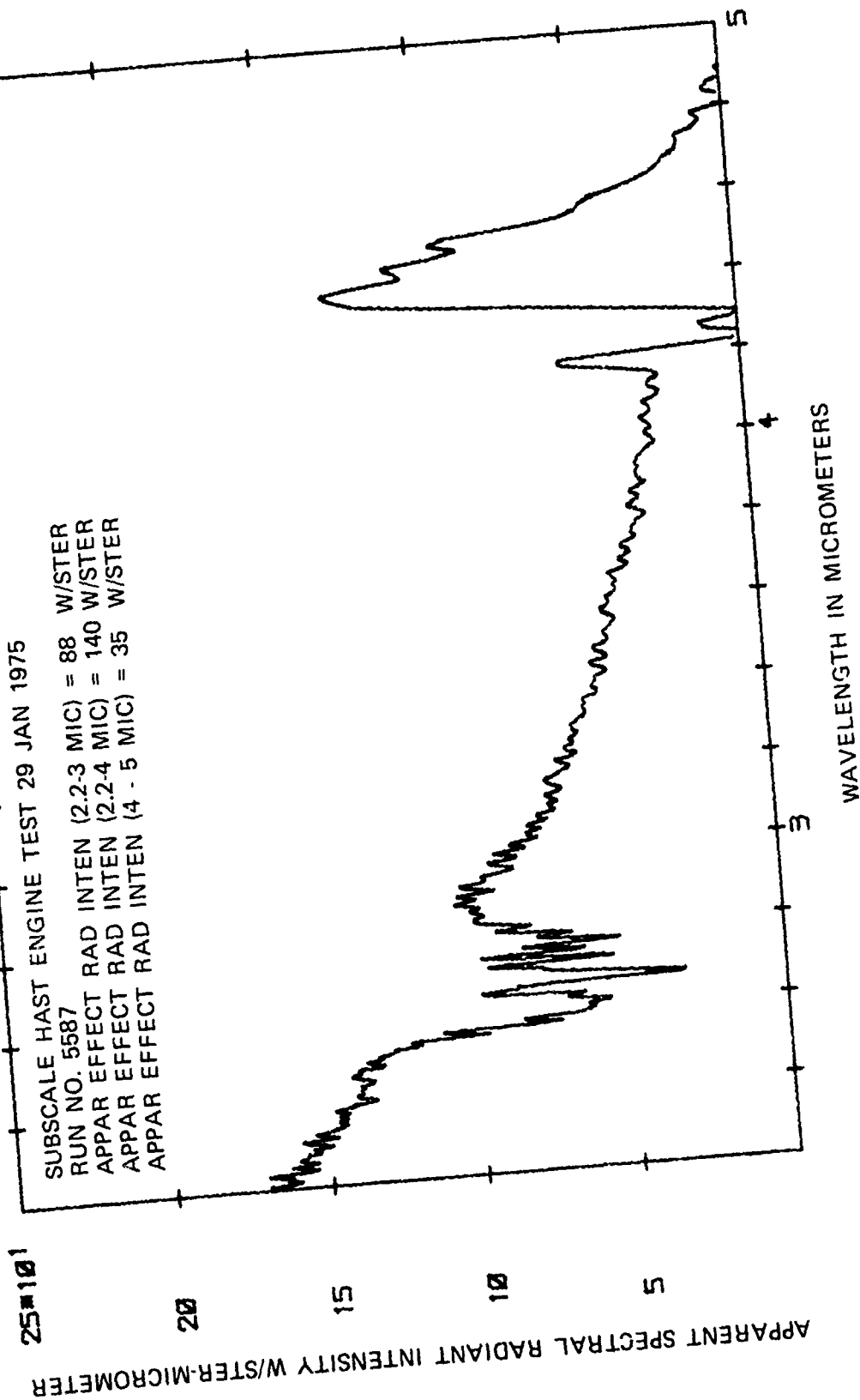


Figure 15. Subscale Engine Spectrum, POPS Injection, No Flow

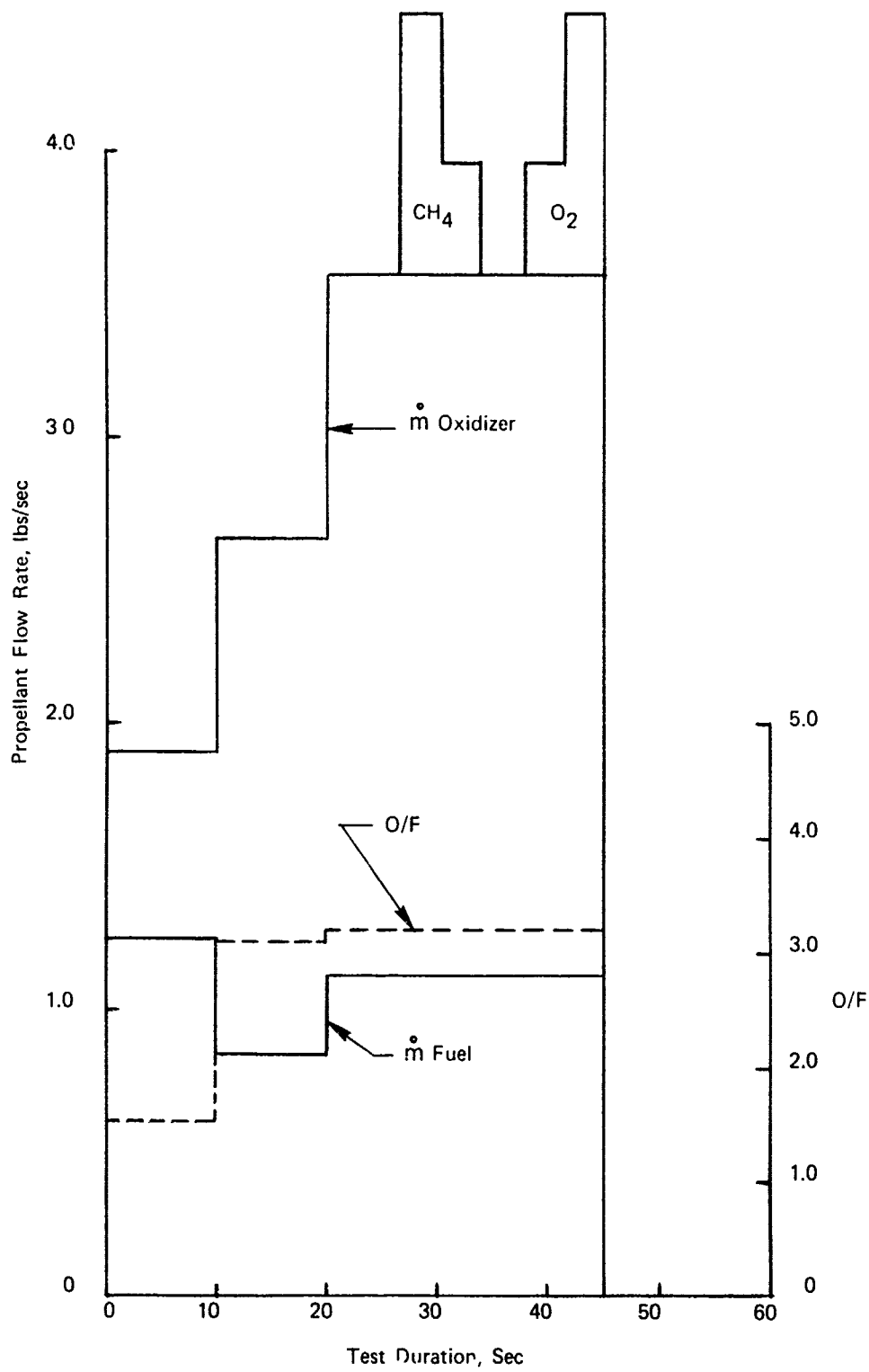


Figure 16. Full-Scale HAST Engine - Boost Phase Duty Cycle

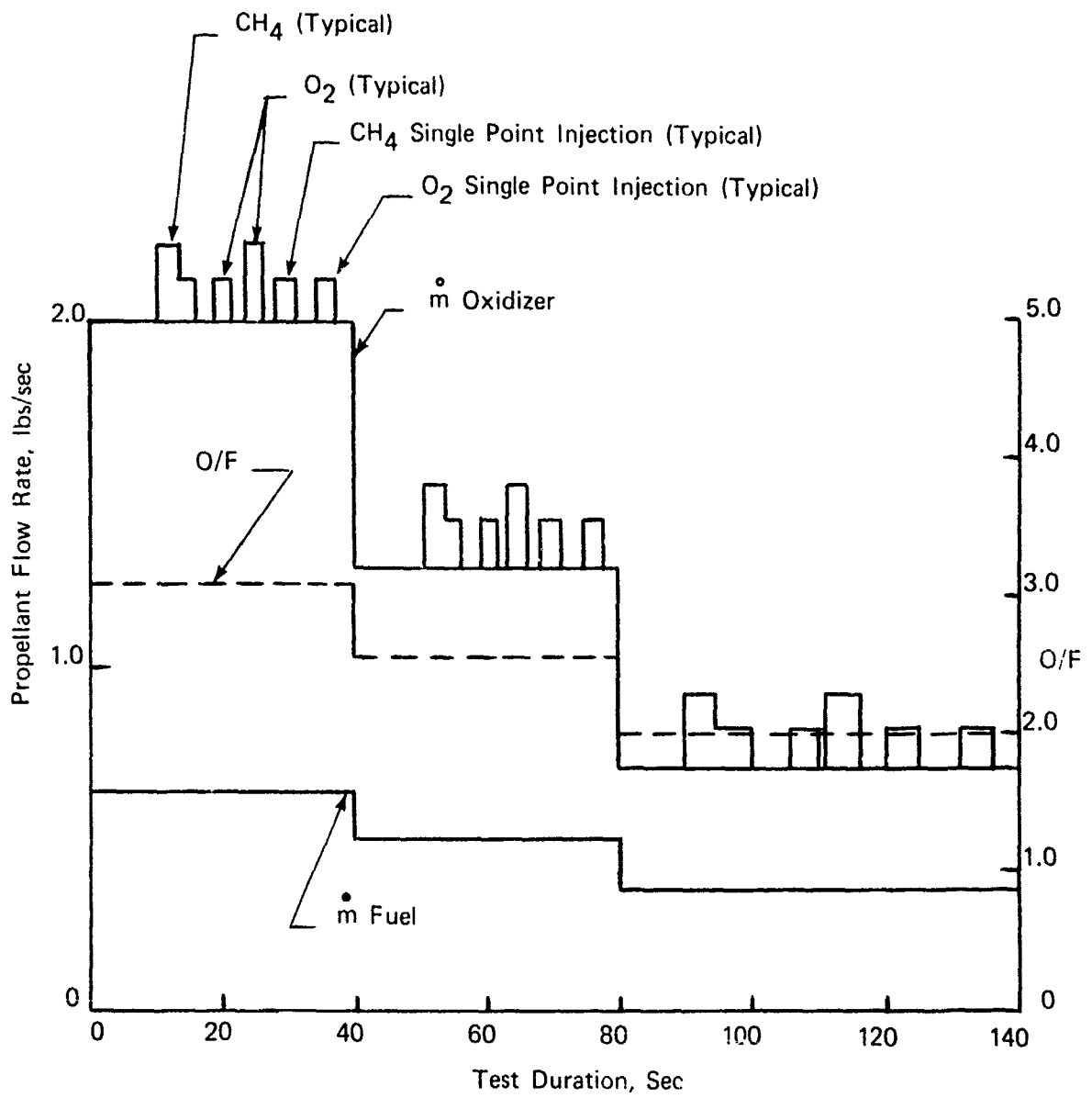


Figure 17. Full-Scale HAST Engine - Sustain Phase Duty Cycle

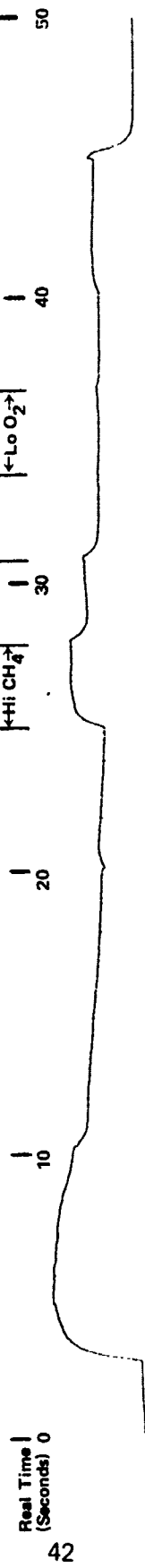


Figure 18. Full-Scale HAST Engine Boost Phase - J (4 to 5 Micrometers) Versus Time

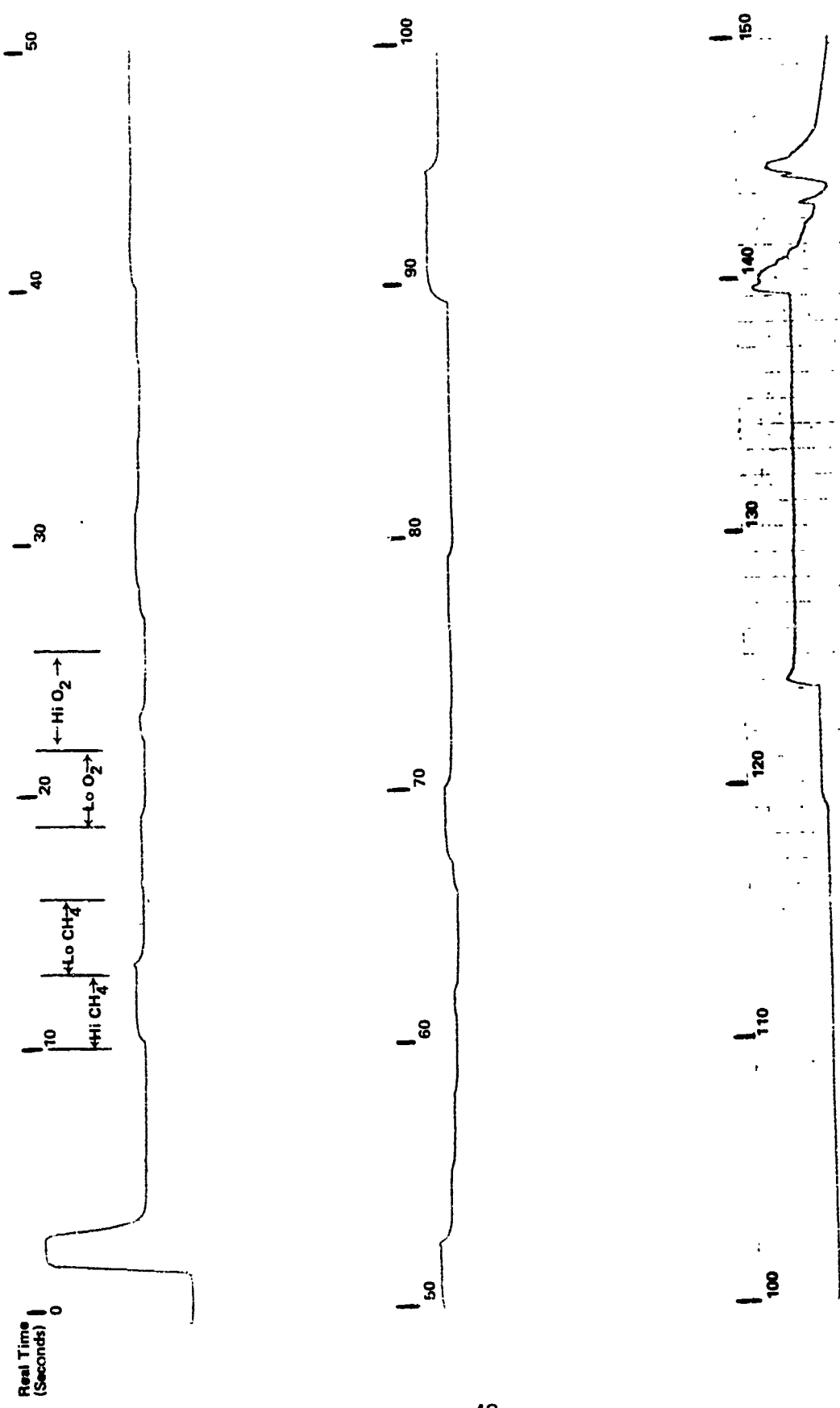


Figure 19. Full-Scale HAST Engine Sustain Phase - J (4 to 5 Micrometers) Versus Time

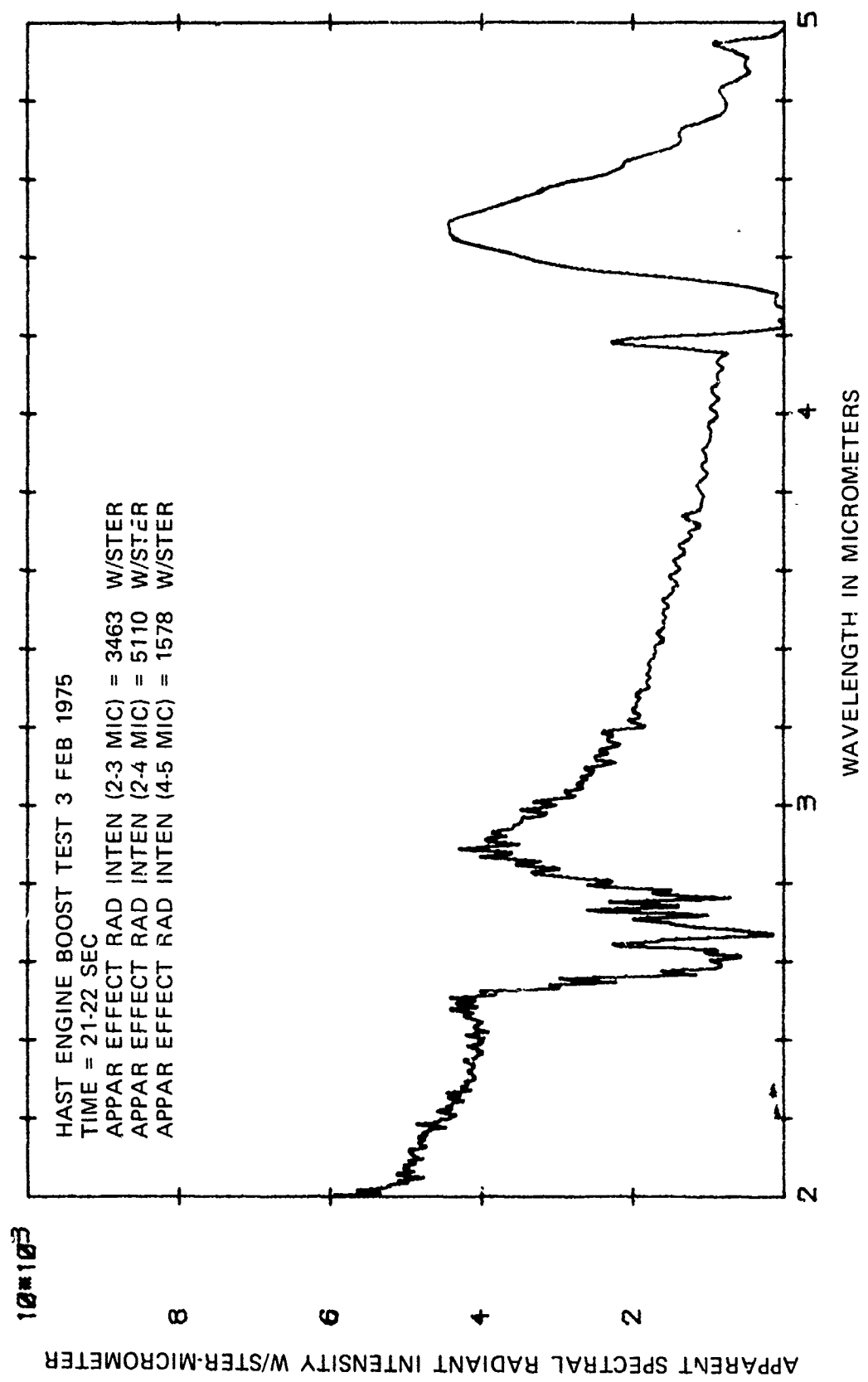


Figure 20. Full-Scale HAST Engine Boost Phase - Typical Spectrum

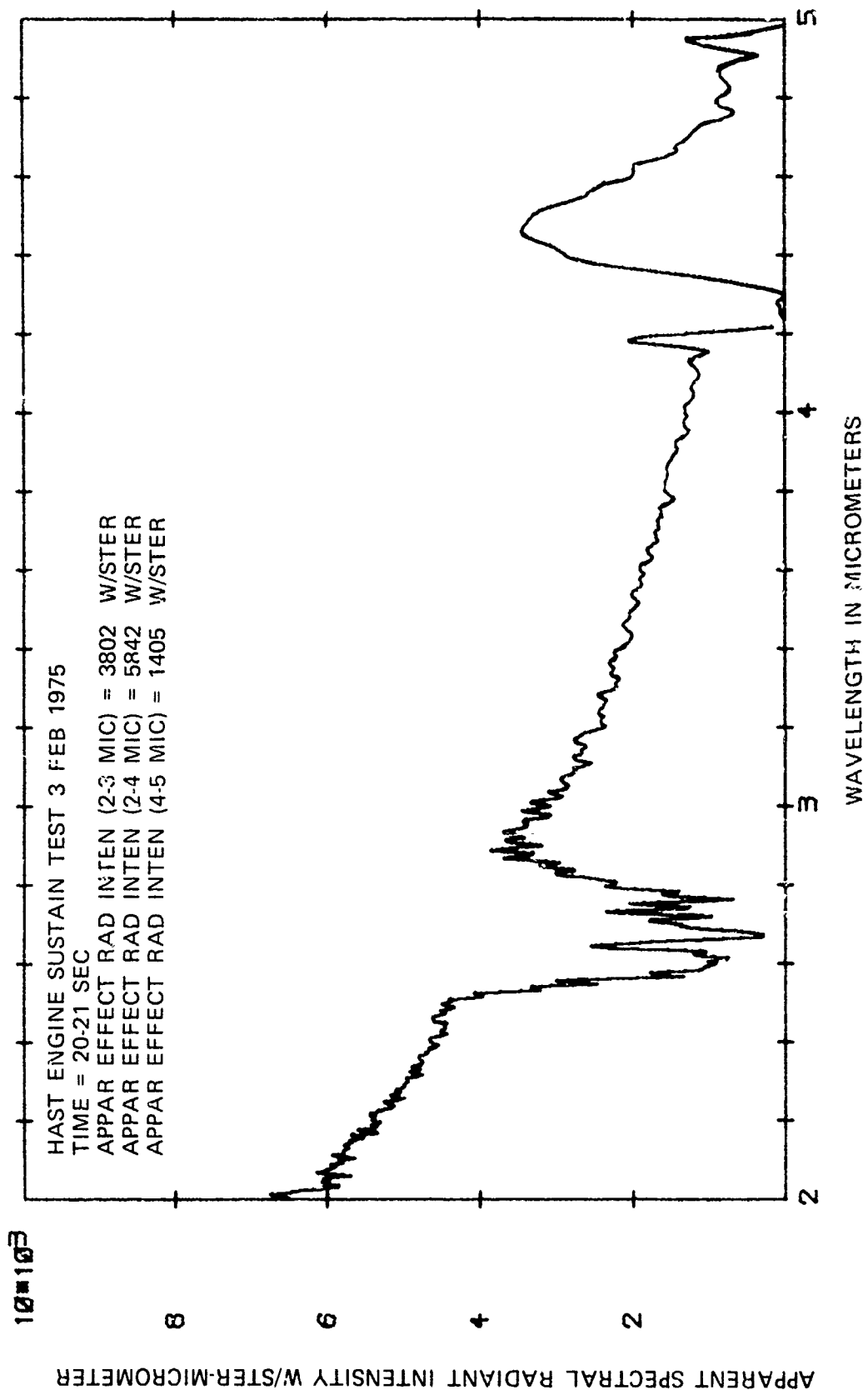


Figure 21 Full-Scale HAST Engine Sustain Phase - Typical Spectrum

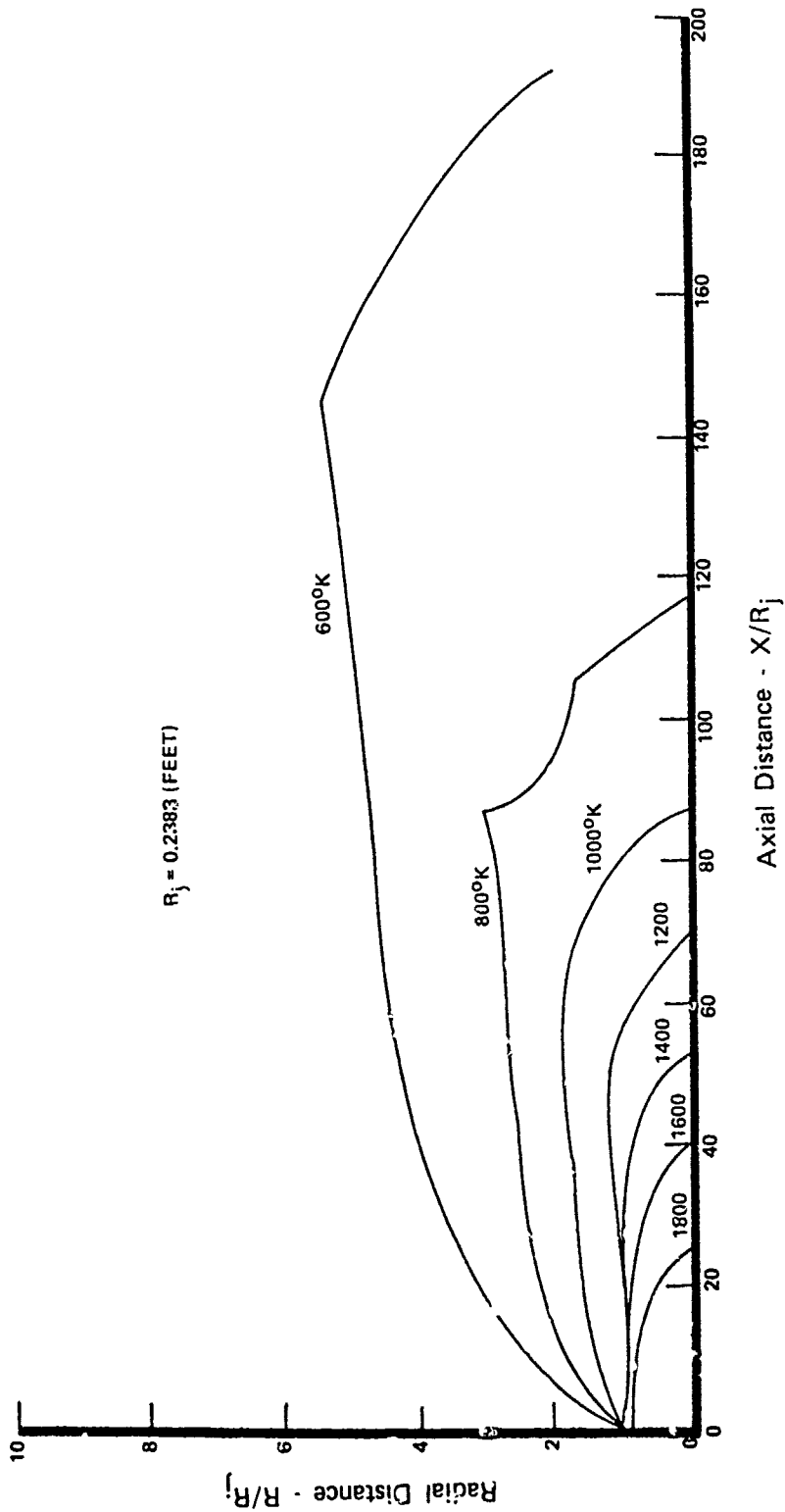


Figure 22. Predicted HAST Plume Isothermal Contours  
(Sea Level Static)-Non-Equilibrium Chemistry

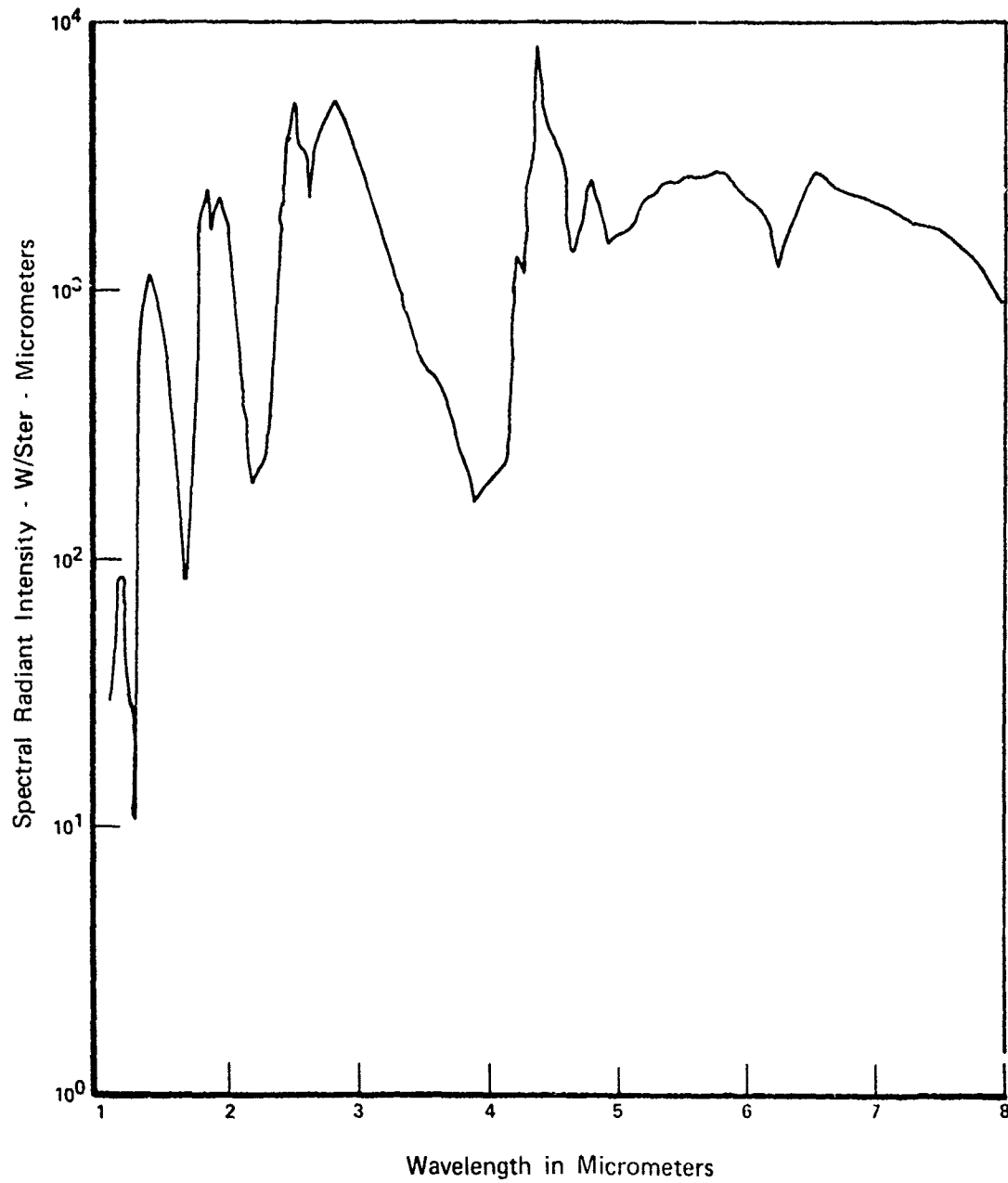


Figure 23. Predicted HAST Plume Spectral Radiant Intensity at 30 Degrees from Tail - 1 to 8 Micrometers

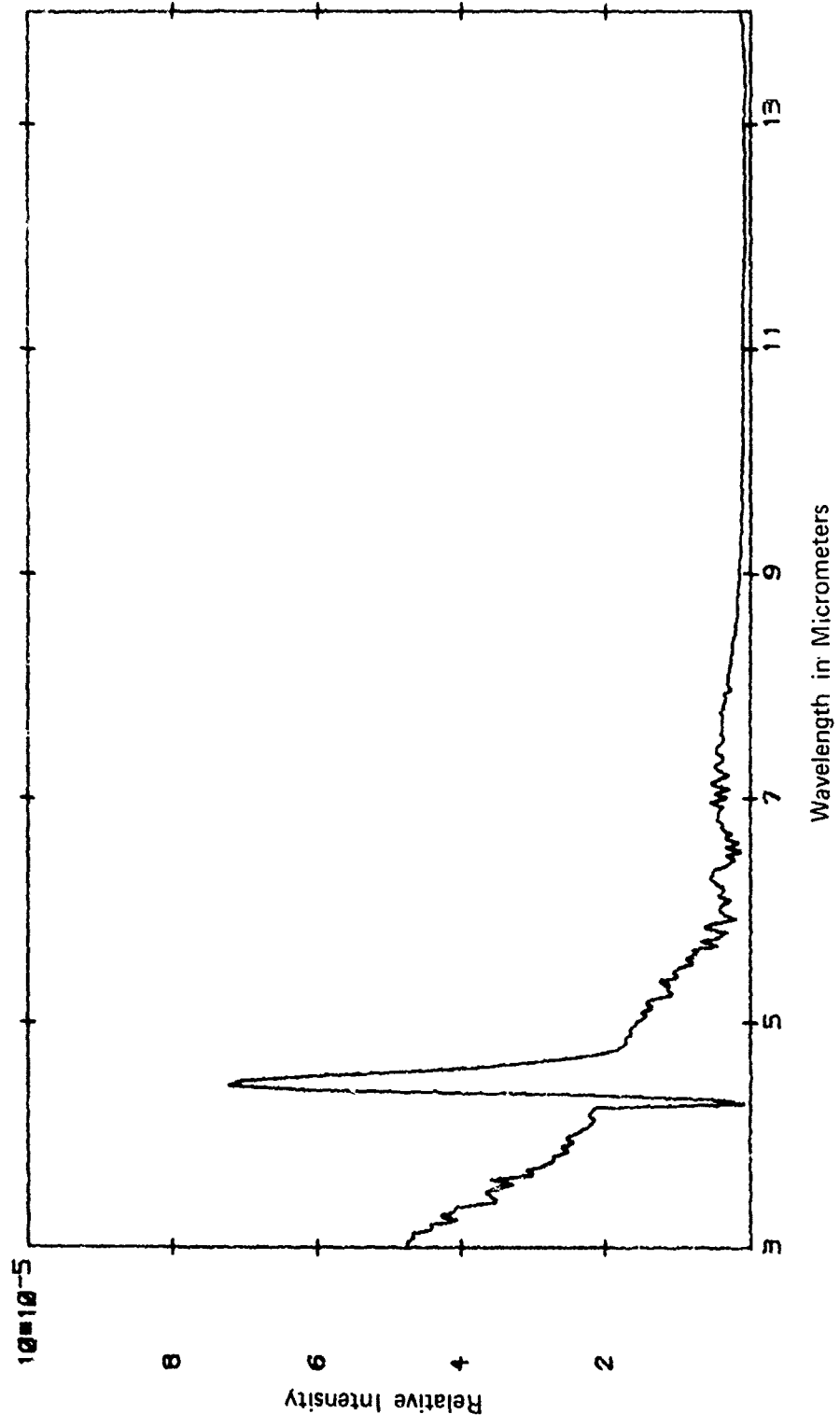


Figure 24. Measured Fuel/Particulate Rich Spectral Distribution from 3 to 14 Micrometers

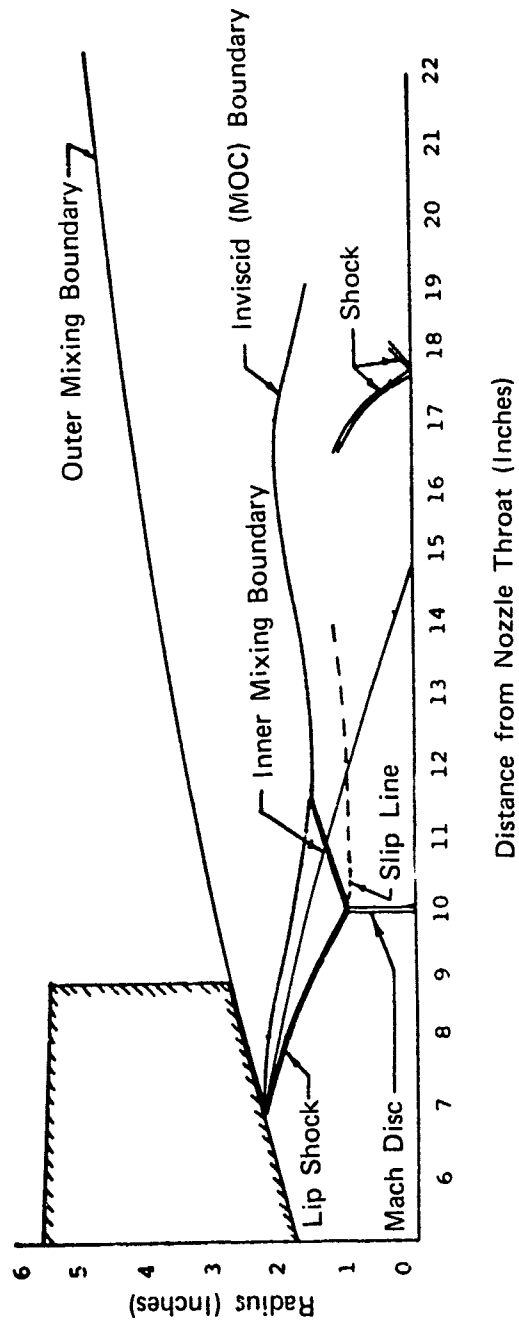


Figure 25. Predicted HAST Plume at Sea Level Static Conditions

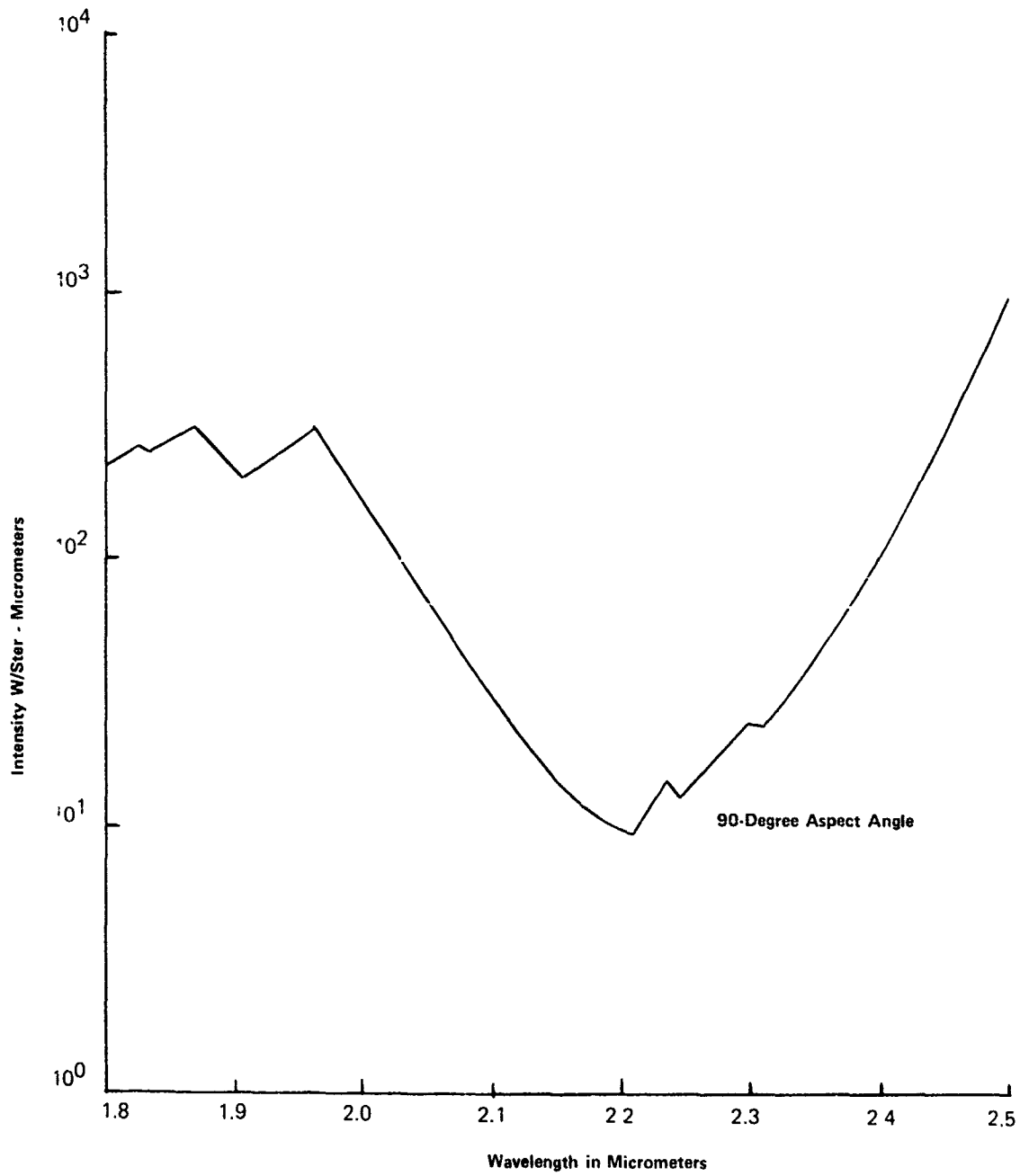


Figure 26. Predicted HAST Plume Spectral Radiant Intensity 1.8 to 2.5 Micrometers (Sea Level Static)

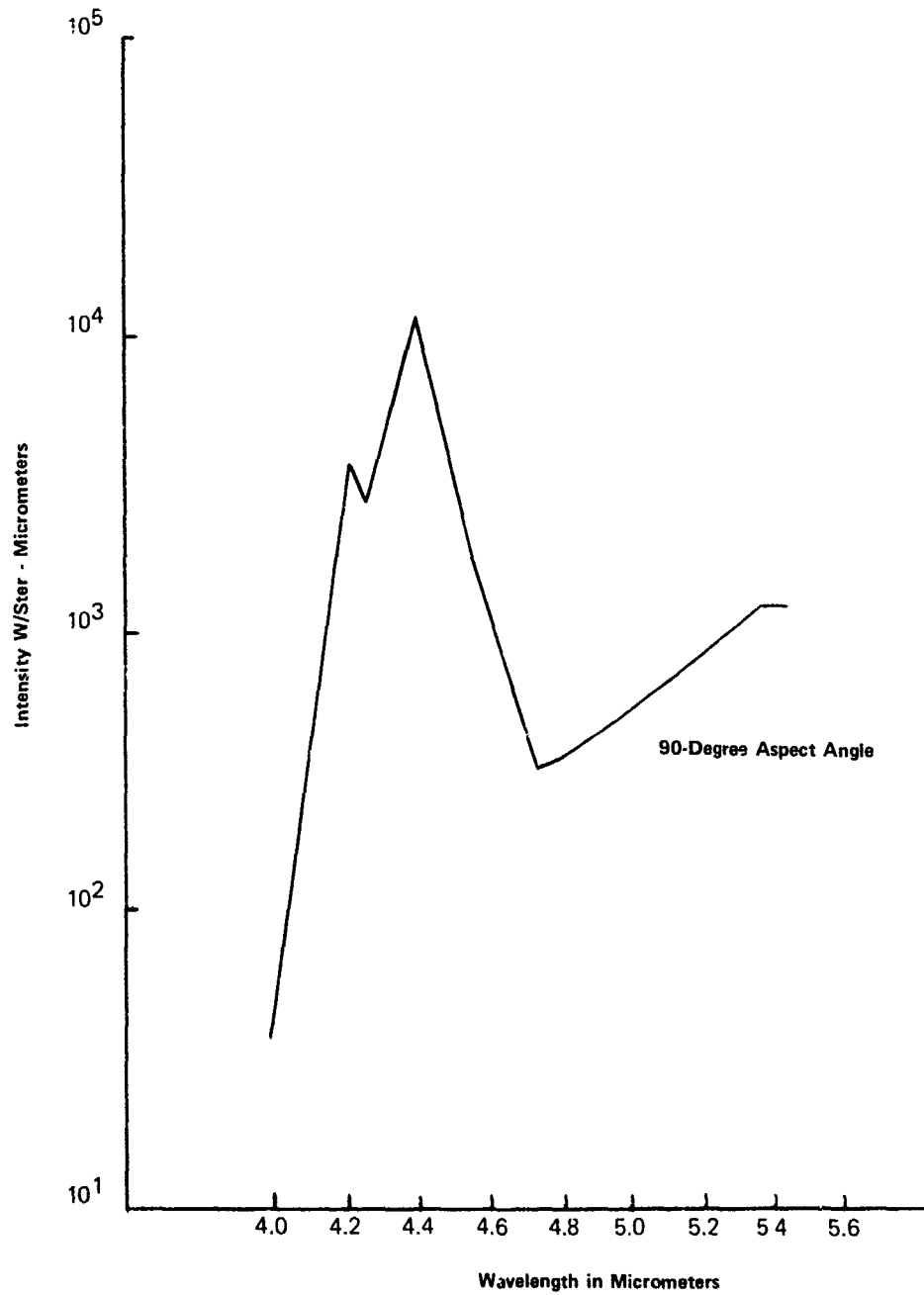


Figure 27. Predicted HAST Plume Spectral Radiant Intensity  
4.0 to 5.5 Micrometers (Sea Level Static)

TABLE 1. TIME SEQUENCES FOR FULL-SCALE HAST ENGINE SECONDARY INJECTION FOR BOOST AND SUSTAIN PHASES

Time (Sec)	Sym Valve	Hi CH <sub>4</sub>	Lo CH <sub>4</sub>	Lo O <sub>2</sub>	Hi O <sub>2</sub>
BOOST SEQUENCE					
5 to 6	*	*	*	*	*
7 to 8	*	*	*	*	*
14 to 15	On	*	*	*	*
21 to 22	On	*	*	*	*
26 to 27	*	On	*	*	*
29 to 30	*	*	On	*	*
32 to 33	*	*	*	*	*
35 to 36	*	*	*	On	*
38 to 39	*	*	*	*	On
41 to 42	*	*	*	*	*
SUSTAIN SEQUENCE					
0 to 2	*	*	*	*	*
2 to 9	*	*	*	*	*
9 to 10	On	*	*	*	*
10 to 13	On	On	*	*	*
13 to 16	On	*	On	*	*
16 to 19	On	*	*	*	*
19 to 22	On	*	*	On	*
22 to 23	On	*	*	*	*
23 to 26	On	*	*	*	On
26 to 27	On	*	*	*	*
27 to 28	*	*	*	*	*
28 to 31	*	*	On	*	*
31 to 34	*	*	*	*	*
34 to 37	*	*	*	On	*
37 to 49	*	*	*	*	*
49 to 50	On	*	*	*	*
50 to 53	On	On	*	*	*
53 to 56	On	*	On	*	*
56 to 59	On	*	*	*	*
59 to 62	On	*	*	On	*
62 to 63	On	*	*	*	*
63 to 66	On	*	*	*	On
66 to 67	On	*	*	*	*
67 to 68	*	*	*	*	*
68 to 71	*	*	On	*	*
71 to 74	*	*	*	*	*
74 to 77	*	*	*	*	*
77 to 89	*	*	*	*	*
89 to 90	On	*	*	*	*

TABLE 1. TIME SEQUENCES FOR FULL-SCALE HAST ENGINE SECONDARY INJECTION FOR BOOST AND SUSTAIN PHASES (CONCLUDED)

Time (Sec)	Sym Valve	Hi CH <sub>4</sub>	Lo CH <sub>4</sub>	Lo O <sub>2</sub>	Hi O <sub>2</sub>
SUSTAIN SEQUENCE					
90 to 95	On	On	*	*	*
95 to 100	On	*	On	*	*
100 to 105	On	*	*	*	*
105 to 110	On	*	*	On	*
110 to 111	On	*	*	*	*
111 to 116	On	*	*	*	On
116 to 117	On	*	*	*	*
117 to 120	*	*	*	*	*
120 to 125	*	*	*	*	*
125 to 130	*	*	*	*	*
130 to 135	*	*	*	*	*
135 to 140	*	*	*	*	*
*Off					

TABLE 2. INFRARED MEASUREMENT COMPARISONS  
AGAINST AN EXTENDED SOURCE

	BOFORS Scanner	Radiometer (Thermopile)	Interferometer Spectrometer
	4 to 5.5 $\mu$	3.9 to 5.0 $\mu$	4 to 5 $\mu$
Plume 1	5.85	5.49	2.79
Plume 2	6.29	5.89	2.91
Plume 3	11.3	9.63	4.49
Plume 4	17.1	14.5	5.57
Plume 5	2.64	2.73	1.16
Plume 6	29.3	25.8	21.72
Plume 7	52.0	52.4	46.86
Plume 8	19.2	17.2	14.42
Plume 9	33.9	30.4	24.71

All units are radiant intensity (W/Ster).  
Plume size of propane/oxygen torch was 1 to 3 feet.

TABLE 3. RADIOMETRIC DATA FOR SUBSCALE HAST ENGINE

Run No.	O/F	Injec- tion	$\dot{m}_s/\dot{m}_p$	$M_\infty$	Rad J	Scanner J	$\bar{J}$	$(J_{aug}/J)_{flow}$	Injection Mode	$J_{static}/J_{flow}$
5570	2.66	*	0	0	139	SAT	1.40			2.57
		O <sub>2</sub>	0.056	0	151	SAT	1.43		SLOT	
		CH <sub>4</sub>	0.058	0	216	SAT	2.05			
		*	0	0.7	54	SAT	0.54	1		
		O <sub>2</sub>	0.056	0.7	82	SAT	0.78	1.52		
5571	2.42	*	0	0	66	SAT	0.63	1.22		2.44
		CH <sub>4</sub>	0.058	0.7	154	SAT	1.51			
		O <sub>2</sub>	0.055	0	170	216	1.57		SLOT	
		CH <sub>4</sub>	0.056	0	232	282	2.15			
		*	0	0.7	63	62	0.62	1		
5572	2.59	*	0	0	92	105	0.85	1.46		2.45
		O <sub>2</sub>	0.055	0.7	85	64	0.79	1.34		
		CH <sub>4</sub>	0.056	0.7	135	163	1.23			
		O <sub>2</sub>	0.073	0	145	178	1.23		SLOT	
		CH <sub>4</sub>	0.076	0	224	271	1.90			
	*	0	0.7	55	57	0.50	1			
	O <sub>2</sub>	0.073	0.7	88	101	0.75	1.60			
	CH <sub>4</sub>	0.076	0.7	65	65	0.55	1.18			

TABLE 3. RADIOMETRIC DATA FOR SUBSCALE HAST ENGINE (CONTINUED)

Run No.	O/F	Injec- tion	$\dot{m}_s/\dot{m}_p$	$M_\infty$	Rad J	Scanner J	$\bar{J}$	$(J_{aug}/J)_{flow}$	Injection Mode	$J_{static}/J_{flow}$
5573	2.28	*	0	0	151	207	1.58			2.60
		O <sub>2</sub>	0.084	0	161	250	1.56		SLOT	
		CH <sub>4</sub>	0.087	0	268	369	2.59			
		*	0	0.7	58	81	0.61	1		
		O <sub>2</sub>	0.084	0.7	91	129	0.88	1.57		
5574	3.40	CH <sub>4</sub>	0.087	0.7	75	108	0.73	1.29		2.28
		*	0	0	68	116	0.71		SLOT	
		O <sub>2</sub>	0.083	0	75	121	0.72			
		CH <sub>4</sub>	0.085	0	139	221	1.32			
		*	0	0.7	30	54	0.31	1		
5575	2.96	O <sub>2</sub>	0.083	0.7	38	52	0.36	1.26		3.95
		CH <sub>4</sub>	0.085	0.7	47	78	0.44	1.54		
		*	0	0	75	SAT	0.79		SLOT	
		O <sub>2</sub>	0.084	0	79	SAT	0.76			
		CH <sub>4</sub>	0.086	0	139	SAT	1.34			
5575	2.96	*	0	0.3 N <sub>2</sub>	19	SAT	0.20	1		
		O <sub>2</sub>	0.084	0.3 N <sub>2</sub>	22	SAT	0.21	1.14		
		CH <sub>4</sub>	0.086	0.3 N <sub>2</sub>	14	SAT	0.13	0.72		

TABLE 3. RADIOMETRIC DATA FOR SUBSCALE HAST ENGINE (CONTINUED)

Run No.	O/F	Injec- tion	$\dot{m}_s/\dot{m}_p$	$M_\infty$	Rad J	Scanner J	$\bar{J}$	( $J_{aug}/J$ ) flow	Injection Mode	$J_{static}/J_{flow}$
5576	2.33	*	0	0	126	SAT	1.32			7.68
		O <sub>2</sub>	0.084	0	130	SAT	1.25		SLOT	
		CH <sub>4</sub>	0.086	0	214	SAT	2.07			
		*	0	0.3 N <sub>2</sub>	16	19	0.17	1		
		O <sub>2</sub>	0.084	0.3 N <sub>2</sub>	24	27	0.23	1.44		
		CH <sub>4</sub>	0.086	0.3 N <sub>2</sub>	14	17	0.13	0.84		
5577	ABORT									
5578	ABORT									
5579	2.72	*	0	0	162	343	1.46		8 Holes	5.64
		O <sub>2</sub>	0.072	0	162	324	1.36			
		CH <sub>4</sub>	0.074	0	236	461	1.97			
		*	0	0.3 N <sub>2</sub>	29	42	0.26	1		
		O <sub>2</sub>	0.072	0.3 N <sub>2</sub>	44	57	0.37	1.53		
		CH <sub>4</sub>	0.074	0.3 N <sub>2</sub>	19	18	0.16	0.64		
5580	ABORT									
5581	ABORT									
5582	ABORT									
5583	2.52	*	0	0	123	163	1.28			2.72
		O <sub>2</sub>	0.084	0	124	175	1.19		SLOT	

TABLE 3. RADIOMETRIC DATA FOR SUBSCALE HAST ENGINE (CONTINUED)

Run No.	O/F	Injec- tion	$\dot{m}_s/\dot{m}_p$	$M_\infty$	Rad $J$	Scanner $J$	$\bar{J}$	$(J_{aug}/J)_{flow}$	Injection Mode	$J_{static}/J_{flow}$
		CO	0.085	0	135	197	1.30			
		*	0	0.7	45	59	0.47	1		
		O <sub>2</sub>	0.084	0.7	71	99	0.69	1.57		
		CO	0.085	0.7	53	52	0.51	1.17		
5584	2.64	*	0	0	107	144	1.13			2.52
		O <sub>2</sub>	0.133	0	93	110	0.87		SLOT	
		CO	0.135	0	128	139	1.20			
		*	0	0.7	43	51	0.45	1		
		O <sub>2</sub>	0.133	0.7	66	96	0.61	1.54		
		CO	0.135	0.7	52	64	0.49	1.23		
5585	2.56	*	0	0	118	198	1.23			2.91
		O <sub>2</sub>	0.084	0	82	111	0.79		1 Hole	
		CH <sub>4</sub>	0.081	0	62	79	0.60			
		*	0	0.7	41	66	0.42	1		
		O <sub>2</sub>	0.084	0.7	39	57	0.38	0.97		
		CH <sub>4</sub>	0.081	0.7	30	35	0.28	0.72		
5586 (POPS)		*		0	2		0.14			
5587	2.46	*	0	0	133	226	1.39			2.86
		POPS	0.145	0	114	85	1.04		1 Hole	

TABLE 3. RADIOMETRIC DATA FOR SUBSCALE HAST ENGINE (CONCLUDED)

Run No.	O/F	Injec- tion	$\dot{m}_s/\dot{m}_p$	$M_\infty$	Rad J	Scanner J	$\bar{J}$	$(J_{aug}/J)_{flow}$	Injection Mode	$J_{static}/J_{flow}$
5588		*	0	0.7	47	77	0.49	1		
		POPS	0.145	0.7	51	38	0.47	1.10		
	3.99	*	0	0	49	47	0.56		1 Hole	1.91
		POPS	0.138	0	74	25	0.73	1		
		*	0	0.7	25	25	0.29			
5589		POPS	0.138	0.7	39	SAT	0.39	1.55		
	3.88	*	0	0	41	59	0.47			2.04
		O <sub>2</sub>	0.144	0	32	27	0.32		1 Hole	
		CH <sub>4</sub>	0.154	0	55	54	0.55			
		*	0	0.7	20	20	0.22	1		
5590		O <sub>2</sub>	0.144	0.7	18	21	0.18	0.88		
		CH <sub>4</sub>	0.154	0.7	24	20	0.24	1.21		
	4.01	*	0	0	85	159	0.53			5.90
		O <sub>2</sub>	0.079	0	47	82	0.28		1 Hole	
		CH <sub>4</sub>	0.084	0	33	67	0.19			
	*	0	0.7	14	11	0.09	1			
	O <sub>2</sub>	0.079	0.7	13	15	0.08	0.91			
	CH <sub>4</sub>	0.084	0.7	9	7	0.05	0.64			
*No injection										

TABLE 4. RELATIVE RADIATION EMITTED BY SUBSCALE HAST  
ENGINE IN THREE SPECTRAL BANDS

Run No.	Injection	$M_\infty$	(2.2 to 3.0 $\mu$ )	(2.2 to 4.0)	(4.0 to 5.0)
5570	*	0	**	**	**
	O <sub>2</sub>	0	**	**	**
	CH <sub>4</sub>	0	**	**	**
	*	0.7	**	**	**
	O <sub>2</sub>	0.7	**	**	**
	CH <sub>4</sub>	0.7	**	**	**
5571	*	0	145	210	96
	O <sub>2</sub>	0	88	119	51
	CH <sub>4</sub>	0	196	277	127
	*	0.7	122	172	48
	O <sub>2</sub>	0.7	120	177	58
	CH <sub>4</sub>	0.7	84	127	39
5572	*	0	83	121	56
	O <sub>2</sub>	0	181	252	124
	CH <sub>4</sub>	0	89	130	80
	*	0.7	143	202	67
	O <sub>2</sub>	0.7	116	176	56
	CH <sub>4</sub>	0.7	87	137	43

TABLE 4. RELATIVE RADIATION EMITTED BY SUBSCALE HAST  
ENGINE IN THREE SPECTRAL BANDS (CONTINUED)

Run No.	Injection	M <sub>∞</sub>	(2.2 to 3.0 μ)	(2.2 to 4.0)	(4.0 to 5.0)
5573	*	0	126	186	106
	O <sub>2</sub>	0	141	201	127
	CH <sub>4</sub>	0	171	246	199
	*	0.7	147	208	66
	O <sub>2</sub>	0.7	105	157	65
	CH <sub>4</sub>	0.7	92	146	45
5574	*	0	94	150	73
	O <sub>2</sub>	0	95	144	79
	CH <sub>4</sub>	0	56	87	30
	*	0.7	44	70	29
	O <sub>2</sub>	0.7	33	51	24
	CH <sub>4</sub>	0.7	64	101	30
5575	*	0	42	64	25
	O <sub>2</sub>	0	41	60	31
	CH <sub>4</sub>	0	106	150	92
	*	0.3 N <sub>2</sub>	17	30	9
	O <sub>2</sub>	0.3 N <sub>2</sub>	18	32	11
	CH <sub>4</sub>	0.3 N <sub>2</sub>	37	62	17

TABLE 4. RELATIVE RADIATION EMITTED BY SUBSCALE HAST  
ENGINE IN THREE SPECTRAL BANDS (CONTINUED)

Run No.	Injection	$M_\infty$	(2.2 to 3.0 $\mu$ )	(2.2 to 4.0)	(4.0 to 5.0)
5576	*	0	64	98	52
	O <sub>2</sub>	0	110	167	104
	CH <sub>4</sub>	0	165	249	133
	*	0.3 N <sub>2</sub>	42	73	23
	O <sub>2</sub>	0.3 N <sub>2</sub>	15	27	8
	CH <sub>4</sub>	0.3 N <sub>2</sub>	18	31	9
5577	ABORT				
5578	ABORT				
5579	*	0	61	77	94
	O <sub>2</sub>	0	66	83	84
	CH <sub>4</sub>	0	56	73	95
	*	0.3 N <sub>2</sub>	60	102	38
	O <sub>2</sub>	0.3 N <sub>2</sub>	22	40	14
	CH <sub>4</sub>	0.3 N <sub>2</sub>	20	34	12
5583	*	0	78	117	39
	O <sub>2</sub>	0	178	257	85
	CO	0	138	216	75
	*	0.7	129	192	40

TABLE 4. RELATIVE RADIATION EMITTED BY SUBSCALE HAST  
ENGINE IN THREE SPECTRAL BANDS (CONTINUED)

Run No.	Injection	$M_{\infty}$	(2.2 to 3.0 $\mu$ )	(2.2 to 4.0)	(4.0 to 5.0)
5584	O <sub>2</sub>	0.7	123	184	46
	CO	0.7	95	150	40
	*	0	145	223	80
	O <sub>2</sub>	0	146	220	73
	CO	0	149	234	82
5585	*	0.7	145	211	45
	O <sub>2</sub>	0.7	52	80	24
	CO	0.7	100	154	40
	*	0	135	204	88
	O <sub>2</sub>	0	113	181	58
	CH <sub>4</sub>	0	112	186	65
	*	0.7	86	131	38
5589	O <sub>2</sub>	0.7	64	102	32
	CH <sub>4</sub>	0.7	66	104	32
	*	0	74	118	52
	O <sub>2</sub>	0	50	82	30
	CH <sub>4</sub>	0	74	119	54
	*	0.7	46	70	21

TABLE 4. RELATIVE RADIATION EMITTED BY SUBSCALE HAST  
ENGINE IN THREE SPECTRAL BANDS (CONCLUDED)

Run No.	Injection	M <sub>∞</sub>	(2.2 to 3.0μ)	(2.2 to 4.0)	(4.0 to 5.0)
5590	O <sub>2</sub>	0.7	39	63	24
	CH <sub>4</sub>	0.7	58	86	26
	*	0	137	209	96
	O <sub>2</sub>	0	181	136	53
	CH <sub>4</sub>	0	88	150	58
	*	0.7	28	43	14
	O <sub>2</sub>	0.7	30	46	14
	CH <sub>4</sub>	0.7	17	26	9
	*No injection **No data				

SUBSCALE HAST

RANGE(DET)= 3.513 M

RUN=579 FILE=477 RANGE (FRONT OF CAMERA)= 3.05 M SENSITIVITY= 75 ATTENUATION= 620 POWER=2.72

1	2	3	4	5	6	7	8	9	10	11	12	13	14	15	16	17	18	19	20	21	22	23	24	25	26	27
3	3	3	3	3	3	3	3	3	3	3	3	3	3	3	3	3	3	3	3	3	3	3	3	3	3	3
1	1	1	1	1	1	1	1	1	1	1	1	1	1	1	1	1	1	1	1	1	1	1	1	1	1	1
2	2	2	2	2	2	2	2	2	2	2	2	2	2	2	2	2	2	2	2	2	2	2	2	2	2	2
3	3	3	3	3	3	3	3	3	3	3	3	3	3	3	3	3	3	3	3	3	3	3	3	3	3	3
4	4	4	4	4	4	4	4	4	4	4	4	4	4	4	4	4	4	4	4	4	4	4	4	4	4	4
5	5	5	5	5	5	5	5	5	5	5	5	5	5	5	5	5	5	5	5	5	5	5	5	5	5	5
6	6	6	6	6	6	6	6	6	6	6	6	6	6	6	6	6	6	6	6	6	6	6	6	6	6	6
7	7	7	7	7	7	7	7	7	7	7	7	7	7	7	7	7	7	7	7	7	7	7	7	7	7	7
8	8	8	8	8	8	8	8	8	8	8	8	8	8	8	8	8	8	8	8	8	8	8	8	8	8	8
9	9	9	9	9	9	9	9	9	9	9	9	9	9	9	9	9	9	9	9	9	9	9	9	9	9	9
10	10	10	10	10	10	10	10	10	10	10	10	10	10	10	10	10	10	10	10	10	10	10	10	10	10	10
11	11	11	11	11	11	11	11	11	11	11	11	11	11	11	11	11	11	11	11	11	11	11	11	11	11	11
12	12	12	12	12	12	12	12	12	12	12	12	12	12	12	12	12	12	12	12	12	12	12	12	12	12	12
13	13	13	13	13	13	13	13	13	13	13	13	13	13	13	13	13	13	13	13	13	13	13	13	13	13	13
14	14	14	14	14	14	14	14	14	14	14	14	14	14	14	14	14	14	14	14	14	14	14	14	14	14	14
15	15	15	15	15	15	15	15	15	15	15	15	15	15	15	15	15	15	15	15	15	15	15	15	15	15	15
16	16	16	16	16	16	16	16	16	16	16	16	16	16	16	16	16	16	16	16	16	16	16	16	16	16	16
17	17	17	17	17	17	17	17	17	17	17	17	17	17	17	17	17	17	17	17	17	17	17	17	17	17	17
18	18	18	18	18	18	18	18	18	18	18	18	18	18	18	18	18	18	18	18	18	18	18	18	18	18	18
19	19	19	19	19	19	19	19	19	19	19	19	19	19	19	19	19	19	19	19	19	19	19	19	19	19	19
20	20	20	20	20	20	20	20	20	20	20	20	20	20	20	20	20	20	20	20	20	20	20	20	20	20	20
21	21	21	21	21	21	21	21	21	21	21	21	21	21	21	21	21	21	21	21	21	21	21	21	21	21	21
22	22	22	22	22	22	22	22	22	22	22	22	22	22	22	22	22	22	22	22	22	22	22	22	22	22	22
23	23	23	23	23	23	23	23	23	23	23	23	23	23	23	23	23	23	23	23	23	23	23	23	23	23	23
24	24	24	24	24	24	24	24	24	24	24	24	24	24	24	24	24	24	24	24	24	24	24	24	24	24	24
25	25	25	25	25	25	25	25	25	25	25	25	25	25	25	25	25	25	25	25	25	25	25	25	25	25	25
26	26	26	26	26	26	26	26	26	26	26	26	26	26	26	26	26	26	26	26	26	26	26	26	26	26	26
27	27	27	27	27	27	27	27	27	27	27	27	27	27	27	27	27	27	27	27	27	27	27	27	27	27	27

COLUMN NO.=

1	2	3	4	5	6	7	8	9	10	11	12	13	14	15	16	17	18	19	20	21	22	23	24	25	26	27
0.0	0.0	0.0	0.0	0.0	2.5	5.1	7.6	10.2	12.7	15.2	17.8	20.3	22.9	25.4	27.9	30.5	33.0	35.6	38.1	40.6	43.2	45.7	48.3	50.8	53.3	55.9

EXIT PLANE IS IN COLUMN 5, FIELD OF VIEW CENTER IS IN COLUMN 28 HORZ INCREMENT= 2.54 CM VERT INCREMENT= .

TABLE 5. SUBSCALE ENGINE PLUME SPATIAL DISTRIBUTION - NO INJE

= 3.513 M  
MER=2.72

BACH

Distance (cm)	23	24	25	26	27	28	29	30	31	32	33	34	35	36	37	38	39	40	41	42	43	44	45	46	47	48	49	50	51	52	53	54
48.3	3	4	4	4	4	4	4	4	4	4	4	4	4	4	4	4	4	4	4	4	4	4	4	4	4	4	4	4	4	4	4	4
50.8	3	4	4	4	4	4	4	4	4	4	4	4	4	4	4	4	4	4	4	4	4	4	4	4	4	4	4	4	4	4	4	4
53.3	3	4	4	4	4	4	4	4	4	4	4	4	4	4	4	4	4	4	4	4	4	4	4	4	4	4	4	4	4	4	4	4
55.9	3	4	4	4	4	4	4	4	4	4	4	4	4	4	4	4	4	4	4	4	4	4	4	4	4	4	4	4	4	4	4	4
58.4	3	4	4	4	4	4	4	4	4	4	4	4	4	4	4	4	4	4	4	4	4	4	4	4	4	4	4	4	4	4	4	4
61.0	3	4	4	4	4	4	4	4	4	4	4	4	4	4	4	4	4	4	4	4	4	4	4	4	4	4	4	4	4	4	4	4
63.5	3	4	4	4	4	4	4	4	4	4	4	4	4	4	4	4	4	4	4	4	4	4	4	4	4	4	4	4	4	4	4	4
66.0	3	4	4	4	4	4	4	4	4	4	4	4	4	4	4	4	4	4	4	4	4	4	4	4	4	4	4	4	4	4	4	4
68.6	3	4	4	4	4	4	4	4	4	4	4	4	4	4	4	4	4	4	4	4	4	4	4	4	4	4	4	4	4	4	4	4
71.1	3	4	4	4	4	4	4	4	4	4	4	4	4	4	4	4	4	4	4	4	4	4	4	4	4	4	4	4	4	4	4	4
73.7	3	4	4	4	4	4	4	4	4	4	4	4	4	4	4	4	4	4	4	4	4	4	4	4	4	4	4	4	4	4	4	4
76.2	3	4	4	4	4	4	4	4	4	4	4	4	4	4	4	4	4	4	4	4	4	4	4	4	4	4	4	4	4	4	4	4
78.7	3	4	4	4	4	4	4	4	4	4	4	4	4	4	4	4	4	4	4	4	4	4	4	4	4	4	4	4	4	4	4	4
81.3	3	4	4	4	4	4	4	4	4	4	4	4	4	4	4	4	4	4	4	4	4	4	4	4	4	4	4	4	4	4	4	4
83.8	3	4	4	4	4	4	4	4	4	4	4	4	4	4	4	4	4	4	4	4	4	4	4	4	4	4	4	4	4	4	4	4
86.4	3	4	4	4	4	4	4	4	4	4	4	4	4	4	4	4	4	4	4	4	4	4	4	4	4	4	4	4	4	4	4	4
88.9	3	4	4	4	4	4	4	4	4	4	4	4	4	4	4	4	4	4	4	4	4	4	4	4	4	4	4	4	4	4	4	4
91.4	3	4	4	4	4	4	4	4	4	4	4	4	4	4	4	4	4	4	4	4	4	4	4	4	4	4	4	4	4	4	4	4
94.0	3	4	4	4	4	4	4	4	4	4	4	4	4	4	4	4	4	4	4	4	4	4	4	4	4	4	4	4	4	4	4	4
96.5	3	4	4	4	4	4	4	4	4	4	4	4	4	4	4	4	4	4	4	4	4	4	4	4	4	4	4	4	4	4	4	4
99.1	3	4	4	4	4	4	4	4	4	4	4	4	4	4	4	4	4	4	4	4	4	4	4	4	4	4	4	4	4	4	4	4
101.6	3	4	4	4	4	4	4	4	4	4	4	4	4	4	4	4	4	4	4	4	4	4	4	4	4	4	4	4	4	4	4	4
104.1	3	4	4	4	4	4	4	4	4	4	4	4	4	4	4	4	4	4	4	4	4	4	4	4	4	4	4	4	4	4	4	4
106.7	3	4	4	4	4	4	4	4	4	4	4	4	4	4	4	4	4	4	4	4	4	4	4	4	4	4	4	4	4	4	4	4
109.2	3	4	4	4	4	4	4	4	4	4	4	4	4	4	4	4	4	4	4	4	4	4	4	4	4	4	4	4	4	4	4	4
111.8	3	4	4	4	4	4	4	4	4	4	4	4	4	4	4	4	4	4	4	4	4	4	4	4	4	4	4	4	4	4	4	4
114.3	3	4	4	4	4	4	4	4	4	4	4	4	4	4	4	4	4	4	4	4	4	4	4	4	4	4	4	4	4	4	4	4
116.8	3	4	4	4	4	4	4	4	4	4	4	4	4	4	4	4	4	4	4	4	4	4	4	4	4	4	4	4	4	4	4	4
119.4	3	4	4	4	4	4	4	4	4	4	4	4	4	4	4	4	4	4	4	4	4	4	4	4	4	4	4	4	4	4	4	4
121.9	3	4	4	4	4	4	4	4	4	4	4	4	4	4	4	4	4	4	4	4	4	4	4	4	4	4	4	4	4	4	4	4
124.0	3	4	4	4	4	4	4	4	4	4	4	4	4	4	4	4	4	4	4	4	4	4	4	4	4	4	4	4	4	4	4	4

MERT INCREMENT = .72 CM











TABLE 7. SUBSCALE ENGINE PLUME SPATIAL DISTRIBUTION - CH<sub>4</sub> INJECTION

UNITS=  
BACKGROUND=

25	26	27	28	29	30	31	32	33	34	35	36	37	38	39	40	41	42	43	44	45	46	47	48	49	50	51	52	53	54	55	
0.8	53.3	55.9	58.4	61.0	63.5	66.0	68.6	71.1	73.7	76.2	78.7	81.3	83.8	86.4	88.9	91.4	94.0	96.5	99.1	101.6	104.1	106.7	109.2	111.8	114.3	116.8	119.4	121.9	124.5	127.0	
4	4	4	4	4	4	4	4	4	4	4	4	4	4	4	4	4	4	4	4	4	4	4	4	4	4	4	4	4	4	4	
3	3	3	3	3	3	3	3	3	3	3	3	3	3	3	3	3	3	3	3	3	3	3	3	3	3	3	3	3	3	3	
10	10	10	10	10	10	10	10	10	10	10	10	10	10	10	10	10	10	10	10	10	10	10	10	10	10	10	10	10	10	10	
15	15	15	15	15	15	15	15	15	15	15	15	15	15	15	15	15	15	15	15	15	15	15	15	15	15	15	15	15	15	15	
20	20	20	20	20	20	20	20	20	20	20	20	20	20	20	20	20	20	20	20	20	20	20	20	20	20	20	20	20	20	20	
25	25	25	25	25	25	25	25	25	25	25	25	25	25	25	25	25	25	25	25	25	25	25	25	25	25	25	25	25	25	25	
30	30	30	30	30	30	30	30	30	30	30	30	30	30	30	30	30	30	30	30	30	30	30	30	30	30	30	30	30	30	30	
35	35	35	35	35	35	35	35	35	35	35	35	35	35	35	35	35	35	35	35	35	35	35	35	35	35	35	35	35	35	35	
40	40	40	40	40	40	40	40	40	40	40	40	40	40	40	40	40	40	40	40	40	40	40	40	40	40	40	40	40	40	40	
45	45	45	45	45	45	45	45	45	45	45	45	45	45	45	45	45	45	45	45	45	45	45	45	45	45	45	45	45	45	45	45
50	50	50	50	50	50	50	50	50	50	50	50	50	50	50	50	50	50	50	50	50	50	50	50	50	50	50	50	50	50	50	
55	55	55	55	55	55	55	55	55	55	55	55	55	55	55	55	55	55	55	55	55	55	55	55	55	55	55	55	55	55	55	55

INCREMENT = .72 CM

2



SUBSCALE HAST

RANGE(DET)= 3.513 M

RUN=579 FILE=497 RANGE (FRONT OF CAMERA)= 3.05 M SENSITIVITY= 75 ATTENUATION= 620 POWER=2.72

3

1	2	3	4	5	6	7	8	9	10	11	12	13	14	15	16	17	18	19	20	21	22	23	24	25	26	27
1	2	3	4	5	6	7	8	9	10	11	12	13	14	15	16	17	18	19	20	21	22	23	24	25	26	27
0.0	0.0	0.0	0.0	0.0	2.5	5.1	7.6	10.2	12.7	15.2	17.8	20.3	22.9	25.4	27.9	30.5	33.0	35.6	38.1	40.6	43.2	45.7	48.3	50.8	53.3	55.9

COLUMN NO. =

EXIT PLANE IS IN COLUMN 5, FIELD OF VIEW CENTER IS IN COLUMN 28    HORZ INCREMENT= 2.54 CM    VERT INCREMENT= .7

TABLE 8. SUBSCALE ENGINE PLUME SPATIAL DISTRIBUTION - O<sub>2</sub> INJECTION,

3.513 M  
 MER=2.72

BAI

23	24	25	26	27	28	29	30	31	32	33	34	35	36	37	38	39	40	41	42	43	44	45	46	47	48	49	50	51	52	53
48.3	50.8	53.3	55.9	58.4	61.0	63.5	66.0	68.6	71.1	73.7	76.2	78.7	81.3	83.8	86.4	88.9	91.4	94.0	96.5	99.1	101.6	104.1	106.7	109.2	111.8	114.3	116.8	119.4	121.9	124.4
3	3	3	3	4					3	3				3	3															
1	1	1	1	1	1	1	1	1	1	1	1	1	1	1	1	1	1	1	1	1	1	1	1	1	1	1	1	1	1	1

VERT INCREMENT= .72 CM

TABLE 8. SUBSCALE ENGINE PLUME SPATIAL DISTRIBUTION - O<sub>2</sub> INJECTION, MACH 0.3 N<sub>2</sub> FLOW/

UNITS=WATTS/STER X  
BACKGROUND= 153

3 3  
3 3  
4 3 3 3

6 41  
33 42  
66 43  
82 44  
156 45  
241 46  
437 47  
581 48  
730 49  
717 50  
645 51  
453 52  
312 53  
214 54  
119 55  
72 56  
32 57  
9 58

31 32 33 34 35 36 37 38 39 40 41 42 43 44 45 46 47 48 49 50 51 52 53 54 55 56  
68.6 71.1 73.7 76.2 78.7 81.3 83.8 86.4 88.9 91.4 94.0 96.5 99.1 101.6 104.1 106.7 109.2 111.8 114.3 116.8 119.4 121.9 124.5 127.0 129.5





TABLE 9. SUBSCALE ENGINE PLUME SPATIAL DISTRIBUTION - CH<sub>4</sub> INJECTION, MACH 0.3 N<sub>2</sub> FLOW

UNITS=WATTS/STER X  
BACKGROUND= 153

3

36 45  
81 46  
138 47  
215 48  
263 49  
307 50  
348 51  
387 52  
424 53  
458 54  
489 55

30	31	32	33	34	35	36	37	38	39	40	41	42	43	44	45	46	47	48	49	50	51	52	53	54	55	56
66.0	71.1	76.2	81.3	86.4	91.4	96.5	101.6	106.7	111.8	116.8	121.9	127.0														
68.6	73.7	78.7	83.8	88.9	94.0	99.1	104.1	109.2	114.3	119.4	124.5	129.5														

3

SUBSCALE HAST

RANGE(DET)= 3.513 M

RUN=579 FILE=505 RANGE (FRONT OF CAMERA)= 3.05 M SENSITIVITY= 75 ATTENUATION= 620 POWER=2.72

1	2	3	4	5	6	7	8	9	10	11	12	13	14	15	16	17	18	19	20	21	22	23	24	25	26	27
10	15	16	17	19	21	23	24	25	26	27	28	29	30	31	32	33	34	35	36	37	38	39	40	41	42	43
4	4	4	4	4	4	4	4	4	4	4	4	4	4	4	4	4	4	4	4	4	4	4	4	4	4	4

COLUMN NO.=

1	2	3	4	5	6	7	8	9	10	11	12	13	14	15	16	17	18	19	20	21	22	23	24	25	26	27
0.0	0.0	0.0	0.0	0.0	2.5	5.1	7.6	10.2	12.7	15.2	17.8	20.3	22.9	25.4	27.9	30.5	33.0	35.6	38.1	40.6	43.2	45.7	48.3	50.8	53.3	55.9

EXIT PLANE IS IN COLUMN 5, FIELD OF VIEW CENTER IS IN COLUMN 28 HORZ INCREMENT= 2.54 CM VERT INCREMENT= .



TABLE 10. SUBSCALE ENGINE PLUME SPATIAL DISTRIBUTION, - NO INJECTION, MACH 0.3 N<sub>2</sub> FLOW

UNITS=MAHIS/STER X  
 BACKGROUND= 153

2	33	34	35	36	37	38	39	40	41	42	43	44	45	46	47	48	49	50	51	52	53	54	55	56
71.1	73.7	76.2	78.7	81.3	83.8	86.4	88.9	91.4	94.0	96.5	99.1	101.6	104.1	106.7	109.2	111.8	114.3	116.8	119.4	121.9	124.5	127.0	129.5	

3  
 25  
 44  
 78  
 151  
 270  
 467  
 615  
 634  
 482  
 427  
 312  
 191  
 111  
 74  
 22  
 7

41  
 43  
 44  
 45  
 46  
 47  
 48  
 49  
 50  
 51  
 52  
 53  
 54  
 55  
 56  
 57  
 59

3



TABLE 11. SUBSCALE ENGINE PLUME SPATIAL DISTRIBUTION - NO INJEC

3.513 M  
R=2.46

UN  
BACKGR

Station	24	25	26	27	28	29	30	31	32	33	34	35	36	37	38	39	40	41	42	43	44	45	46	47	48	49	50	51	52	53	54
Pressure	3.2	45.7	48.3	50.8	53.3	55.9	58.4	61.0	63.5	66.0	68.6	71.1	73.7	76.2	78.7	81.3	83.8	86.4	88.9	91.4	94.0	96.5	99.1	101.6	104.1	106.7	109.2	111.8	114.3	116.8	119.4
Temperature	110	110	110	110	110	110	110	110	110	110	110	110	110	110	110	110	110	110	110	110	110	110	110	110	110	110	110	110	110	110	110
Velocity	10	10	10	10	10	10	10	10	10	10	10	10	10	10	10	10	10	10	10	10	10	10	10	10	10	10	10	10	10	10	10
Angle	3	3	3	3	3	3	3	3	3	3	3	3	3	3	3	3	3	3	3	3	3	3	3	3	3	3	3	3	3	3	3

3.3 INCREMENT = .72 CM

TABLE 11. SUBSCALE ENGINE PLUME SPATIAL DISTRIBUTION - NO INJECTION, NO FLOW

UNITS=WATTS/STER X  
BACKGROUND= 153

34	71.1	73.7	76.2	78.7	81.3	83.8	86.4	88.9	91.4	94.0	96.5	99.1	101.6	104.1	106.7	109.2	111.8	114.3	116.8	119.4	121.9	124.5
35	10	11	11	11	11	11	11	11	11	11	11	11	11	11	11	11	11	11	11	11	11	11
36	10	11	11	11	11	11	11	11	11	11	11	11	11	11	11	11	11	11	11	11	11	11
37	10	11	11	11	11	11	11	11	11	11	11	11	11	11	11	11	11	11	11	11	11	11
38	10	11	11	11	11	11	11	11	11	11	11	11	11	11	11	11	11	11	11	11	11	11
39	10	11	11	11	11	11	11	11	11	11	11	11	11	11	11	11	11	11	11	11	11	11
40	10	11	11	11	11	11	11	11	11	11	11	11	11	11	11	11	11	11	11	11	11	11
41	10	11	11	11	11	11	11	11	11	11	11	11	11	11	11	11	11	11	11	11	11	11
42	10	11	11	11	11	11	11	11	11	11	11	11	11	11	11	11	11	11	11	11	11	11
43	10	11	11	11	11	11	11	11	11	11	11	11	11	11	11	11	11	11	11	11	11	11
44	10	11	11	11	11	11	11	11	11	11	11	11	11	11	11	11	11	11	11	11	11	11
45	10	11	11	11	11	11	11	11	11	11	11	11	11	11	11	11	11	11	11	11	11	11
46	10	11	11	11	11	11	11	11	11	11	11	11	11	11	11	11	11	11	11	11	11	11
47	10	11	11	11	11	11	11	11	11	11	11	11	11	11	11	11	11	11	11	11	11	11
48	10	11	11	11	11	11	11	11	11	11	11	11	11	11	11	11	11	11	11	11	11	11
49	10	11	11	11	11	11	11	11	11	11	11	11	11	11	11	11	11	11	11	11	11	11
50	10	11	11	11	11	11	11	11	11	11	11	11	11	11	11	11	11	11	11	11	11	11
51	10	11	11	11	11	11	11	11	11	11	11	11	11	11	11	11	11	11	11	11	11	11
52	10	11	11	11	11	11	11	11	11	11	11	11	11	11	11	11	11	11	11	11	11	11
53	10	11	11	11	11	11	11	11	11	11	11	11	11	11	11	11	11	11	11	11	11	11
54	10	11	11	11	11	11	11	11	11	11	11	11	11	11	11	11	11	11	11	11	11	11
55	10	11	11	11	11	11	11	11	11	11	11	11	11	11	11	11	11	11	11	11	11	11
56	10	11	11	11	11	11	11	11	11	11	11	11	11	11	11	11	11	11	11	11	11	11

6	31
159	32
71	33
33	34
35	35
36	36
37	37
38	38
39	39
40	40
41	41
42	42
43	43
44	44
45	45
46	46
47	47
48	48
49	49
50	50
51	51
52	52
53	53
54	54
55	55
56	56
57	57
58	58
59	59
60	60
61	61
62	62
63	63
64	64
65	65
66	66
67	67
68	68
69	69
70	70











TABLE 13. SUBSCALE ENGINE PLUME SPATIAL DISTRIBUTION - POPS INJECTION, MACH (

UNIT:  
BACKGROU

13 M  
46

24	25	26	27	28	29	30	31	32	33	34	35	36	37	38	39	40	41	42	43	44	45	46	47	48	49	50	51	52	53	54	55
45.7	48.3	50.8	53.3	55.9	58.4	61.0	63.5	66.0	68.6	71.1	73.7	76.2	78.7	81.3	83.8	86.4	88.9	91.4	94.0	96.5	99.1	101.6	104.1	106.7	109.2	111.8	114.3	116.8	119.4	121.9	
3	3	3	3	3	3	3	3	3	3	3	3	3	3	3	3	3	3	3	3	3	3	3	3	3	3	3	3	3	3	3	

INCREMENT= .72 CM

2





TABLE 14. SUBSCALE ENGINE PLUME SPATIAL DISTRIBUTION - POPS INJECTIO

3 M  
46

UNITS  
BACKGROUND

25	26	27	28	29	30	31	32	33	34	35	36	37	38	39	40	41	42	43	44	45	46	47	48	49	50	51	52	53	54	55
45.7	48.3	50.8	53.3	55.9	58.4	61.0	63.5	66.0	68.6	71.1	73.7	76.2	78.7	81.3	83.8	86.4	88.9	91.4	94.0	96.5	99.1	101.6	104.1	106.7	109.2	111.8	114.3	116.8	119.4	121.9

INCREMENT = .72 CM

*2*

ON

TABLE 14. SUBSCALE ENGINE PLUME SPATIAL DISTRIBUTION - POPS INJECTION, NO FLOW

S=H  
VD=

UNITS=WATTS/STER X  
BACKGROUND= 153

6	43
12	44
18	45
24	46
30	47
36	48
42	49
48	50
54	51
60	52
66	53
72	54
78	55
84	56
90	57
96	58
102	59
108	60
114	61

24	33	34	35	36	37	38	39	40	41	42	43	44	45	46	47	48	49	50	51	52	53	54	55	56
	68.6	71.1	73.7	76.2	78.7	81.3	83.8	86.4	88.9	91.4	94.0	96.5	99.1	101.6	104.1	106.7	109.2	111.8	114.3	116.8	119.4	121.9	124.5	

3

TABLE 15. SUBSCALE HAST ENGINE SCANNER, RADIOMETRIC DATA  
WITH AND WITHOUT REFLECTED RADIATION

Run No.	Injection	$M_{\infty}$	J (With Reflection)	J (Without Reflection)	Percent Reflection
5570	*	0	SAT	SAT	
	O <sub>2</sub>	0	SAT	SAT	
	CH <sub>4</sub>	0	SAT	SAT	
	*	0.7	SAT	SAT	
	O <sub>2</sub>	0.7	SAT	SAT	
	CH <sub>4</sub>	0.7	SAT	SAT	
5571	*	0	185	173	6
	O <sub>2</sub>	0	216	201	7
	CH <sub>4</sub>	0	282	256	9
	*	0.7	62	59	5
	O <sub>2</sub>	0.7	105	100	5
	CH <sub>4</sub>	0.7	64	59	8
5572	*	0	163	155	5
	O <sub>2</sub>	0	178	167	6
	CH <sub>4</sub>	0	271	259	4
	*	0.7	53	51	4
	O <sub>2</sub>	0.7	101	94	7
	CH <sub>4</sub>	0.7	65	62	5

TABLE 15. SUBSCALE HAST ENGINE SCANNER, RADIOMETRIC DATA WITH AND WITHOUT REFLECTED RADIATION (CONTINUED)

Run No.	Injection	$M_{\infty}$	J (With Reflection)	J (Without Reflection)	Percent Reflection
5573	*	0	207	190	8
	O <sub>2</sub>	0	250	226	10
	CH <sub>4</sub>	0	369	343	7
	*	0.7	81	74	8
	O <sub>2</sub>	0.7	129	116	10
5574	CH <sub>4</sub>	0.7	108	99	8
	*	0	116	104	10
	O <sub>2</sub>	0	121	109	10
	CH <sub>4</sub>	0	221	199	10
	*	0.7	54	48	11
5575	O <sub>2</sub>	0.7	52	45	13
	CH <sub>4</sub>	0.7	78	72	8
	*	0	SAT	SAT	
	O <sub>2</sub>	0	SAT	SAT	
	CH <sub>4</sub>	0	SAT	SAT	
	*	0.3 N <sub>2</sub>	SAT	SAT	
	O <sub>2</sub>	0.3 N <sub>2</sub>	SAT	SAT	
	CH <sub>4</sub>	0.3 N <sub>2</sub>	SAT	SAT	

TABLE 15. SUBSCALE HAST ENGINE SCANNER, RADIOMETRIC DATA WITH AND WITHOUT REFLECTED RADIATION (CONTINUED)

Run No.	Injection	$M_{\infty}$	J (With Reflection)	J (Without Reflection)	Percent Reflection
5576	*	0	SAT	SAT	
	O <sub>2</sub>	0	SAT	SAT	
	CH <sub>4</sub>	0	SAT	SAT	
	*	0.3 N <sub>2</sub>	19	18	5
	O <sub>2</sub>	0.3 N <sub>2</sub>	27	25	7
	CH <sub>4</sub>	0.3 N <sub>2</sub>	17	16	6
5577	ABORT				
5578	ABORT				
5579	*	0	343	310	10
	O <sub>2</sub>	0	324	293	10
	CH <sub>4</sub>	0	461	421	9
	*	0.3 N <sub>2</sub>	43	39	9
	O <sub>2</sub>	0.3 N <sub>2</sub>	57	49	14
	CH <sub>4</sub>	0.3 N <sub>2</sub>	18	16½	8
5580	ABORT				
5581	ABORT				
5582	ABORT				
5583	*	0	163	150	8
	O <sub>2</sub>	0	175	163	7

TABLE 15. SUBSCALE HAST ENGINE SCANNER, RADIOMETRIC DATA WITH AND WITHOUT REFLECTED RADIATION (CONTINUED)

Run No.	Injection	$M_{\infty}$	J (With Reflection)	J (Without Reflection)	Percent Reflection
5584	CO	0	197	183	7
	*	0.7	60	57	5
	O <sub>2</sub>	0.7	99	91	8
	CO	0.7	52	49	6
	*	0	144	135	6
	O <sub>2</sub>	0	110	102	7
	CO	0	139	130	6
	*	0.7	51	50	2
	O <sub>2</sub>	0.7	96	90	6
	CO	0.7	64	60	6
5585	*	0	198	177	11
	O <sub>2</sub>	0	111	101	10
	CH <sub>4</sub>	0	79	76	4
	*	0.7	66	59	11
5586 (POPS)	O <sub>2</sub>	0.7	57	52	9
	CH <sub>4</sub>	0.7	35	32	9
			**		
5587	*	0	226	200	12
	POPS	0	85	74	13

TABLE 15. SUBSCALE HAST ENGINE SCANNER, RADIOMETRIC DATA WITH AND WITHOUT REFLECTED RADIATION (CONCLUDED)

Run No.	Injection	$M_{\infty}$	J (With Reflection)	J (Without Reflection)	Percent Reflection
5588	*	0.7	77	66	14
	POPS	0.7	38	29	24
	*	0	47	45	4
	POPS	0	25	23	8
	*	0.7	25	24	4
5589	POPS	0.7	SAT	SAT	
	*	0	59	57	3
	O <sub>2</sub>	0	27	25	7
	CH <sub>4</sub>	0	54	47	13
	*	0.7	20	19	5
5590	O <sub>2</sub>	0.7	21	20	5
	CH <sub>4</sub>	0.7	20	19	5
	*	0	159	141	11
	O <sub>2</sub>	0	82	74	10
	CH <sub>4</sub>	0	67	48	28
	*	0.7	11	10	9
	O <sub>2</sub>	0.7	15	14	7
	CH <sub>4</sub>	0.7	7	6	14

\*No injection

\*\*No data

TABLE 16. FULL-SCALE HAST ENGINE BOOST PHASE - INFRARED RADIANT INTENSITY BETWEEN 4 AND 5 $\mu$

$\dot{\omega}_t$ gm/sec	Time from t = 0 (sec)	$J_{60^\circ}$		$J_{30^\circ}$		Scanner $J_{90^\circ}$		Percent Reflection	Interferometer $J_{90^\circ}$
		W/Ster	W/Ster	$\mu$ /Ster	$\mu$ /Ster	With Reflection	Without Reflection		
1429	5 to 6	8734	4100	7710	7000	13	*		
1429	7 to 8	8353 to 8135	3985	7440	6650	16	*		
1528	14 to 15	4914 to 4641	2930	3390	3050	17	3606		
2132	21 to 22	3986 to 3822	2348	3040	2360	18	3156		
(2278) Hi F	26 to 27	6552	4226	4910	4540	13	5032		
(2192) Lo F	29 to 30	4914 to 5078	3228	*	*	*	4342		
2132	32 to 33	3822	2583	*	*	*	3334		
(2191) Lo O	35 to 36	3713	2524	*	*	*	3186		
(2273) Hi O	38 to 39	3549	2348	*	*	*	3094		
2132	41 to 42	4204	2583	*	*	*	3648		

\*No measurements were taken.

TABLE 17. FULL-SCALE HAST ENGINE SUSTAIN PHASE - INFRARED  
RADIANT INTENSITY BETWEEN 4 AND 5 $\mu$

$\dot{\omega}_t$ gm/sec	Time from t = 0 (sec)	J 60° W/Ster	Interferometer J 90°	J 60° W/Ster/gm/sec
1197	5 to 6	4368	*	3.65
(1240) Hi F	11 to 12	4859	4438	3.89
(1220) Lo F	15 to 16	3549	3370	2.91
1197	18 to 19	3549	3296	2.96
(1221) Lo O	20 to 21	2894	2810	2.37
(1250) Hi O	24 to 25	2675	2356	2.14
(1220) Asy F	29 to 30	3385	3454	2.77
1197	32 to 33	2894	2888	2.42
(1221) Asy F	35 to 36	2730	2508	2.24
(869) Hi F	51 to 52	4696	4652	5.4
(834) Lo F	54 to 55	3385	3474	4.03
816	56 to 57	3003	*	3.68
(840) Lo O	60 to 61	2675	2594	3.19
(869) Hi O	64 to 65	2184	2196	2.51
(840) Asy F	69 to 70	3330	3324	3.97
816	72 to 73	2675	2574	3.28
(840) Asy F	75 to 76	2348	2470	2.80
(529) Hi F	91 to 92	4095	3544	7.74
(499) Lo F	96 to 97	2730	2338	5.47
476	101 to 102	1801	1628	3.79
(500) Lo O	106 to 107	1801	1674	3.61
(528) Hi O	112 to 113	1692	1574	3.21
(499) Asy F	121 to 122	2238	2156	4.48
476	126 to 127	1557	1556	3.27
(500) Lo O	131 to 132	1539	1512	3.08
476	136 to 137	1470	1576	3.09

\*No data taken.





18. FULL-SCALE HAST ENGINE BOOST PHASE SPATIAL DISTRIBUTION, T = 5 TO 6 SECONDS

UNITS=WATTS/STER X

BACKGROUND= 156

32	33	34	35	36	37	38	39	40	41	42	43	44	45	46	47	48	49	50	51	52	53	54	55	56	Total
1	1	1	1	1	1	1	1	1	1	1	1	1	1	1	1	1	1	1	1	1	1	1	1	1	136
1	1	1	1	1	1	1	1	1	1	1	1	1	1	1	1	1	1	1	1	1	1	1	1	1	130
1	1	1	1	1	1	1	1	1	1	1	1	1	1	1	1	1	1	1	1	1	1	1	1	1	102
1	1	1	1	1	1	1	1	1	1	1	1	1	1	1	1	1	1	1	1	1	1	1	1	1	75
1	1	1	1	1	1	1	1	1	1	1	1	1	1	1	1	1	1	1	1	1	1	1	1	1	107
1	1	1	1	1	1	1	1	1	1	1	1	1	1	1	1	1	1	1	1	1	1	1	1	1	127
1	1	1	1	1	1	1	1	1	1	1	1	1	1	1	1	1	1	1	1	1	1	1	1	1	125
1	1	1	1	1	1	1	1	1	1	1	1	1	1	1	1	1	1	1	1	1	1	1	1	1	104
1	1	1	1	1	1	1	1	1	1	1	1	1	1	1	1	1	1	1	1	1	1	1	1	1	44
1	1	1	1	1	1	1	1	1	1	1	1	1	1	1	1	1	1	1	1	1	1	1	1	1	50
1	1	1	1	1	1	1	1	1	1	1	1	1	1	1	1	1	1	1	1	1	1	1	1	1	46
1	1	1	1	1	1	1	1	1	1	1	1	1	1	1	1	1	1	1	1	1	1	1	1	1	42
1	1	1	1	1	1	1	1	1	1	1	1	1	1	1	1	1	1	1	1	1	1	1	1	1	44
1	1	1	1	1	1	1	1	1	1	1	1	1	1	1	1	1	1	1	1	1	1	1	1	1	19
1	1	1	1	1	1	1	1	1	1	1	1	1	1	1	1	1	1	1	1	1	1	1	1	1	14
1	1	1	1	1	1	1	1	1	1	1	1	1	1	1	1	1	1	1	1	1	1	1	1	1	13
1	1	1	1	1	1	1	1	1	1	1	1	1	1	1	1	1	1	1	1	1	1	1	1	1	13
1	1	1	1	1	1	1	1	1	1	1	1	1	1	1	1	1	1	1	1	1	1	1	1	1	14
1	1	1	1	1	1	1	1	1	1	1	1	1	1	1	1	1	1	1	1	1	1	1	1	1	7
1	1	1	1	1	1	1	1	1	1	1	1	1	1	1	1	1	1	1	1	1	1	1	1	1	13
1	1	1	1	1	1	1	1	1	1	1	1	1	1	1	1	1	1	1	1	1	1	1	1	1	11
1	1	1	1	1	1	1	1	1	1	1	1	1	1	1	1	1	1	1	1	1	1	1	1	1	18
1	1	1	1	1	1	1	1	1	1	1	1	1	1	1	1	1	1	1	1	1	1	1	1	1	13
1	1	1	1	1	1	1	1	1	1	1	1	1	1	1	1	1	1	1	1	1	1	1	1	1	6
1	1	1	1	1	1	1	1	1	1	1	1	1	1	1	1	1	1	1	1	1	1	1	1	1	14
1	1	1	1	1	1	1	1	1	1	1	1	1	1	1	1	1	1	1	1	1	1	1	1	1	9
1	1	1	1	1	1	1	1	1	1	1	1	1	1	1	1	1	1	1	1	1	1	1	1	1	11
1	1	1	1	1	1	1	1	1	1	1	1	1	1	1	1	1	1	1	1	1	1	1	1	1	12
1	1	1	1	1	1	1	1	1	1	1	1	1	1	1	1	1	1	1	1	1	1	1	1	1	22
1	1	1	1	1	1	1	1	1	1	1	1	1	1	1	1	1	1	1	1	1	1	1	1	1	45
1	1	1	1	1	1	1	1	1	1	1	1	1	1	1	1	1	1	1	1	1	1	1	1	1	50
1	1	1	1	1	1	1	1	1	1	1	1	1	1	1	1	1	1	1	1	1	1	1	1	1	59
1	1	1	1	1	1	1	1	1	1	1	1	1	1	1	1	1	1	1	1	1	1	1	1	1	78
1	1	1	1	1	1	1	1	1	1	1	1	1	1	1	1	1	1	1	1	1	1	1	1	1	104
1	1	1	1	1	1	1	1	1	1	1	1	1	1	1	1	1	1	1	1	1	1	1	1	1	109
1	1	1	1	1	1	1	1	1	1	1	1	1	1	1	1	1	1	1	1	1	1	1	1	1	136
1	1	1	1	1	1	1	1	1	1	1	1	1	1	1	1	1	1	1	1	1	1	1	1	1	161
1	1	1	1	1	1	1	1	1	1	1	1	1	1	1	1	1	1	1	1	1	1	1	1	1	180
1	1	1	1	1	1	1	1	1	1	1	1	1	1	1	1	1	1	1	1	1	1	1	1	1	226
1	1	1	1	1	1	1	1	1	1	1	1	1	1	1	1	1	1	1	1	1	1	1	1	1	271
1	1	1	1	1	1	1	1	1	1	1	1	1	1	1	1	1	1	1	1	1	1	1	1	1	265
1	1	1	1	1	1	1	1	1	1	1	1	1	1	1	1	1	1	1	1	1	1	1	1	1	315
1	1	1	1	1	1	1	1	1	1	1	1	1	1	1	1	1	1	1	1	1	1	1	1	1	336
1	1	1	1	1	1	1	1	1	1	1	1	1	1	1	1	1	1	1	1	1	1	1	1	1	351
1	1	1	1	1	1	1	1	1	1	1	1	1	1	1	1	1	1	1	1	1	1	1	1	1	367
1	1	1	1	1	1	1	1	1	1	1	1	1	1	1	1	1	1	1	1	1	1	1	1	1	410
1	1	1	1	1	1	1	1	1	1	1	1	1	1	1	1	1	1	1	1	1	1	1	1	1	368
1	1	1	1	1	1	1	1	1	1	1	1	1	1	1	1	1	1	1	1	1	1	1	1	1	359
1	1	1	1	1	1	1	1	1	1	1	1	1	1	1	1	1	1	1	1	1	1	1	1	1	344
1	1	1	1	1	1	1	1	1	1	1	1	1	1	1	1	1	1	1	1	1	1	1	1	1	333
1	1	1	1	1	1	1	1	1	1	1	1	1	1	1	1	1	1	1	1	1	1	1	1	1	291
1	1	1	1	1	1	1	1	1	1	1	1	1	1	1	1	1	1	1	1	1	1	1	1	1	278
1	1	1	1	1	1	1	1	1	1	1	1	1	1	1	1	1	1	1	1	1	1	1	1	1	217
1	1	1	1	1	1	1	1	1	1	1	1	1	1	1	1	1	1	1	1	1	1	1	1	1	155
1	1	1	1	1	1	1	1	1	1	1	1	1	1	1	1	1	1	1	1	1	1	1	1	1	177
1	1	1	1	1	1	1	1	1	1	1	1	1	1	1	1	1	1	1	1	1	1	1	1	1	141
1	1	1	1	1	1	1	1	1	1	1	1	1	1	1	1	1	1	1	1	1	1	1	1	1	104
1	1	1	1	1	1	1	1	1	1	1	1	1	1	1	1	1	1	1	1	1	1	1	1	1	67
1	1	1	1	1	1	1	1	1	1	1	1	1	1	1	1	1	1	1	1	1	1	1	1	1	51
1	1	1	1	1	1	1	1	1	1	1	1	1	1	1	1	1	1	1	1	1	1	1	1	1	51
1	1	1	1	1	1	1	1	1	1	1	1	1	1	1	1	1	1	1	1	1	1	1	1	1	47
1	1	1	1	1	1	1	1	1	1	1	1	1	1	1	1	1	1	1	1	1	1	1	1	1	27
1	1	1	1	1	1	1	1	1	1	1	1	1	1	1	1	1	1	1	1	1	1	1	1	1	32
1	1	1	1	1	1	1	1	1	1	1	1	1	1	1	1	1	1	1	1	1	1	1	1	1	22
1	1	1	1	1	1	1	1	1	1	1	1	1	1	1	1	1	1	1	1	1	1	1	1	1	19
1	1	1	1	1	1	1	1	1	1	1	1	1	1	1	1	1	1	1	1	1	1	1	1	1	7
1	1	1	1	1	1	1	1	1	1	1	1	1	1	1	1	1	1	1	1	1	1	1	1	1	3
1	1	1	1	1	1	1	1	1	1	1	1	1	1	1	1	1	1	1	1	1	1	1	1	1	0

J Total = 8.08 KW/STER

t = 5 to 6 seconds

3















TABLE 21. FULL-SCALE HAST ENGINE BOOST PHASE SPATIAL DISTRIBUTION, T = 21 TO

9.609 M  
FR=

BACK

24	25	26	27	28	29	30	31	32	33	34	35	36	37	38	39	40	41	42	43	44	45	46	47	48	49	50	51	52	53	
1	1	1	1	1	1	1	1	1	1	1	1	1	1	1	1	1	1	1	1	1	1	1	1	1	1	1	1	1	1	1
1	1	1	1	1	1	1	1	1	1	1	1	1	1	1	1	1	1	1	1	1	1	1	1	1	1	1	1	1	1	1
0.0	0.0	0.0	0.0	0.0	0.1	0.0	0.0	0.0	0.0	0.0	0.0	0.0	0.0	0.0	0.0	0.0	0.0	0.0	0.0	0.0	0.0	0.0	0.0	0.0	0.0	0.0	0.0	0.0	0.0	0.0

J Total = 2.78 KW/STER

t = 21 to 22 seconds

ERT INCREMENT = 2.14 C

2

TABLE 21. FULL-SCALE HAST ENGINE BOOST PHASE SPATIAL DISTRIBUTION, T = 21 TO 22 SECONDS

UNITS=WATTS/STER X  
BACKGROUND= 159

Node	Value	Node	Value
1	0.0	31	0.0
2	0.0	32	0.0
3	0.0	33	0.0
4	0.0	34	0.0
5	0.0	35	0.0
6	0.0	36	0.0
7	0.0	37	0.0
8	0.0	38	0.0
9	0.0	39	0.0
10	0.0	40	0.0
11	0.0	41	0.0
12	0.0	42	0.0
13	0.0	43	0.0
14	0.0	44	0.0
15	0.0	45	0.0
16	0.0	46	0.0
17	0.0	47	0.0
18	0.0	48	0.0
19	0.0	49	0.0
20	0.0	50	0.0
21	0.0	51	0.0
22	0.0	52	0.0
23	0.0	53	0.0
24	0.0	54	7.6
25	0.0	55	15.2
26	0.0	56	22.9

J Total = 2.78 KW/STER

t = 21 to 22 seconds

Node	Value	Node	Value
1	0.0	31	0.0
2	0.0	32	0.0
3	0.0	33	0.0
4	0.0	34	0.0
5	0.0	35	0.0
6	0.0	36	0.0
7	0.0	37	0.0
8	0.0	38	0.0
9	0.0	39	0.0
10	0.0	40	0.0
11	0.0	41	0.0
12	0.0	42	0.0
13	0.0	43	0.0
14	0.0	44	0.0
15	0.0	45	0.0
16	0.0	46	0.0
17	0.0	47	0.0
18	0.0	48	0.0
19	0.0	49	0.0
20	0.0	50	0.0
21	0.0	51	0.0
22	0.0	52	0.0
23	0.0	53	0.0
24	0.0	54	7.6
25	0.0	55	15.2
26	0.0	56	22.9

3







FULL SCALE HAST "BOOST" FIRING STATIC 14,000 FT ALTITUDE MODIFIED A(F)/A(IT) RANGE (DET) = 9.609 M  
 RUN= 46 FILE=132 RANGE (FRONT OF CAMERA)= 9.14 M SENSITIVITY= 50 ATTENUATION=2455 POWER=

1	2	3	4	5	6	7	8	9	10	11	12	13	14	15	16	17	18	19	20	21	22	23	24	25	26	27	28

COLUMN NO.=

1	2	3	4	5	6	7	8	9	10	11	12	13	14	15	16	17	18	19	20	21	22	23	24	25	26	27	28
0.0	0.0	0.0	0.0	0.0	0.0	0.0	0.0	0.0	0.0	0.0	0.0	0.0	0.0	0.0	0.0	0.0	0.0	0.0	0.0	0.0	0.0	0.0	0.0	0.0	0.0	0.0	

EXIT PLANE IS IN COLUMN 27, FIELD OF VIEW CENTER IS IN COLUMN 29 HORIZ INCREMENT= 7.62 CM VERT INCREMENT= 2.14 CM



TABLE 23. FULL-SCALE HAST ENGINE BOOST PHASE SPATIAL DISTRIBUTION, T = 41 TO 42 SECONDS

		UNITS=WATTS/STER X	
		BACKGROUND= 159	
32	0.0	1	68
33	0.0	1	69
34	0.0	1	44
35	0.0	1	44
36	0.0	1	51
37	0.0	1	28
38	0.0	1	0
39	0.0	1	0
40	0.0	1	0
41	0.0	1	0
42	0.0	1	0
43	0.0	1	0
44	0.0	1	0
45	0.0	1	0
46	0.0	1	0
47	0.0	1	0
48	0.0	1	0
49	0.0	1	0
50	0.0	1	0
51	0.0	1	0
52	0.0	1	0
53	0.0	1	0
54	7.6	1	0
55	15.2	1	0
56	22.9	1	0

		UNITS=WATTS/STER X	
		BACKGROUND= 159	
32	0.0	1	68
33	0.0	1	69
34	0.0	1	44
35	0.0	1	44
36	0.0	1	51
37	0.0	1	28
38	0.0	1	0
39	0.0	1	0
40	0.0	1	0
41	0.0	1	0
42	0.0	1	0
43	0.0	1	0
44	0.0	1	0
45	0.0	1	0
46	0.0	1	0
47	0.0	1	0
48	0.0	1	0
49	0.0	1	0
50	0.0	1	0
51	0.0	1	0
52	0.0	1	0
53	0.0	1	0
54	7.6	1	0
55	15.2	1	0
56	22.9	1	0

J Total = 3.27 KW/STER

t = 41 to 42 seconds

32	0.0	1	13
33	0.0	1	15
34	0.0	1	17
35	0.0	1	20
36	0.0	1	25
37	0.0	1	24
38	0.0	1	22
39	0.0	1	21
40	0.0	1	20
41	0.0	1	17
42	0.0	1	14
43	0.0	1	11
44	0.0	1	9
45	0.0	1	8
46	0.0	1	7
47	0.0	1	6
48	0.0	1	5
49	0.0	1	4
50	0.0	1	3
51	0.0	1	2
52	0.0	1	1
53	0.0	1	0
54	7.6	1	0
55	15.2	1	0
56	22.9	1	0

3







TABLE 25. COMPARISON BETWEEN CALCULATED AND MEASURED DATA  
(SEA LEVEL STATIC CONDITIONS - SUSTAIN PHASE)

J (W/STER)			
Degrees	O/F = 3.2 Calculation 1 (4.17 to 4.88 $\mu$ )	O/F = 3.2 Calculation 2 (4.0 to 5.56 $\mu$ )	O/F = 3.1 Measurement (4 to 5 $\mu$ )
30	2220	3440	Not observed
60	2540	3060	2900 to 3500
90	3770	5600*	3000 to 3300
120	4110	6100*	Not observed
*Extrapolated			

TABLE 26. COMPARISON BETWEEN CALCULATED AND MEASURED  
DATA (SEA LEVEL STATIC - BOOST PHASE)

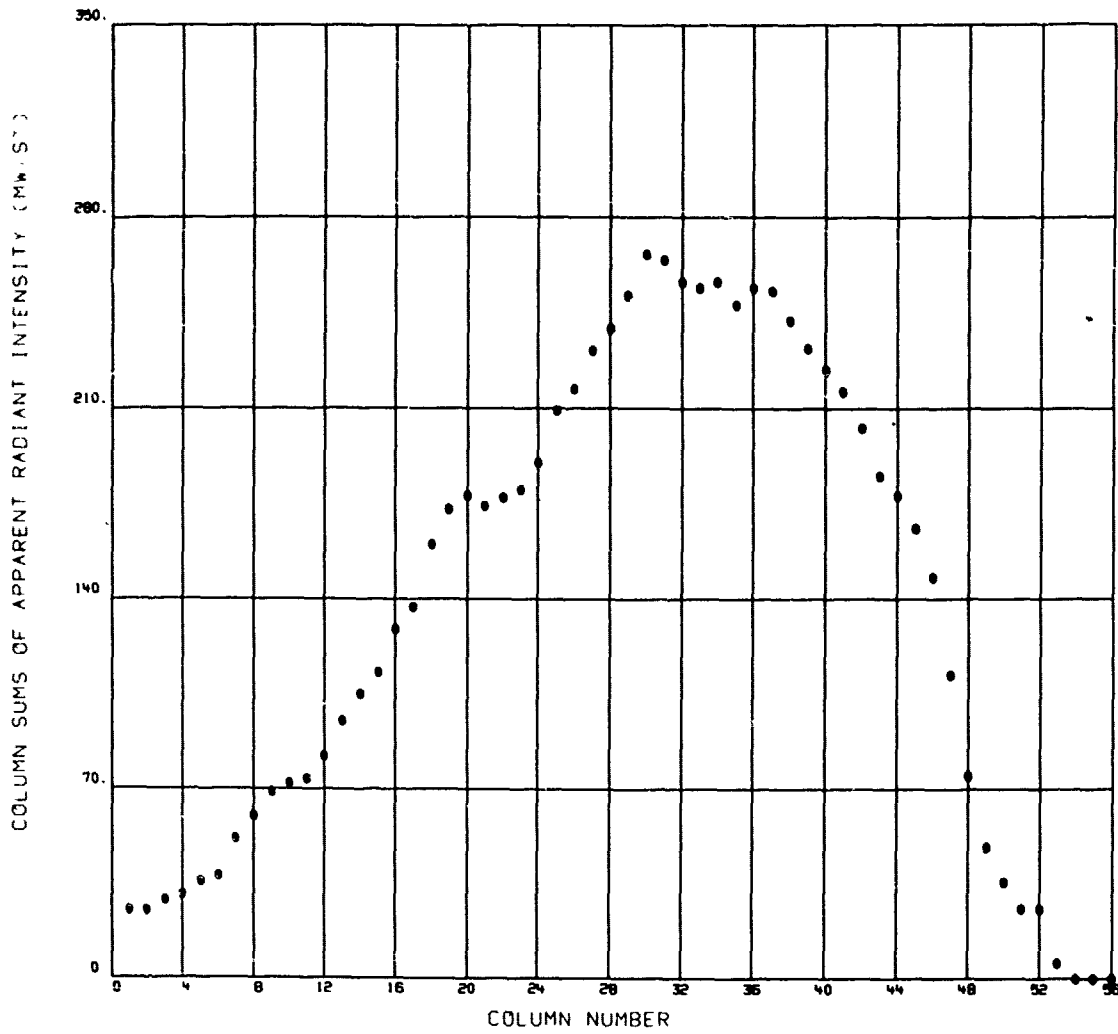
J (W/STER)		
Degrees	O/F = 3.5 Calculation 3 (4.0 to 5.5 $\mu$ )	O/F = 3.2 Measurement (4.0 to 5 $\mu$ )
30	5910	2400 to 2900
60	3660	3800 to 4000
90	3410	2800 to 3600

APPENDIX A

ADDITIONAL FULL-SCALE HAST ENGINE PLUME  
, THERMAL SCANNER DATA DISPLAYS

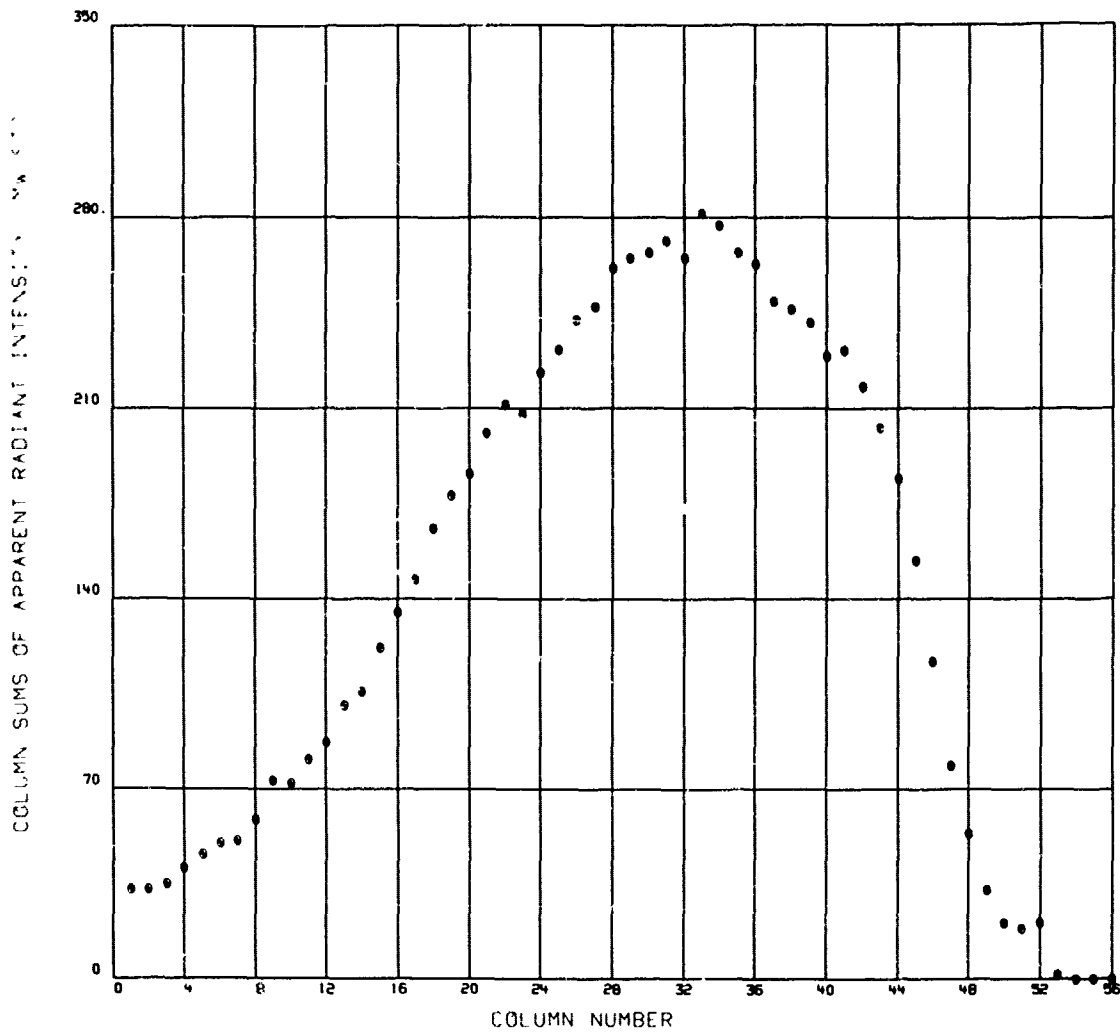
# ONE DIMENSIONAL DISPLAYS

FULL SCALE HAST 8BOOST8 FIRING      STATIC 1400 FT ALTITUDE      MODIFIED ACE) / AS  
FILE 35 RUN NO. = 12      POWER90000



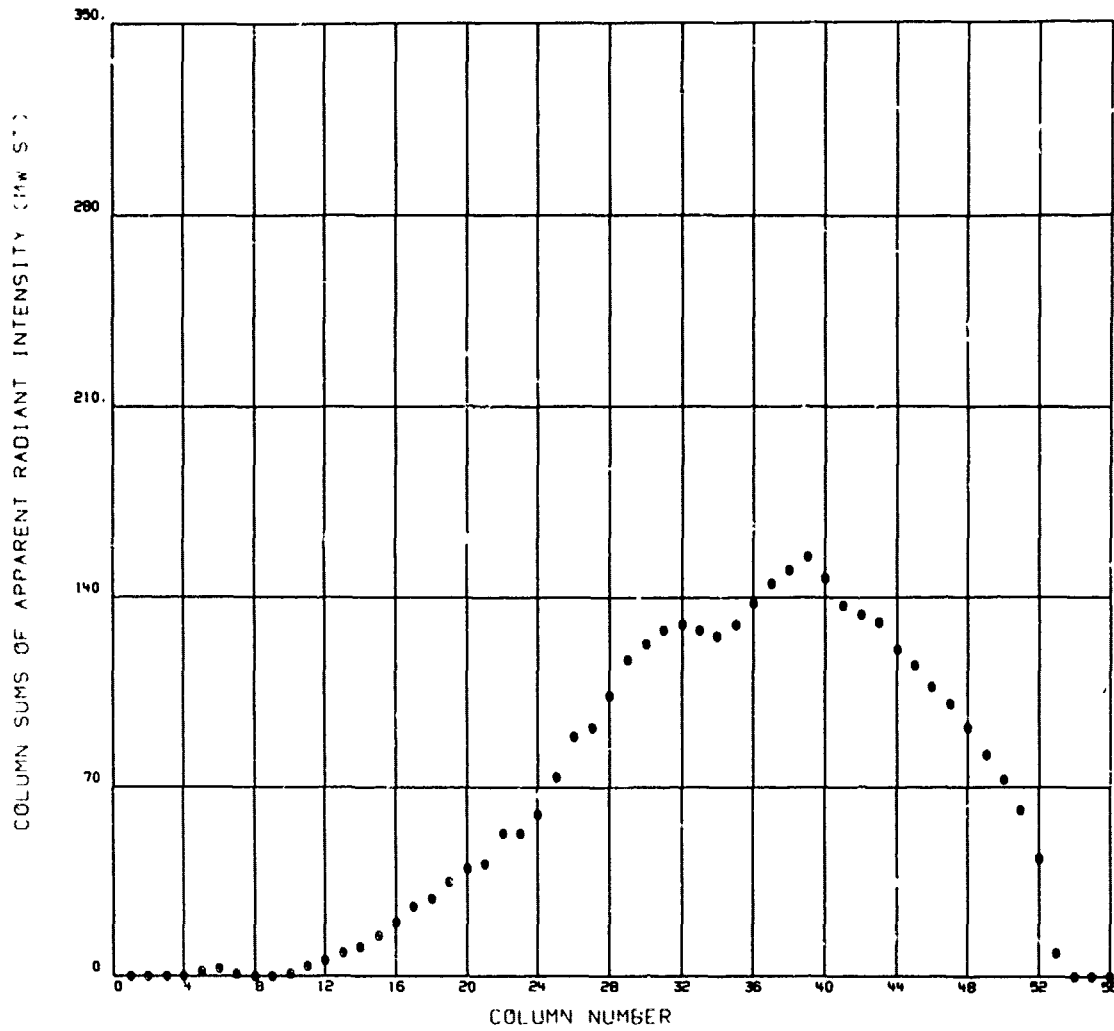
### ONE DIMENSIONAL DISPLAYS (CONTINUED)

A 1 - NAST BB00079 FIRING      DATE: 14 JUL 64      MODIFIED BY: A1  
 24 - RUN NO.      POWER: 500



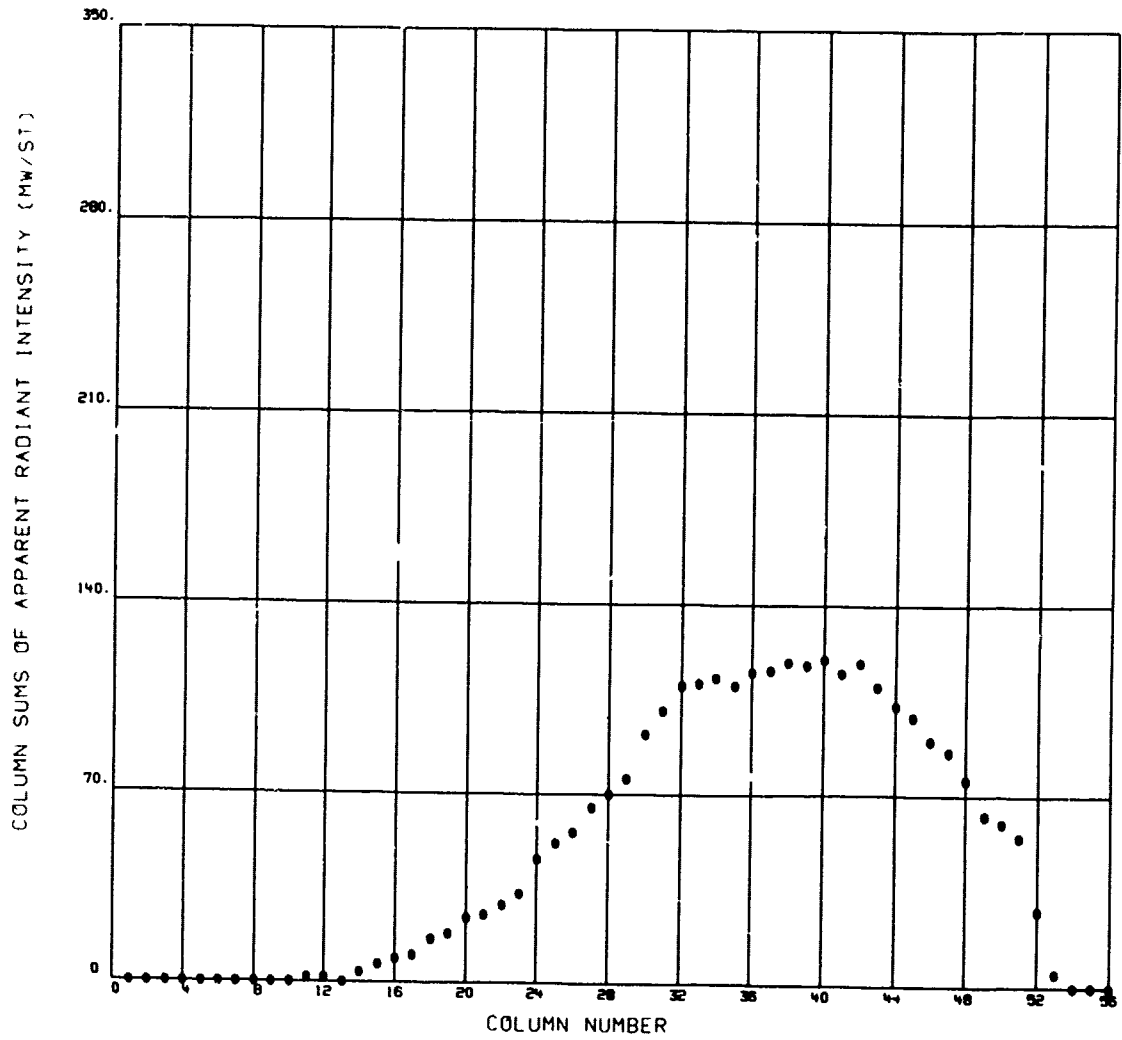
# ONE DIMENSIONAL DISPLAYS (CONTINUED)

FULL SCALE HAST 8BOOST8 FIRING      STATIC 1400 FT ALTITUDE      MODIFIED AERIAL  
FILE 56 RUN NO. - 20      POWER50000



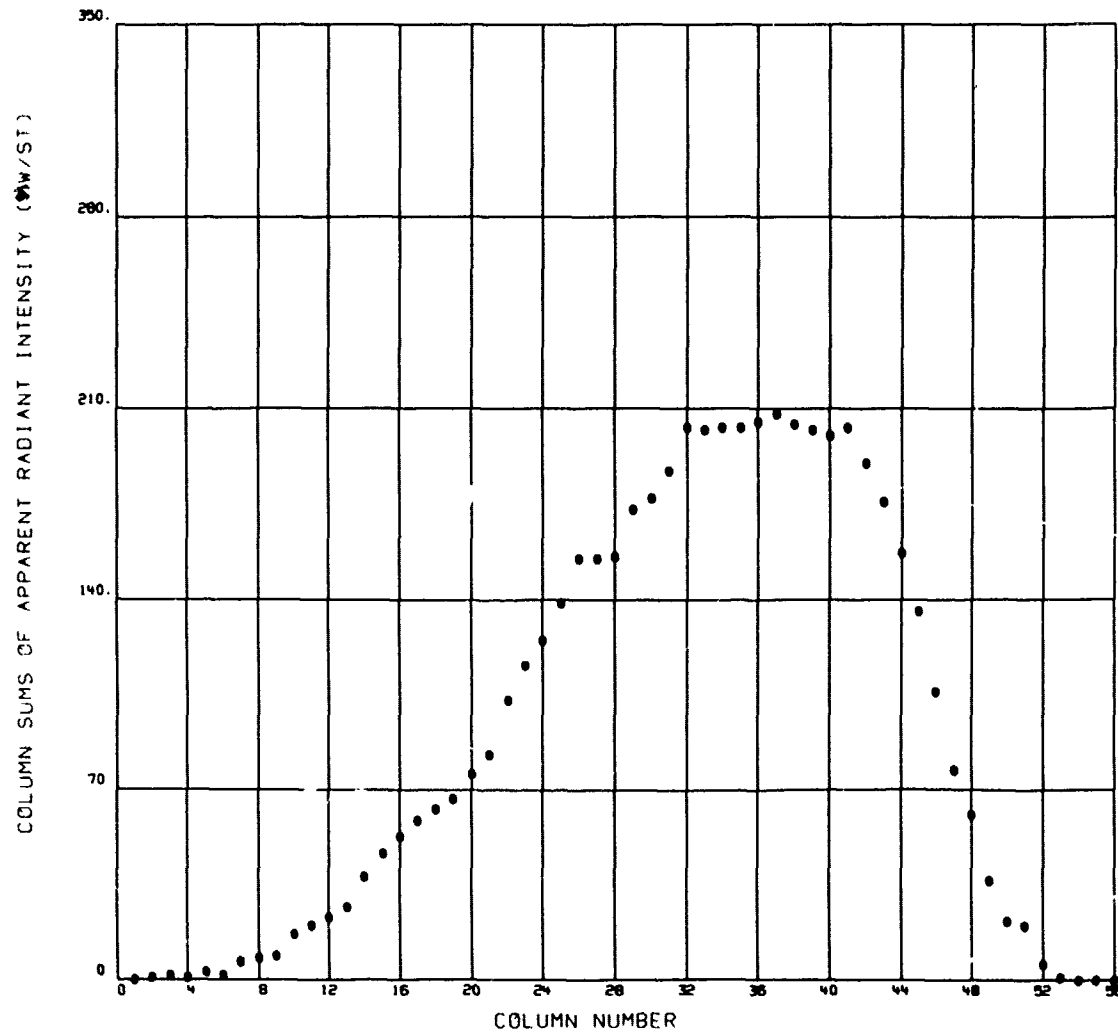
# ONE DIMENSIONAL DISPLAYS (CONTINUED)

FULL SCALE HAST BOOSTER FIRING      STATIC 1400 FT ALTITUDE      MODIFIED ACE)/AC  
FILE '6 RUN NO. 27      POWER50000



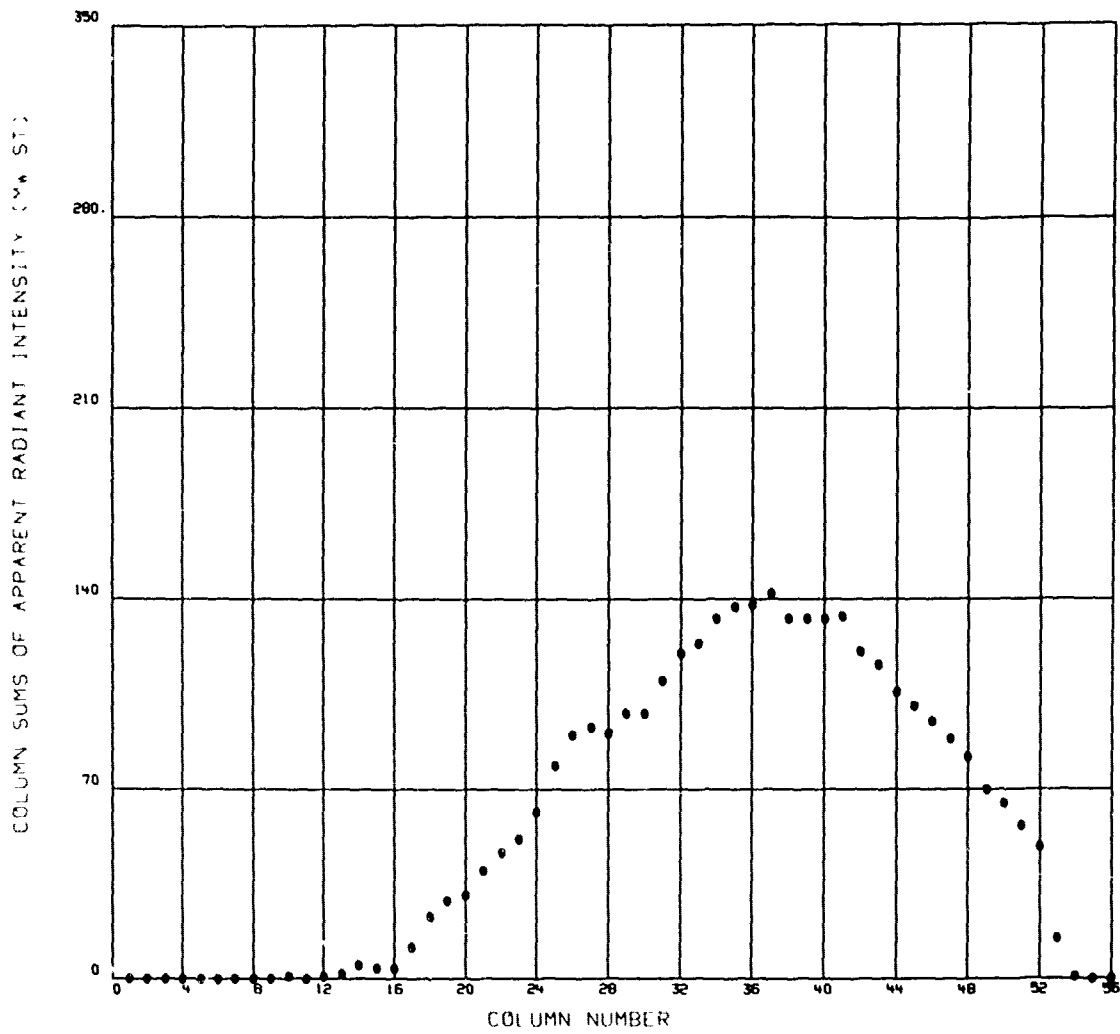
# ONE DIMENSIONAL DISPLAYS (CONTINUED)

FULL SCALE HAST BOOSTER FIRING      STATIC 1400 FT ALTITUDE      MODIFIED ACE 1/AC  
 FILE 91 RUN NO. = 32      POWER 50000



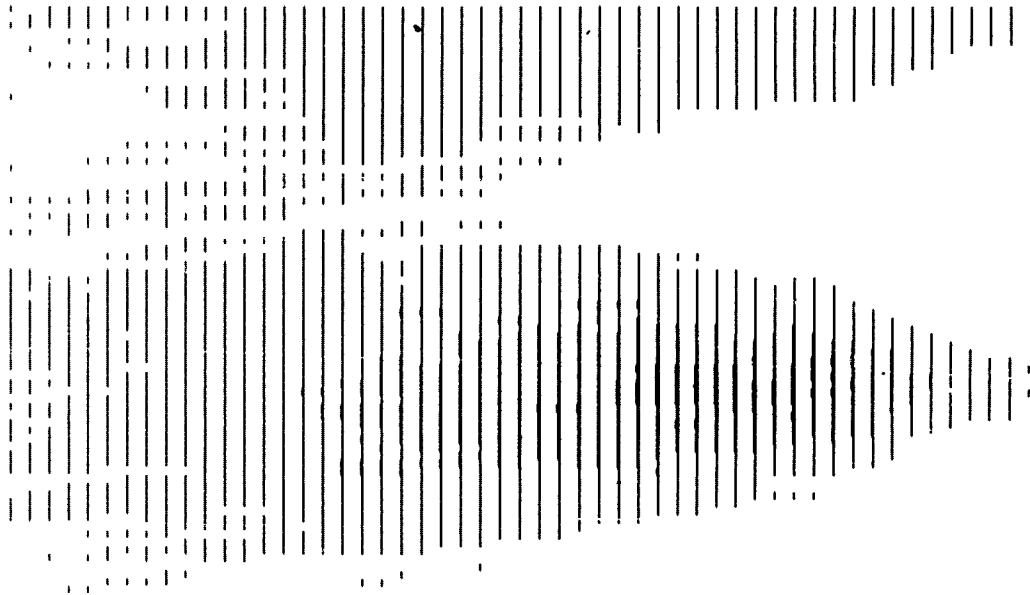
# ONE DIMENSIONAL DISPLAYS (CONCLUDED)

FULL SCALE HAST 8800518 FIRING      STATIC 1400 FT ALTITUDE      MODIFIED ACD/AO  
FILE 132    RUN NO. - 46    POWER50000



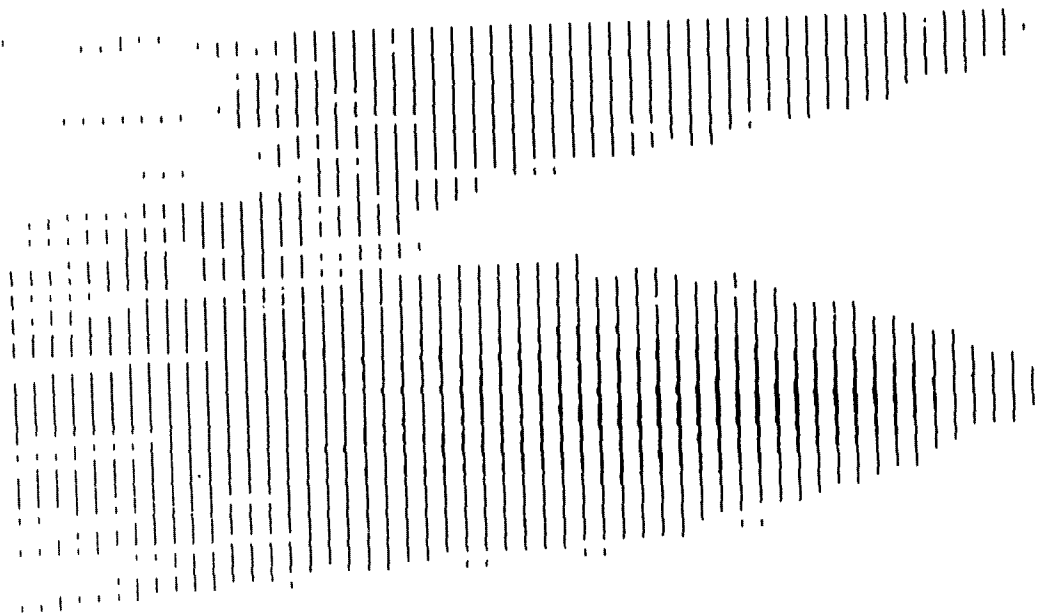
## TWO DIMENSIONAL DISPLAYS

FULL SCALE HAST 0800ST8 FIRING      STATIC 1400 FT ALTITUDE      MODIFIED A(E)/A  
FILE= 29    RUN NO.= 10    POWER50000  
MINIMUM VALUE= 1    MAXIMUM VALUE= 101    INCREMENT= 6



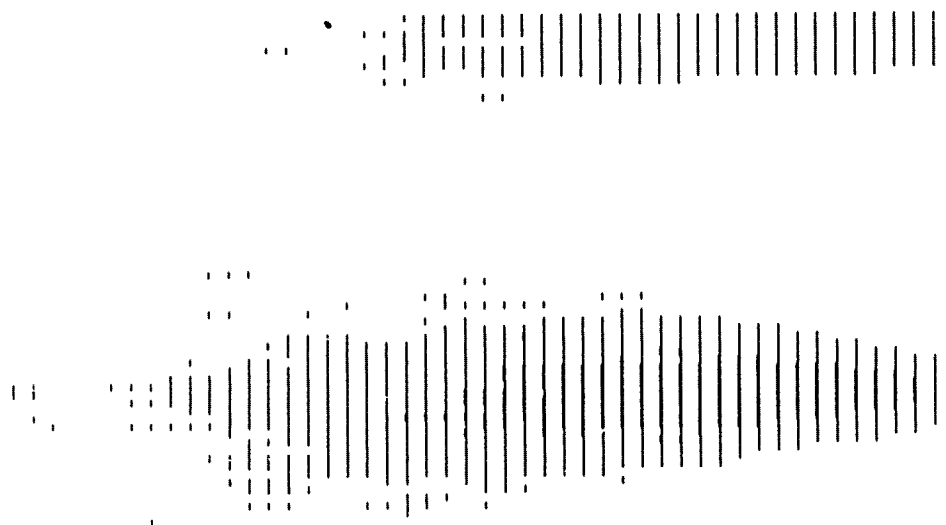
TWO DIMENSIONAL DISPLAYS (CONTINUED)

FULL SCALE HAST @BOOST@ FIRING      STATIC 1400 FT ALTITUDE      MODIFIED ACE)/AC  
FILE= 35    RUN NO.= 12    POWER@0000  
MINIMUM VALUE= 1    MAXIMUM VALUE= 101    INCREMENT= 6



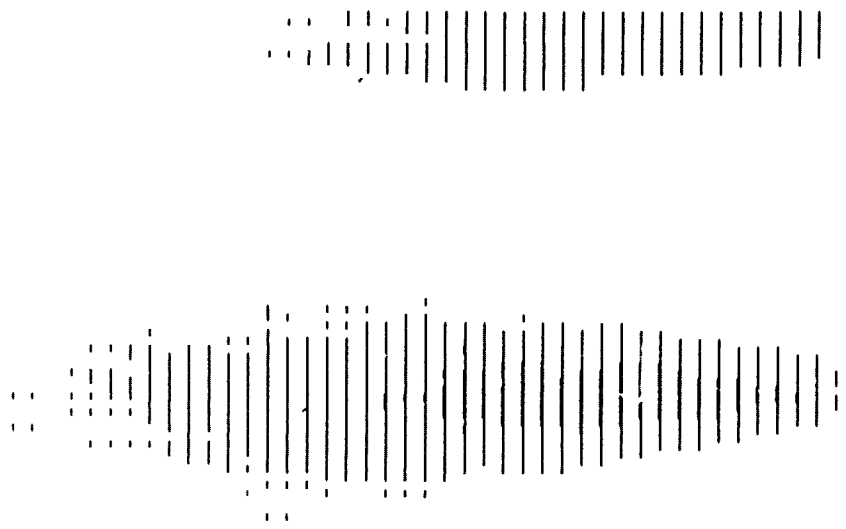
TWO DIMENSIONAL DISPLAYS (CONTINUED)

FULL SCALE HAST 0800ST0 FIRING      STATIC 1400 FT ALTITUDE      MODIFIED ACE)/AC  
FILE= 56    RUN NO.= 20    POWER50000  
MINIMUM VALUE= 1    MAXIMUM VALUE= 101    INCREMENT= 6



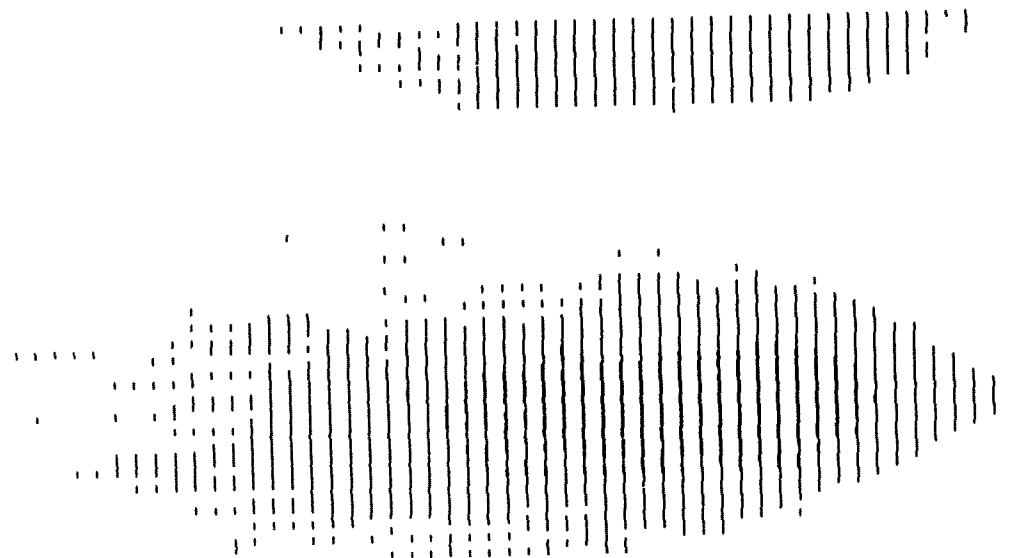
TWO DIMENSIONAL DISPLAYS (CONTINUED)

FULL SCALE HAST 8800ST8 FIRING      STATIC 1400 FT ALTITUDE      MODIFIED A(E)/A(I)  
FILE= 76 RUN NO.= 27      POWER50000  
MINIMUM VALUE= 1      MAXIMUM VALUE= 101      INCREMENT= 6



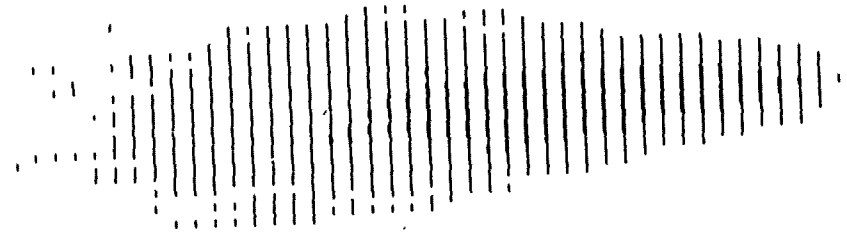
TWO DIMENSIONAL DISPLAYS (CONTINUED)

FULL SCALE HAST BOOSTER FIRING      STATIC 1400 FT ALTITUDE      MODIFIED A(E)/AC  
FILE= 91    RUN NO.= 32    POWER=0000  
MINIMUM VALUE= 1    MAXIMUM VALUE= 101    INCREMENT= 6



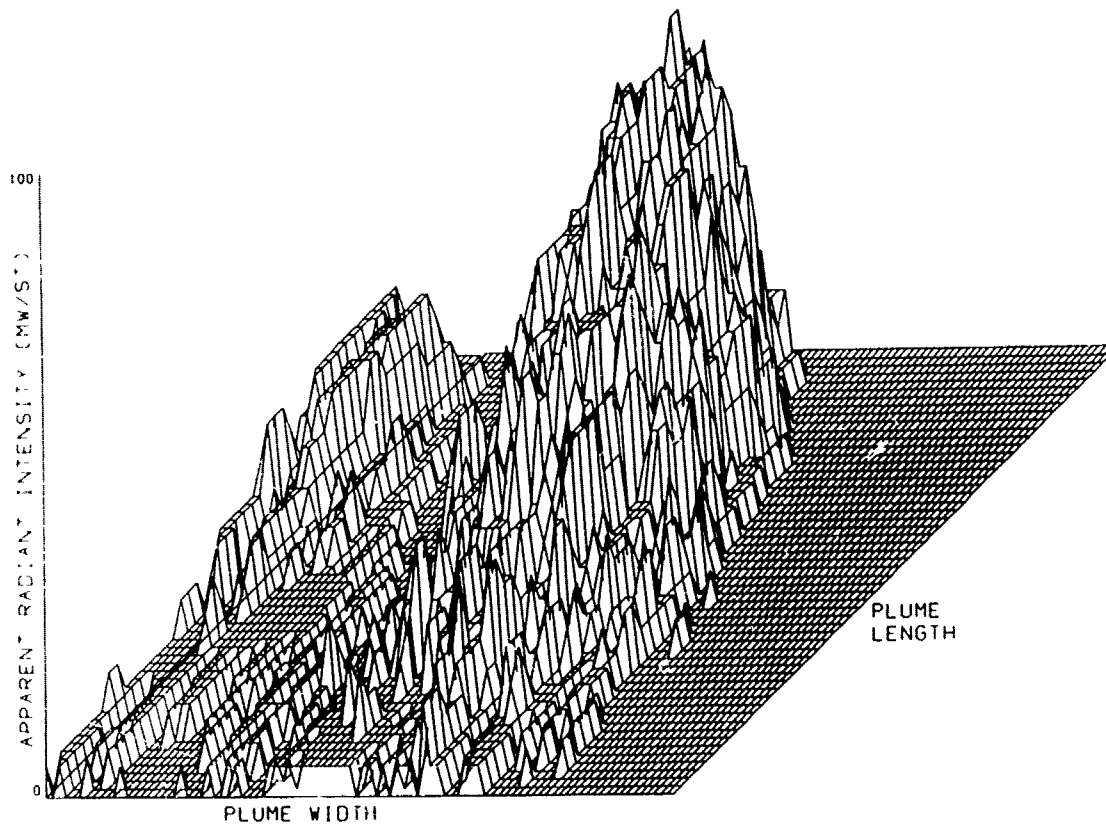
TWO DIMENSIONAL DISPLAYS (CONCLUDED)

FULL SCALE HAST 8800ST8 FIRING      STATIC 1400 FT ALTITUDE      MODIFIED A(E)/AC  
FILE= 132 RUN NO.= 46      POWER50000  
MINIMUM VALUE= 1      MAXIMUM VALUE= 101      INCREMENT= 6



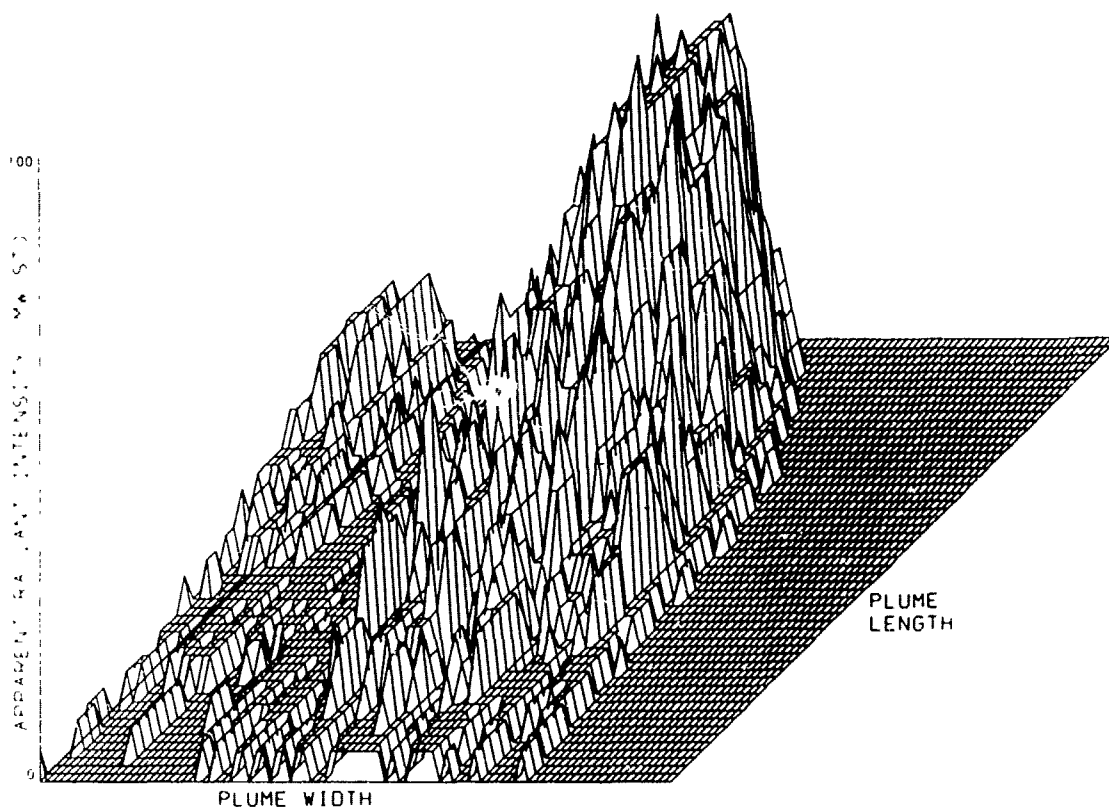
# THREE DIMENSIONAL DISPLAYS

FULL SCALE WAST BOOSTER FIRING STA 10 1400 FT ALTITUDE MODIFIED AED AC  
FILE 19 RUN NO. 10 3 50000



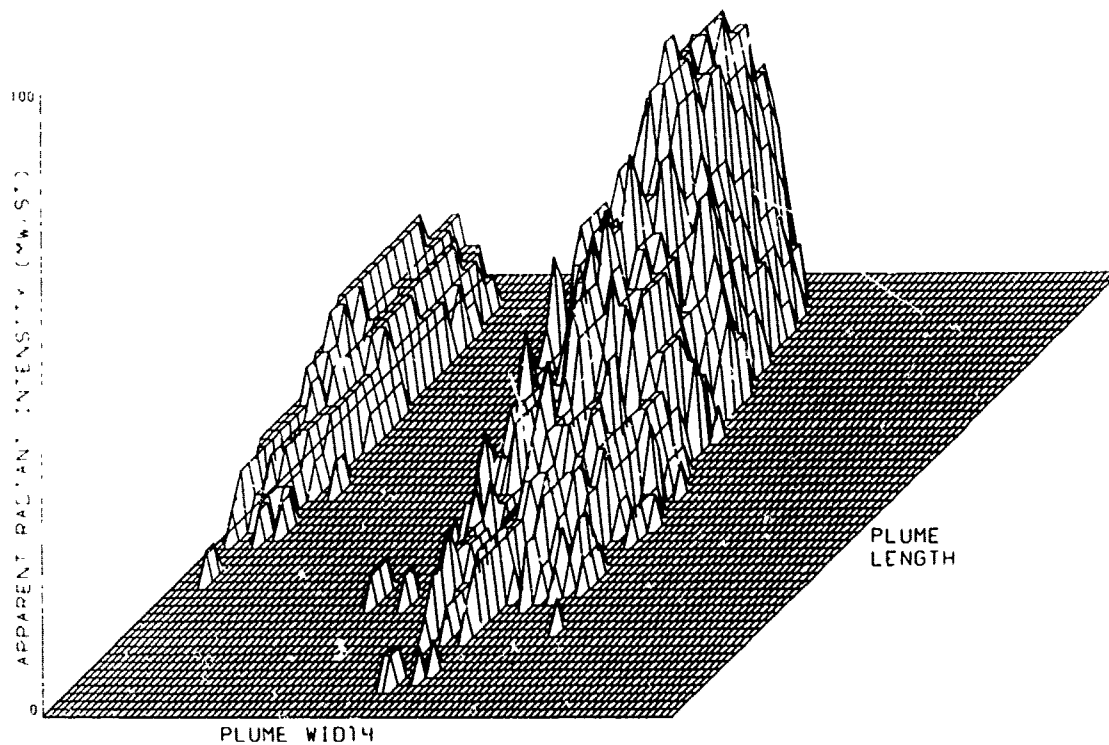
### THREE DIMENSIONAL DISPLAYS (CONTINUED)

SCALE HAST 8800STB FIRING      STATIC 1400 FT ALTITUDE      MODIFIED ACD/AC  
35 RUN NO. 12      O/F 50000



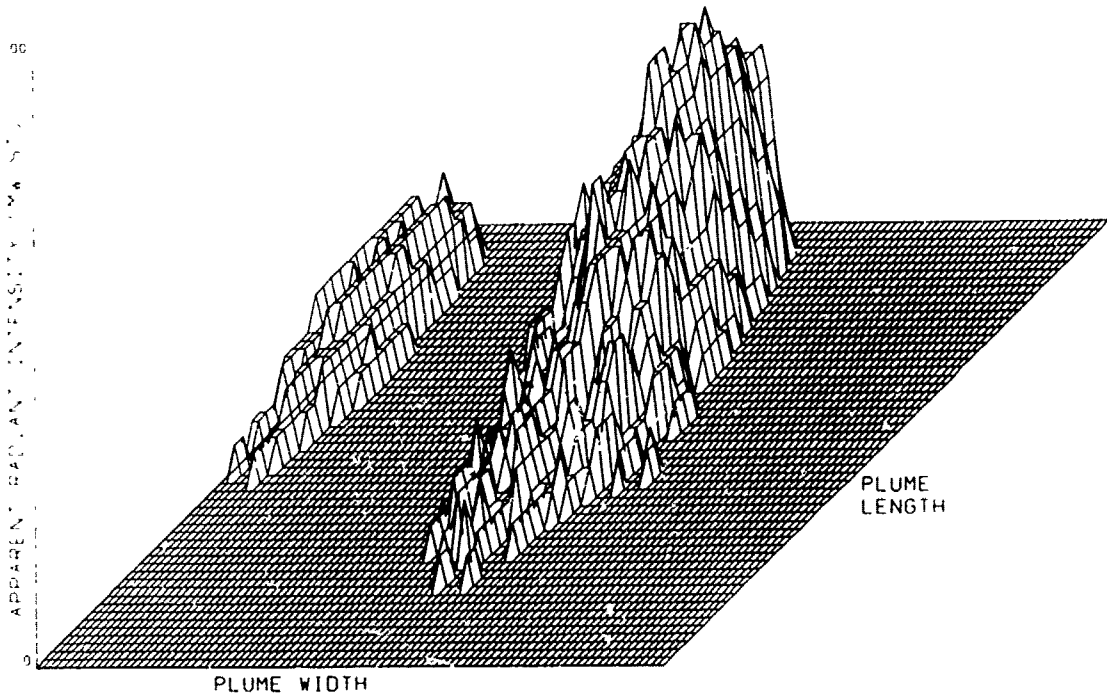
### THREE DIMENSIONAL DISPLAYS (CONTINUED)

DATA FILE 2800572.FIT1.D      DATE: 1400    ALTITUDE    MODIFIED    A    A  
FILE    P.A. NO    20    03    55566



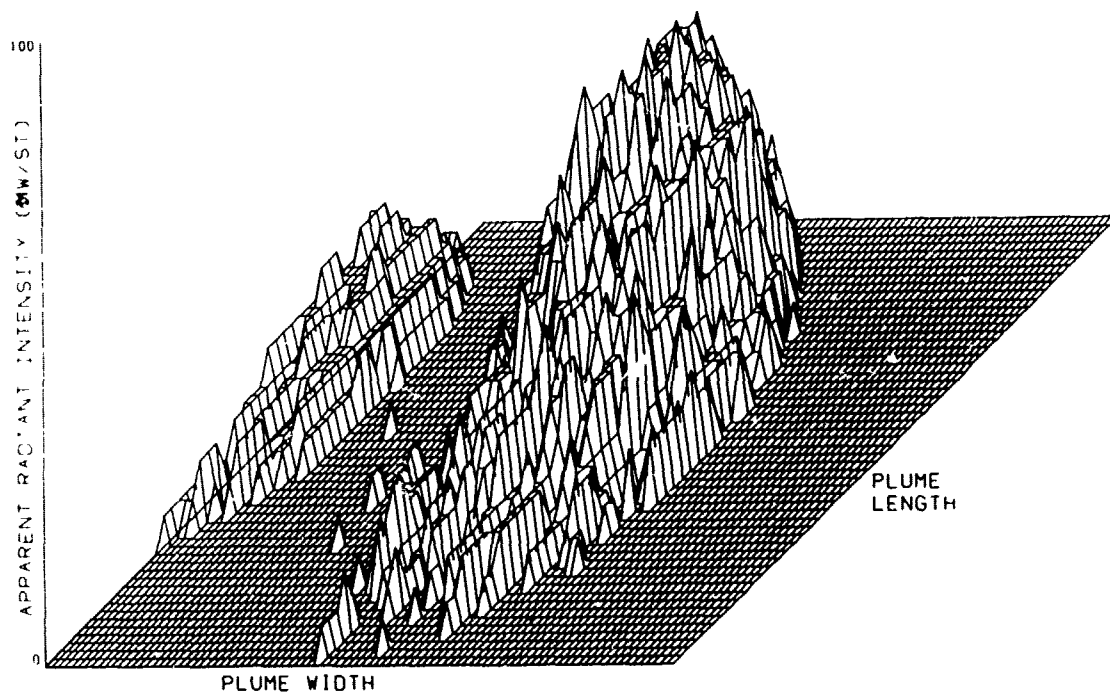
### THREE DIMENSIONAL DISPLAYS (CONTINUED)

SCALE WAST BOOSTER FIRING      STATIC 1400 FT ALTITUDE      MODIFIED ALTITUDE  
RUN NO. 27      OF 5000



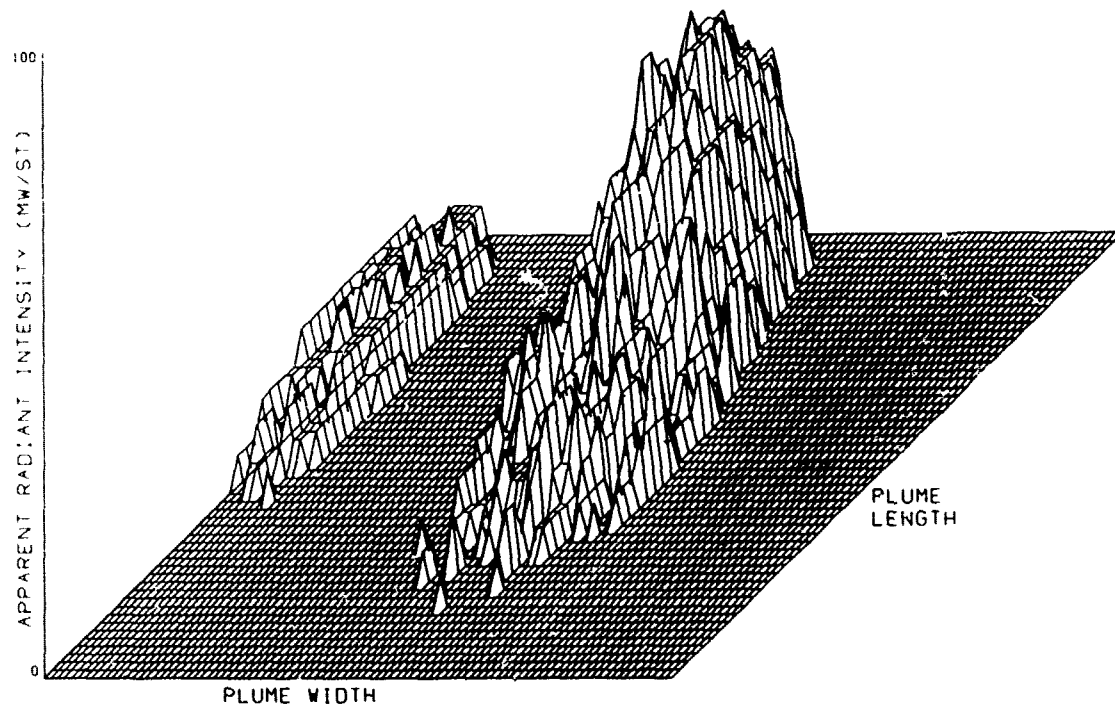
### THREE DIMENSIONAL DISPLAYS (CONTINUED)

FULL SCALE HAST BOOSTER FIRING      STATIC 1400 FT ALTITUDE      MODIFIED ACE      A  
FILE 91 RUN NO. 32      O/F 50000



### THREE DIMENSIONAL DISPLAYS (CONCLUDED)

FULL SCALE HAST 8800ST8 FIRING      STATIC 1400 FT ALTITUDE      MODIFIED ACE)2AC  
FILE = 132    RUN NO. = 46    O/F = 50000



## INITIAL DISTRIBUTION

USAF/SAMI	1	Celesco Industries	1
USAF/RDPA	2	Ordnance Research, Inc	1
USAF/RDQRM	2	United Technologies	20
USAF/XOOW	2	ASD/ENYEHM	1
USAF/XOOPA	1	AFIS/INTA	1
AFSC/DLCAW	2	IDA/Lib	1
TAC/DRW	1	IDA/Wolfhard	1
AFAL/TE	1	AFOSR/NAE	1
AFAL/NV	1	FTD/ENDA	1
ASD/ENYS	1	ASD/XR	1
ASD/RYE	2	AFAPL/RJT	1
AUL/AUL-LSE-70-239	1	AFCRL/OPS	1
ODDR&E/TST&E	1	AFCRL/OPI	1
DARPA/TIO	1	AFRPL/DYSP	1
DDC	2	AEDC (Aro Inc/Lib/Doc)	1
ADTC/PMR	1	Aro Inc/McGregor	1
TAWC/TRADOCLO	1	NWC/Code 4513/Victor	1
TAWC/TERR	1	NWC/Code 4514/Breit	1
ADTC/XR	1	NRL/Code 4004B/Balwanz	1
AFATL/DL	1	Aerochem/Pergament	1
AFATL/DLB	1	Aerodyne/Draper	1
AFATL/DLM	1	Aerodyne/Mann	1
AFATL/DLMI	1	Aeronautical RA/Fishburne	1
AFATL/DLMH	3	Aerospace Corp/Lee	1
AFATL/DLMQ	10	Aerospace Corp/Thomas	1
AFATL/DLOSL	2	Atlantic Research/Goede	1
AFTEC/XR	1	Calspan Corp/Boyer	1
AFTEC/TET	1	Calspan/Marrone	1
4950 Test W/TIHM	1	Grumman Corp/Slack	1
Ogden ALC/MMNOP	2	Lockheed Msl & Space/Mikatarian	1
AFWL/LR	1	Lockheed Msl & Space/Smith	1
NWC/Code 5143	1	Martin-Marietta Corp/Hetrick	1
ADC/DOV	1	Physical Dynamics, Inc/Boynton	1
Redstone Arsenal (AMSMI-TM)	2	Thiokol Corp/Webb	1
Redstone Arsenal (AMSMI-REI)	1	Brigham Young Univ/Smoot	1
ADWC/50th TES	1	ADTC/TSGPA	1
Pacific Missile Test Cntr/Code 1252	1	NRL/Code 7126	1
COMPTREVFOR	1	AFOSR/NP	1
TFWC/TAF	1	Univ of Maryland/Anderson	1
Warner-Robins (ALC/MMYQ)	1	Rocketdyne/Flanagan	1
NASC/PMA-247	1	Envir Research Inst of Michigan	1
NSWSES/Code 4221	2	NASA/JPL/Ryason	1
NADC/Targets Office	1	AFAL/WRD	1
Mitre Corp	2	SAMSO/RSSP	1
Beech Aircraft Corp	2	Flight Systems, Inc	1
Atlantic Research Corp	1	Motorola, Inc	1
Teledyne CAE	1	DARPA	1
Teledyne Ryan Aeronautical	1		
Northrup Ventura	1		
Hayes International Corp	1		
Sanders Associates, Inc	1		